POLITECNICO DI TORINO

Collegio di Ingegneria Chimica e dei Materiali

Corso di Laurea Magistrale
in Ingegneria Chimica e dei Processi Sostenibili

Tesi di Laurea Magistrale

“An example of crystal engineering: the case study of Levofloxacin-Quercetin cocrystals”.

Relatrice

Prof.ssa Elena Simone

Correlatrice

Dott.ssa Cecilia Fiore

Candidato

Simone Tedeschi

Anno accademico 2024/2025
Sessione di Laurea Ottobre 2024

ABSTRACT

In the last century crystal engineering gained more attention within the scientific community, due to its many potential applications. Notable among these are the enhancement of the physicochemical properties of drugs, the development of controlled drug release systems, the creation of organic semiconductors, the design of chemical sensors, and the production of controlled-release fertilizers. Engineering crystal structures with tailored properties implies that their design and synthesis is guided by precise control of intermolecular interactions that occur between molecules within crystal lattice. In particular, the pharmaceutical sector finds very promising a specific crystal engineering strategy: the use of cocrystals. Pharmaceutical cocrystals are defined as crystalline structures composed of at least an active pharmaceutical ingredient (API) and one or more partner molecules ,in a stoichiometric ratio, hereinafter referred to as "coformers".

In a previous work, the efficiency of the crystal engineering approach was presented in showing the combination between flavonoids and antibiotics as an advanced approach to fight a pathogen called *Helicobacter pylori* (Uivarosi et al., 2024). In the aforementioned work, the solid-state combination of Levofloxacin (LEVO), an antibiotic and Quercetin (QUE) a flavonoid gave a new crystal structure, a cocrystal-solvate of Ethanol. In this thesis four different cocrystals solvents of LEVO and QUE were synthetized via slurring at room temperature for 72 hours in the dark, with a stoichiometric ratio 1:1 using four different solvents: methanol (MeOH), ethanol (EtOH), 1-propanol (1PR) and isopropanol (IPA) and their desolvated products were analyzed as well. Powder X-ray diffraction and Raman Spectroscopy were applied for the solid-state characterization of these novel materials. Differential Scanning Calorimetry and Thermogravimetric analysis were useful to determine the thermal behavior and stability of these new crystal structures. Performance characterization such as solubility, dissolution tests and wettability measurements were also performed.

The wettability of the cocrystals powder in water and sunflower oil was evaluated by contact angle measurements, which showed that cocrystals have a worse wettability than levofloxacin with water, but a slowly better wettability with sunflower oil.

Solubility tests were performed using dynamic experiments with the commercial platform Crystal16. Each cocrystal solubility profile was studied in the respective solvent of crystallization.

Dissolution tests were conducted both in milli Q water and in a pH=1 solution, to study the difference in release rate between the different cocrystals, levofloxacin, and the physical

mixture. The results provided evidence that cocrystallization can be used to control the release rate of the active ingredient over the time. Also, tentative tablets were produced to observe different dissolution behavior in the presence of two routinely used excipients, mannitol and cellulose nanocrystals.

Summury in Italian:

1 Introduzione

Nell'ultimo secolo l'ingegneria dei cristalli ha ricevuto molte attenzioni grazie alle numerose potenziali applicazioni che ha mostrato, quali un rilascio controllato di un farmaco o un fertilizzante, la modifica di proprietà chimico-fisiche di un farmaco, tra cui stabilità o solubilità, e la creazione di sensori chimici o semiconduttori organici. Di particolare interesse in questo lavoro sono i cocristalli farmaceutici, definiti come strutture composte da almeno un ingrediente farmaceutico attivo (API) e una o più molecole, in rapporto stechiometrico, denominate coformers. I Coformers sono solitamente selezionati dalla lista GRAS "Generally Regarded As Safe" e comprendono vitamine, biomolecole, additivi alimentari, minerali e amminoacidi. L'ingegneria dei cristalli sta conquistando così tanto spazio nell'ambito farmaceutico a causa dell'aumento della resistenza dei patogeni ai comuni antibiotici, che sta portando all'esigenza di trovare e costruire nuove soluzioni. In particolare, in questa tesi si riprende un lavoro condotto da (Uivarosi et al., 2024) contro *Helicobacter pylori,* un patogeno Gram-negativo che nel 2017 è stato inserito nella prima lista di patogeni resistenti agli antibiotici che necessitano di priorità nella ricerca di una soluzione dalla Word Health Organization. Nello studio sopra-menzionato si faceva riferimento a diverse combinazioni di antibiotici e flavonoidi per combattere questo patogeno, tra queste è stata ritenuta interessante quella tra la levofloxacina (un fluorochinolone) e la quercetina (flavonoide). Il cocristallo da queste due sostanze è stato ottenuto in una soluzione slurry per 72 ore in assenza di luce, con rapporto stechiometrico 1:1, con 4 diversi solventi: etanolo, metanolo, 1-propanolo e isopropanolo. Lo scopo è osservare il differente comportamento e studiarne le proprietà strutturali e chimico-fisiche. La levofloxacina appartiene alla famiglia dei Fluorochinoloni, capaci di bloccare l'attività batterica agendo su due enzimi essenziali: DNA girasi e Topoisomerasi IV, risultando efficace sia contro i batteri Gram- che contro quelli Gram+. La quercetina appartiene alla famiglia dei flavonoidi e può essere trovata in diversi vegetali, semi e frutti e possiede molte attività farmacologiche come antiossidante, antimicrobico, anticancro, e antiinfiammatorio. Sono state studiate le differenze nel rilascio tra la miscela fisica, ottenuto semplicemente mescolando levofloxacina e quercetina, con pura levofloxacina e i vari cocristalli. La ragione per cui si è ritenuto necessario introdurre questa casistica è dovuta dal fatto che sia cocristallo che miscela fisica hanno registrato dai test antimicrobici condotti dallo studio di Fiore et al. un comportamento simile, in particolar modo in entrambi i casi era necessaria

metà della dose di levofloxacina per giungere allo stesso risultato antimicrobico, rispetto alla pura levofloxacina. Lo scopo della tesi è di meglio capire e mostrare come la cocristallizzazione possa essere un potente strumento, partendo da un esempio pratico.
La tesi è composta da 5 capitoli. Il contenuto dei prossimi capitoli può essere così sintetizzato:

- *Capitolo 2:* fornisce un riassunto teorico, con lo scopo di capire meglio l'origine dell'ingegneria dei cristalli e la sua funzione, i reagenti coinvolti- levofloxacina e quercetina- le tecniche di analisi applicate come la diffrazione ai raggi X e la spetroscopia Raman per la caratterizzazione della struttura, calorimetria a scansione differenziale e analisi termogravimetriche per lo studio della perdita di solvente nelle strutture dei cocristalli e i fenomeni di fusione e degradazione.
- *Capitolo 3*: descrive i materiali, gli strumenti utilizzati e i metodi performati.
- *Capitolo 4*: è dedicato alla discussione dei risultati principali ottenuti durante lo svolgimento di questo lavoro
- *Capitolo 5*: conclude la tesi.
- Appendice A mostra il tentativo con diversi modelli di dissoluzione per una migliore comprensione della scelta del modello di questa tesi.
- Appendice B contiene le immagini dei diversi angoli di contatto registrati nel lavoro.

2 Panoramica Teorica

Nel 1989 Desiraju ha dato una prima definizione dell'ingegneria dei cristalli intesa come comprensione delle interazioni intermolecolari usato nel disegnare nuovi soliti con specifiche proprietà chimico-fisiche. La Food and Drug Administration ha poi fornito la definizione di cocristalli intesi come "materiali cristallini compostati da due o più molecole diverse, tipicamente un ingrediente farmaceutico attivo e uno o più coformers, nello stesso reticolo cristallino". La differenza con i Sali consiste nel fatto che i componenti che si trovano nel reticolo interagiscono con interazioni non-ioniche. I cocristalli possono essere suddivisi in due principali classi: cocristalli ionici e cocristalli molecolari. Si definisce la solubilità come la massima quantità di soluto che si può dissolvere in una determinata quantità di solvente, in specifiche condizioni. Lo studio procede con la descrizione della nucleazione e della crescita cristallina, due processi guidati dalla supersaturazione. È possibile dividere la regione di supersaturazione in due zone: una metastabile dove avviene solo la crescita dei cristalli e una labile in cui avvengono sia nucleazione che crescita. La

nucleazione primaria è definita come la formazione di una nuova particella da molecole disciolte nella fase continua e può essere omogenea, processo governato dalla sola super saturazione, oppure eterogenea se avviene grazie alla presenza di superfici solide che favoriscono la nucleazione. La nucleazione secondaria si riferisce alla creazione di nuovi nuclei d cristalli già esistenti. L'operazione di crescita cristallina è un processo in cui un cristallo aumenta di dimensione. Questo fenomeno occorre quando materiale da una soluzione si deposita nella superficie di un cristallo già esistente, seguendo la struttura cristallina. La crescita cristallina si compone di due fasi: una fase di diffusione e una di deposizione. Una parentesi particolare è stata aperta sulle tecniche di "seeding" che involvono l'introduzione di cristalli precedentemente formati, per permettere l'aggregazione di molecole addizionali, e poiché fungono da stampo per le molecole di assemblarsi in cristalli con le stesse caratteristiche di quelli introdotti. Vengono poi illustrati i metodi di preparazione dei cocristalli differenziando tra quelli in soluzione e quelli solidi. Particolare attenzione è posta alla cocristallizzazione via slurry, in quanto tecnica adoperata in questo lavoro, che consiste nella sospensione dei reagenti in una minima quantità di solvente.

Si passa poi allo studio dell'angolo di contatto, ovvero l'angolo formato tra il perimetro di una goccia di liquido e la superficie su cui poggia, dopo una descrizione dei reagenti utilizzati in questo studio e delle loro classi di appartenenza. Questo valore viene di solito applicato per quantificare la bagnabilità di un materiale. Si parte dalla definizione di Young fino ad arrivare alla descrizione dei diversi scenari possibili, compresi le micro-eterogeneità e l'isteresi.

Segue poi una descrizione teorica delle tecniche analitiche presenti nello studio. Tra queste troviamo la diffrazione dei raggi X, tecnica non invasiva applicata per esaminare una grande varietà di materiali. Questa tecnica permette di esaminare e caratterizzare la posizione degli atomi, il loro arrangiamento all'interno di una cella unitaria e lo spazio tra piani atomici. I raggi X colpiscono materiali solidi e sono dispersi dagli elettroni che orbitano attorno al nucleo atomico. L'interferenza delle onde disperse può essere costruttiva o distruttiva, se costruttiva avviene la diffrazione. Lo strumento è composto da una sorgente di raggi X che colpisce il campione posto su un piano d'appoggio e i raggi sono diffratti verso un detector. Nella diffrazione di polveri è applicata una polvere, piuttosto che un solo cristallo. Un diffrattogramma mostra l'intensità della radiazione diffratta in reloazione con l'angolo di Bragg (2θ). Contiene numerosi picchi caratterizzati dalla posizione, dal profilo e dall'intensità.

Altra tecnica analizzata è la spettroscopia Raman, una tecnica spettroscopica vibrazionale non distruttiva. Un campione viene esposto a fotoni da una sorgente laser monocromatica, provocando la dispersione in tutte le direzioni. La maggior parte delle radiazioni ha una frequenza uguale a quella incidente (scattering elastico), mentre solo una piccola frazione differisce (scattering anelastico). La variazione della luce incidente dipende dalla composizione chimica. Le vibrazioni molecolari causano cambi nella polarizzabilità molecolare e queste corrispondo a frequenze specifiche e dipendono dal tipo di legame coinvolto. Lo strumento è composto da una sorgente luminosa, con specifiche frequenza e lunghezza d'onda, che colpisce un campione posto su un apposito ripiano. La luce diffusa è analizzata da un apposito detector per determinarne la frequenza. Uno spettro Raman si presenta come intensità vs lo spostamento Raman espresso in cm^{-1}.

Tra le analisi termiche applicate troviamo l'analisi termogravimetrica, tecnica usata per determinare il cambiamento delle proprietà chimico-fisiche di un campione in risposta a una rampa di temperatura appositamente impostata. L'analisi è condotta in una fornace chiusa equipaggiata con un analizzatore che contiene una microbilancia, fortemente sensitiva a fenomeni come degradazione, ossidazione e decomposizione. L'atmosfera è mantenuta controllata grazie all'uso di un gas inerte. Il risultato consiste in un termogramma che contiene il cambiamento di massa vs la temperatura impostata o il tempo durante il quale l'analisi è condotta.

Altra tecnica termica è la calorimetria differenziale a scansione, comunemente applicata per determinare le temperature di fusione, cristallizzazione e transizione vetrosa, ma anche gli associati cambi in entalpia ed entropia. Lo strumento è composto da due porta campioni identici, di cui solo su uno viene effettivamente depositato il campione da analizzare. In questo modo le differenze nel comportamento sono dovute alla presenza del campione da un lato o dalla sua assenza nell'altro. Un tipico grafico ottenuto è costituito dalla differenza di flusso di calore tra il campione e il riferimento all'asse-y e la temperatura o il tempo in asse-x.

La legge di Lambert-Beer, successivamente descritta, consiste nella relazione tra l'assorbimento della luce da parte di una sostanza e le sue proprietà. La legge mostra come l'assorbimento sia direttamente proporzionale alla concentrazione della sostanza e alla lunghezza ottica del cammino.

Successivamente una serie di modelli di dissoluzione è stata descritta, con lo scopo di capire il comportamento di dissoluzione dei cocristalli. Si parte dalla descrizione di un modello di ordine zero, in cui la dissoluzione del farmaco avviene a velocità costante e indipendente dalla quantità di soluto rimanente. Si passa al modello di primo ordine in cui la velocità di dissoluzione è proporzionale alla concentrazione del soluto rimanente. Si è descritto il modello di Weibull,

modello empirico senza alcune base teorica. Il modello mostra la frazione di farmaco rilasciato ad un determinato tempo come funzione di due parametri: la scala temporale del processo e il parametro di forma. Il modello di Higuchi descrive la dissoluzione di un principio attivo da una matrice solida, principalmente diffusiva. Il modello è governato dalla legge di Fick, dipendente dalla radice quadrata del tempo. Ha trovato, infine, forte applicazione un nuovo modello basato sulle cinetiche dispersive. Questo è un modello semi-empirico realizzato per studiare e caratterizzare cinetiche di dissoluzione complesse. Il concetto alla base prevede un cambiamento della barriera energetica di attivazione che può avvenire in alcuni casi. In particolare, ci si è concentrati sul modello "deceleratory", che consente di studiare conversioni omogenee come la decomposizione di diversi tipi di cristalli.

3 Materiali e Metodi

La levofloxacina è stata acquistata da TCI Europe (TCI Europe N.V., Belgium-Tokyo Chemical Industry, Japan), mentre la quercetina da Sigma-Aldrich (Merck, Massachusetts, U.S.).

I cocristalli di levofloxacina e quercetina sono stati sintetizzati via slurry a temperatura ambiente, per 72 ore al buio, con una stechiometria di reazione 1:1, utilizzando quattro diversi solventi: metanolo, etanolo, 1-propanolo e isopropanolo. Le sospensioni sono state mantenute in agitazione con una velocità di circa 250 rpm in una fiala da 10 ml, chiusa con parafilm. Diverse stechiometrie sono state testate per verificare che non si parlasse di soluzione solida, ma bensì di un cocristallo con una struttura ben definita.

La diffrazione di polveri su raggi X è stata collezionata applicando una geometria Bragg-Bentano su un diffrattometro Empyrean (Malvern Panalytical, U.K.). I Diffrattogrammi sono stati ottenuti a 2θ range 4-40° e 0.0001 come minima dimensione del passo 2θ, grazie ad una radiazione CuK_α con una lunghezza d'onda (λ) di 1.54 Å. Lo strumento ha operato con una corrente di 40 mA e un voltaggio di 40 kV con un Soller slit di 0.04 rad, anti-scatter slit di $^1/_2$ e uno slit di divergenza di $^1/_4$.

Per la spettroscopia Raman è stato utilizzato uno spettrofotometro LabRAM HR Evolution (Horiba, Japan). Una lunghezza d'onda e un detector Synapse Plus (Horiba) sono stati utilizzati. Sono state registrate scansioni della regione spettrale tra 200 e 1700 cm^{-1} con un tempo di acquisizione di 10 secondi ed un numero di accumulazione di 40.

Le misure del flusso di calore sono state ottenute grazie ad un Mettler Toledo DSC (Mettler Toledo, USA). Ogni campione, all'incirca di 3 mg, è stato riscaldato da 20°C fino a 350°C, con una velocità di 10°C/min.

L’analisi termogravimetrica si è condotta con un Mettler Toledo 1600 (Mettler Toledo, USA), con argon come gas inerte. All’incirca 6 mg di campione sono stati disposti con un programma di temperatura da 20°C fino a 400°C, con una velocità di 10°C/min.

Le misure dell’angolo di contatto sono state effettuate grazie a un analizzatore della forma della goccia DSA25 (Kruss Scientific), equipaggiato con una micro-siringa ed una camera ad alta velocità. I campioni analizzati sono stati realizzati sotto forma di dischi da 1 cm di diametro, grazie all’uso di una pressa idraulica in cui sono stati inseriti 100-120 mg di campione per 30 secondi sotto una pressione di 200 bar. Le misure sono state effettuate e registrate sia per acqua che per olio di semi di girasole, con una goccia di 2 μl. La goccia è stata analizzata con il metodo di Young-Laplace grazie al software Kruss Advance 1.12.0.35401, permettendo in questo modo di registrare gli angoli di contatto tra la superficie del disco e la goccia.

La misura della solubilità è stata realizzata grazie all’ausilio del Crystal 16 (technobis Crystallization Systems), equipaggiato con un laser con lunghezza d’onda di 645 nm per misurare la torbidità delle soluzioni. Quantità di cocristalli da 1 mg a 15 mg sono state inserite in 1 ml di solvente all’interno di fiale di vetro da 1.5 ml. L’analisi prevede l’impostazione da parte dell’utente di vari cicli di temperatura, opportunamente personalizzati per ogni cocristallo. I valori di trasmissività registrati nel tempo e per ogni specifica temperatura sono stati analizzati usando il software CrystalClear e approssimati con l’equazione di van’t Hoff, per ottenere le curve di solubilità. Le equazioni sono state poi linearizzate per permettere di estrapolare valori di solubilità a temperature differenti da quelle analizzate, per un possibile scale-up della produzione.

Per condurre i test di dissoluzione borse di dissoluzione fatte in cellulosa, con un cut-off in peso di 14,000 Da (Sigma-Aldrich, Cesano Maderno, Italia), sono state immerse in acqua milli Q per almeno 10 minuti, per consentirne l’apertura e il corretto funzionamento. Successivamente opportune quantità di polveri da analizzare sono state inserite nella membrana insieme ad una biglia di vetro per garantirne la completa immersione ed evitare fenomeni di galleggiamento. I test di dissoluzione sono condotti sia in acqua milli Q che in una soluzione a pH 1, in un baker con un volume di 100 ml. Il tutto è mantenuto sotto continua agitazione (intorno a 85 rpm) per assicurare un’omogeneità della soluzione. I prelievi sono stati fatti a specifici intervalli di tempo e i campioni estratti sono stati analizzati in uno spettrofotometro Multiskan Sky high UV/Vis (ThermoFisher Scientific).

È stato cruciale identificare la lunghezza d’onda della levofloxacina, in quanto unica a dissolversi all’interno della soluzione. Per fare ciò sono stati condotti dei test di dissoluzione di levofloxacina ed analizzati in una regione che va da 220 nm a 500 nm. Il picco di assorbimento maggiore corrisponde alla lunghezza d’onda della sostanza, 289 nm per la levofloxacina, come

mostrato in figure 3.2. A questo punto è stato calcolato il coefficiente costante della legge di Lambert-Beer, partendo da concentrazioni di levofloxacina note, sia per la dissoluzione in acqua milli Q che nella soluzione a pH 1.
È stata studiata la dissoluzione anche di opportune compresse usando il 5% in peso di nanocristalli di cellulosa e il 20% in peso di mannitolo, due degli eccipienti più diffusi. Anche in questo caso entrambe le soluzioni, pH 1 ed acqua milli Q, sono state analizzate.
Questo capitolo termina con la descrizione dei conti eseguiti per valutare i differenti modelli di dissoluzione studiati durante questo lavoro di tesi.

4 Risultati e discussione

Questo capitolo comincia con la figura 4.1 con l'obiettivo di mostrare che si viene a formare una struttura diversa da quella dei reagenti, in quanto non consiste in una semplice sovrapposizione di diffrattogrammi. Le differenze tra strutture solvate e desolvate sono state analizzate per tutti e quattro i cocristalli. Per etanolo e metanolo si registra un leggero cambiamento di struttura dopo il trattamento termico. C'è da dire che specialmente nel caso del metanolo, come mostrato in figura 4.18, non si riesce ad osservare un vero cambiamento in massa, questo perché essendo un solvente con bassa temperatura di ebollizione è facile credere che arrivi ad evaporare completamente già a temperatura ambiente. Le due forme senza solvente sono diverse e per questo motivo denominate LEVOQUE_FORM I, quella ottenuta dalla rimozione dell'etanolo e LEVOQUE_FORM III, quella ottenuta dalla rimozione del metanolo. Interessante è il caso dei cocristalli formati da isopropanolo e 1-propanolo che una volta sottoposti a trattamenti termici conservano la struttura originale ed in particolare risultano isomorfi tra loro, come mostrato in figura 4.17. Per questo la forma ottenuta è denominata LEVOQUE_FORM II. Nel tempo tutte queste forme polimorfiche tendono ad evolvere e trasformarsi in LEVOQUE_FORM II, probabilmente in quanto più stabile. In figura 4.7 uno schema riassuntivo delle forme polimorfiche è stato riportato. Da notare che per forme polimorfiche si intendono le diverse strutture in cui il cocristallo si presenta, private del loro solvente di origine. Durante questo lavoro, a volte, il solvente di origine viene citato per facilitare il lettore nel comprendere l'origine del cocristallo. Tramite la combinazione delle analisi termogravimetriche e della calorimetria a scansione differenziale, sono state individuate le perdite in massa dovute all'evaporazione del solvente, segnando così un passaggio da una forma solvatata ad una senza più solvente. Inoltre,
dalle analisi termiche si sono potuti osservare i fenomeni di fusione e degradazione dei singoli cocristalli. Un cambiamento della stechiometria di reazione è stato effettuato per analizzare se effettivamente si formasse una nuova struttura ordinata o se invece si parlasse di soluzione

solida. I test sono stati condotti con una stechiometria di reazione 1:2 e 1:3 (levofloxacina:quercetina), osservando che il diffrattogramma in entrambi i casi coincide con quello dei cocristalli ottenuti con un rapporto stechiometrico 1:1, più l'eccesso di reagente, in questo caso quercetina. È stato poi mostrato un esempio di nucleazione secondaria, in particolar modo della tecnica del "seeding", in quanto non risultava più possibile ottenere il cocristallo in etanolo, nella sua forma pura. Sono stati studiati gli spettri Raman di quercetina e levofloxacina, analizzando le posizioni dei picchi principali e comparandole con quelle ritrovate negli spettri Raman dei cocristalli. Un cambiamento di posizione che vale la pena di menzionare è quello che si viene a formare a 1625 cm^{-1}, tipico dei legami ammidici o C(O)N, originariamente assente in entrambi i reagenti.

Le misure dell'angolo di contatto sono state applicate per studiare la bagnabilità della superficie dei cocristalli. Bisogna tuttavia considerare che l'angolo di contatto è una proprietà di superficie ed essendo impossibile realizzare tante compresse perfettamente uguali, alcune discordanze nei valori registrati sono possibili da osservare anche nella stessa classe di cocristalli analizzate. Sicuramente si parla di differenze piccole, che non vanno ad inficiare con il comportamento generale dei vari cocristalli. Lo studio dell'angolo di contatto per i cocristalli ottenuti da isopropanolo e 1-propanolo è stato condotto sia per le strutture contenenti ancora il solvente, sia per quelle private dello stesso. Lo scopo di quest'analisi era osservare se si presentasse un comportamento molto diverso, o comunque scostato, tra i due diversi casi. L'origine di questo studio è da attribuirsi alla coincidenza dei diffrattogrammi ottenuti dall'analisi ai raggi X per entrambe le strutture. Si è osservato che in generale i valori di angolo di contatto sono tutti maggiori di 90° per l'acqua, mostrando che i cocristalli hanno una forte tendenza a repellere l'acqua. In linea di massima si osserva una leggera differenza di valori tra i casi con e senza solvente, più facilmente attribuibile alla diversità della superficie e del peso delle compresse, piuttosto che a una differenza di struttura o proprietà chimico-fisiche. Con l'olio di semi di girasole, invece, mostrano una buona affinità arrivando a valori di 20° circa, mostrando una buona bagnabilità. Per lo studio dell'angolo di contatto dei cocristalli ottenuti da metanolo ed etanolo, nessun trattamento in forno è stato ritenuto necessario, in quanto in entrambi i casi si è già precedentemente mostrato quanto fossero volatili, per cui è ragionevole che le strutture fossero già prive di solvente. I valori ottenuti sono in linea con gli altri cocristalli, non mostrando una grande differenza di comportamento. Compresse di levofloxacina sono state realizzate e analizzate nelle stesse condizioni dei cocristalli. è possibile, però, osservare in questo caso una tendenza della levofloxcina ad essere bagnata dall'acqua. Questo mostra che la non bagnabilità della superficie del cocristallo è attribuibile alla presenza della quercetina nella struttura. Con l'olio di semi di girasole i valori di angolo di contatto mostrati dall'analizzatore sono stati

leggermente maggiori, a prova del comportamento superficiale più idrofobico attribuito dalla presenza della quercetina nella struttura.

Test di solubilità sono stati condotti per ottenere dati per gli esperimenti di cristallizzazione e un possibile scale up. Il profilo di solubilità di ogni cocristallo è stato studiato nel rispettivo solvente di cristallizzazione. L'esperimento consiste nel raggiungimento dalla temperatura iniziale di 20°C di una temperatura massima a cui rimanere per mezz'ora, impostata ad hoc per ogni cocristallo, seguita da una fase di raffreddamento fino a 0°C, anche qui temperatura mantenuta per mezz'ora. La velocità di riscaldamento/raffreddamento prevede una velocità di 0.2 °C/min / -0.2 °C/min. Il ciclo si ripete per due volte successive fino al raggiungimento della conclusione dell'esperimento.

La solubilità del cocristallo ottenuto da metanolo è stata studiata in metanolo con una concentrazione che va da 3.91 mg/g a 13.76 mg/g. la temperatura massima raggiunta in questo caso è stata di 52°C per evitare qualsiasi fenomeno di evaporazione del solvente che avrebbe inevitabilmente cambiato la concentrazione.

La solubilità del cocristallo ottenuto da etanolo è stata studiata in etanolo con una concentrazione che va da 2.69 mg/g a 13.69 mg/g. la temperatura massima raggiunta in questo caso è stata di 65°C per evitare qualsiasi fenomeno di evaporazione del solvente che avrebbe inevitabilmente cambiato la concentrazione.

La solubilità del cocristallo ottenuto da 1-propanolo è stata studiata in 1-propanolo con una concentrazione che va da 2.61 mg/g a 11.19 mg/g. la temperatura massima raggiunta in questo caso è stata di 75°C, questo perché il solvente presenta una temperatura di ebollizione maggiore rispetto agli altri due casi.

La solubilità del cocristallo ottenuto da isopropanolo è stata studiata in isopropanolo con una concentrazione che va da 3.69 mg/g a 13.36 mg/g. la massima temperatura raggiunta è stata di 75°C.

In tutti i casi sono stati raccolti i denominati "clear points", ovvero quei punti che corrispondono ad un valore di trasmissività pari al 100% a determinate temperature. Questi punti sono stati approssimati con l'equazione di van't Hoff, successivamente linearizzata. Tutte le figure e le equazioni risultanti sono state riportate in questo lavoro. Di particolare interesse è risultato un paragone effettuato dai differenti valori di entalpia di dissoluzione estrapolati dai coefficienti angolari delle rette delle equazioni linearizzate. Valori più alti di entalpia si traducono in una maggiore richiesta energetica per far avvenire la transizione dallo stato solido a quello disciolto. Di conseguenza, temperature più basse sono associate ad una bassa solubilità, mentre un aumento della temperatura porta ad un aumento

significativo della solubilità per i composti con entalpie di soluzione più elevate. Il valore di entalpia più grande è stato registrato per il cocristallo ottenuto da isopropanolo.
Durante lo studio della solubilità è stato possibile osservare inusuali comportamenti di trasmissività per il cocristallo ottenuto i isopropanolo. Questo accade perché durante il secondo ciclo di temperatura applicato dal sistema, un iniziale incremento di trasmissività è stato registrato, seguito da una repentina diminuzione, il tutto mentre la temperatura stava aumentando. Questo comportamento potrebbe essere attribuito ad una trasformazione polimorfica in una forma meno solubile. È possibile osservare quanto detto in figura 4.23.
Lo studio ha coinvolto la scelta di un opportuno modello di dissoluzione appropriato per descrivere il complesso meccanismo di dissoluzione dei campioni analizzati. L' appendice A è completamente dedicata a questa scelta, mostrando come i modelli comunemente utilizzati come quello di ordine zero, ordine uno o il modello di Higuchi non fossero appropriati. Ragione che ha spinto verso un nuovo modello semi-empirico, precedentemente descritto, chiamato "deceleratory model", basato su un cambiamento delle energie di attivazione durante il processo di dissoluzione che segue la distribuzione di Maxwell-Boltzman. I risultati dei test di dissoluzione vengono poi mostrati sia per le polveri che per le compresse contenenti gli eccipienti. Il rilascio della levofloxacina nella forma del cocristallo è molto più lento rispetto a quella che avviene nella sua forma pura o nella miscela fisica, ottenuta semplicemente mescolando quercetina e levofloxacina. Questo probabilmente è dovuto alla formazione di una nuova struttura che sicuramente rallenta questo processo. Dalle polveri in acqua milli Q non si osserva una significativa differenza nel comportamento dei cocristalli ottenuti dalle 4 differenti classi di solventi. Le polveri analizzate nella soluzione a pH 1 mostrano come la dissoluzione delle polveri sia accentuata ad un pH più acido, opportunamente selezionato per simulare l'effetto all'interno dello stomaco umano. Se prima le polveri di levofloxacina avevano bisogno di 21 ore per raggiungere la dissoluzione completa, adesso ne necessitano solo 7. Questo fenomeno di accelerazione del processo è registrato anche per i cocristalli. il fenomeno è in linea con il calcolo dei coefficienti della legge di Lambert-Beer, in quanto a pH 1 è risultato maggiore. Un andamento simile è stato osservato anche per le compresse contenenti gli eccipienti. In acqua milli Q i valori risultano molto più bassi, mentre sono di gran lunga accelerati nella soluzione a pH1. Lo scopo di questi test era di osservare l'applicabilità in campo farmaceutico di questi cocristalli, permettendo, a seconda del rilascio necessario in campo farmacologico, di decidere a quale formulazione ricorrere.

5 Conclusioni

L'obiettivo di questo lavoro è stato dimostrare come l'ingegneria dei cristalli possa essere utilizzata per creare nuovi composti con diversi benefici aggiuntivi. In particolare, è stata considerata la lotta contro *H. pylori* a partire da uno studio precedente, analizzando il cocristallo generato da una soluzione slurry in etanolo di levofloxacina e quercetina. In questo lavoro, sono stati utilizzati quattro solventi differenti (metanolo, etanolo, 1-propanolo e isopropanolo) in una soluzione slurry con un rapporto stechiometrico dei reagenti di 1:1. Lo scopo era osservare le differenze in termini di proprietà chimico-fisiche e profilo di dissoluzione. Differenti strutture sono state evidenziate attraverso la diffrazione a raggi X su polveri e la spettroscopia Raman, e sono state ulteriormente analizzate mediante calorimetria a scansione differenziale e analisi termogravimetrica. Queste ultime analisi hanno permesso di determinare le strutture desolvate e hanno mostrato la presenza di tre diverse forme polimorfiche. La struttura desolvata formata con etanolo come solvente è stata denominata Forma I, quella con isopropanolo e 1-propanolo Forma II e quella con metanolo Forma III. Nel tempo, tutte queste forme tendono a convertirsi nella Forma II, probabilmente la più stabile. Sono stati utilizzati diversi rapporti stechiometrici per dimostrare come la struttura formata sia regolare e non una soluzione solida. Sono state effettuate misurazioni degli angoli di contatto, dimostrando che la presenza della quercetina nella struttura riduce la bagnabilità con l'acqua e la aumenta con l'olio di girasole rispetto alla levofloxacina pura. Sono stati condotti test di solubilità per ottenere dati utili agli esperimenti di cristallizzazione e alla sintesi su scala maggiore. Il profilo di solubilità di ogni cocristallo è stato studiato nel rispettivo solvente di cristallizzazione. Il valore più alto dell'entalpia di van't Hoff è stato ottenuto da LEVOQUE_IPA in isopropanolo, mentre il più basso da LEVOQUE_MeOH in metanolo, indicando che il primo richiede più energia per passare dallo stato solido a quello disciolto. Sono stati registrati test di dissoluzione sia delle polveri dei cocristalli, sia della miscela fisica che della levofloxacina pura, in acqua milli-Q e in soluzione a pH 1. A pH 1, i profili di dissoluzione risultano più rapidi. Sono stati inoltre registrati test di dissoluzione su tablets con eccipienti come mannitolo e nanocristalli di cellulosa, primo tentativo di una possibile formulazione. L'ingegneria dei cristalli è un potente strumento nel definire formulazioni a rilascio sostenuto, in quanto consente un controllo delle proprietà fisiche del farmaco, come la solubilità e la velocità di dissoluzione.

SUMMURY

List of abbreviations

API: Active Pharmaceutical Ingredients

DSC: Differential Scanning Calorimetry

TGA: Thermogravimetrical Analysis

PXRD: Power X-Ray Diffraction

LEVO: Levofloxacin

QUE: Quercetin

EtOH: Ethanol

MeOH: Methanol

IPA: Isopropanol

1PR: 1-Propanol

CNC: Cellulose nanocrystals

FDA: Food and Drug Administration

LEVOQUE_EtOH: cocrystal of Levofloxacin and Quercetin realized in a slurry solution of Ethanol

LEVOQUE_MeOH: cocrystal of Levofloxacin and Quercetin realized in a slurry solution of Methanol

LEVOQUE_IPA: cocrystal of Levofloxacin and Quercetin realized in a slurry solution of Isopropanol

LEVOQUE_1PR: cocrystal of Levofloxacin and Quercetin realized in a slurry solution of 1-propanol

LEVO+QUE: physical mixture of Levofloxacin and Quercetin

LEVOQUE_FORM I: desolvated cocrystal of Levofloxacin and Quercetin realized in a slurry solution of ethanol

LEVOQUE_FORM II: desolvated cocrystal of Levofloxacin and Quercetin realized in a slurry solution of both 1-propanol and isopropanol.

LEVOQUE_FORM III: desolvated cocrystal of Levofloxacin and Quercetin realized in a slurry solution of methanol.

Index of figures

Index of tables

1 Introduction

1.1 Background: Crystal engineering strategies and pharmaceutical application

Crystal engineering focuses on studying the design and synthesis of solid-state structures with desired properties through the control of intermolecular interactions that occur between molecules within crystalline structures. In the last century crystal engineering gained more attention within the scientific community, due to its many potential applications. Notable among these are the enhancement of the physicochemical properties of drugs, the development of controlled drug release systems, the creation of organic semiconductors, the design of chemical sensors, and the production of controlled-release fertilizers. Engineering crystal structures with tailored properties implies that their design and synthesis is guided by precise control of intermolecular interactions that occur between molecules within crystal lattice. In particular, the pharmaceutical sector finds very promising a specific crystal engineering strategy: the use of cocrystals. Pharmaceutical cocrystals are defined as crystalline structures composed of at least an active pharmaceutical ingredient (API) and one or more partner molecules ,in a stoichiometric ratio, hereinafter referred to as "coformers".

This is essential because it gives the chance to take two or more substances together in the same crystal lattice usually to create a new structure, more stable and efficient or because thanks to the synergic effect that is generated it allows to use a minor concentration of the interested API. Coformers are usually selected from the Generally Regarded As Safe (GRAS) list and they can include vitamins, biomolecules, food additives, minerals and amino acids. There are now some powerful applications where it is possible to find two or more APIs and leading to a "codrug". The reason why crystal engineering is hiring so much potential, and interest is the increase of the antimicrobial resistance which leads to need new solutions. *Helicobacter pylori (H. pylori)* is a Gram-negative pathogen included in 2017 in the first list of antibiotic-resistant priority pathogens by the World Health Organization (WHO) (Gonzá Lez et al., n.d.), reason why Fiore et al. decided to study a new solution to fight this pathogen. They used a crystal engineering approach by combining an antibiotic form fluoroquinolones class (Levofloxacin or Ciprofloxacin) and a flavonoid (Quercetin, Myricetin and Hesperetin), synthetized a slurry

solution with a specific stoichiometric ratio. Particular attention has been dedicated to the antimicrobial activity, showing that the physical mixture and cocrystals show a similar effect but a more powerful one in comparison with the only antibiotic (Fiore et al., 2024). In this work it has been decided to focus on the cocrystal obtained by synthetizing, in a slurry solution with a stoichiometric ratio 1:1, Levofloxacin (LEVO) and Quercetin (QUE). Levofloxacin belongs to the family of Fluoroquinolones able to block the bacterial activity targeting two essential enzymes: DNA gyrase and Topoisomerase IV, resulting effective against both Gram-negative and Gram-positive bacteria. Quercetin belongs to the family of flavonoids, and it can be found in several vegetables, seeds and fruits and possesses many pharmacological activities such antioxidant, antimicrobial, anticancer and anti-inflammatory.

1.2 Aim and structure of the thesis

The aim of this thesis was the synthesis and characterization of Levofloxacin and Quercetin cocrystals obtained applying the crystal engineering strategy afore mentioned, the so called cocrystalliazion. Some preliminary tests to assess functional properties of these materials were also performed (e.g. dissolution rate experiments and solubility curves).

This thesis work is composed of five chapters. The content is shown below:

- *Chapter 2* provides a theoretical overview on crystal engineering, the reactants involved – levofloxacin and quercetin- , the analytical methodologies applied, such as X-ray diffraction and Raman spectroscopy for structural characterization, Differential scanning calorimetry and thermogravimetric analysis for the study of solvent loss in the cocrystal structures and the temperature at which this occurs. It contains the description of the contact angle theory, Lambert-Beer's law and the main dissolution models used for pharmaceutical ingredients.
- *Chapter 3* describes the materials, the equipment used and the performed methods.
- *Chapter 4* is dedicated to the results obtained in this work.
- *Chapter 5* concludes the thesis.
- Appendix A shows the trial with different dissolution models, to better understand the model's choice of this work.
- Appendix B contains contact angle images.

2 Theoretical overview

2.1 Cocrystals

The field of crystal engineering emerged in the mid-20th century as a response to the growing interest in understanding and manipulating the crystalline structures of organic and inorganic compounds. Fare clic o toccare qui per immettere il testo.

In 1989 Desiraju defined the crystal engineering as "*the understanding of intermolecular interactions in the context of crystal packing and the utilization of such understanding in the design of new solids with desired physical and chemical properties*." (Rissanen, 2021)

The concept of supramolecular synthons was introduced in 1995, and this was followed by the exploration of heterosynthons and their potential applications in the design of pharmaceutical cocrystals in 2004.

Today, crystal engineering encompasses a wide range of research areas, including the design of pharmaceutical crystals for enhanced drug delivery, the development of new materials with desired physical properties, and the creation of functional molecular assemblies for various technological applications.

The Food and Drug Administration (FDA) defined cocrystals as *"crystalline materials composed of two or more different molecules, typically active pharmaceutical ingredient (API) and cocrystal formers ("coformers"), in the same crystal lattice"*. (Fda et al., 2018)

Cocrystals are distinguished from salts by the fact that, unlike salts, the components coexisting in the cocrystal lattice with a specific stoichiometry interact through nonionic interactions. Furthermore, cocrystals differ from polymorphs, which encompass various forms including single-component crystalline structures with different molecular arrangements or conformations in the lattice, amorphous forms, and multicomponent phases such as solvates and hydrates.

Instead, cocrystals bear more resemblance to solvates, as both contain multiple components within the lattice. From a physical chemistry and regulatory standpoint, cocrystals can be seen as a specialized category of solvates and hydrates, where the second component (the coformer) is not a solvent (including water) and is typically nonvolatile.

There are two main classifications of cocrystals: ionic cocrystals (or charge-assisted) and molecular cocrystals, each with important distinctions. (Kavanagh et al., 2019)

Molecular Cocrystals: Molecular cocrystals consist of two components held together in a definite stoichiometric ratio through non-covalent interactions — typically in the pharmaceutical field, a biologically active molecular compound and a pharmaceutically acceptable molecular coformer.

Ionic Cocrystals: Ionic cocrystals are more complex, as they involve at least three moieties: an anion, a cation, and a neutral component, with one of these being biologically active. This additional complexity results in a significantly larger range of possible compositions and a higher likelihood of discovering a solid form with desirable properties.

Based on the information provided, it can be argued that cocrystals represent a promising pathway towards developing new and improved medicines, offering a potentially low-risk and cost-effective approach with high rewards. Essentially, cocrystals provide a method to manipulate the physicochemical properties of a medicine by incorporating a suitable coformer; for instance, improving the solubility of poorly water-soluble drugs or enhancing the compressibility and tabletability of drugs.

Ideal coformers should possess several key characteristics to optimize their effectiveness in cocrystal formation. They should be affordable, pharmaceutically acceptable, possess low molecular weight, and feature multiple binding sites for the active pharmaceutical ingredient (API), allowing for strong intermolecular interactions. These attributes enable coformers to play a critical role in the development of stable and effective cocrystals that can enhance the overall performance and properties of medicinal formulations.

Ionic cocrystals are stabilized by charge-assisted supramolecular synthons, which are less susceptible to solvent effects and more likely to exhibit substantial variations in properties. This characteristic makes them potentially valuable in pharmaceutical applications.

2.2 Crystal nucleation and growth

Nucleation and crystal growth are rate-dependent processes, driven by the level of supersaturation. As supersaturation increases, so does the nucleation rate, which serves as the driving force for the process. However, nucleation becomes significant only when supersaturation. Surpasses a certain threshold. To explain this, Wilhelm Ostwald divided the supersaturation region into two zones: the labile zone and the metastable zone (Dai et al., 2017). The solubility curve, shown in figure 2.1, primarily depends on temperature but is also influenced by impurities or additives in the solution. This curve offers crucial insights into the crystallization process, as solubility refers to the maximum amount of solute that can dissolve in a certain amount of solvent under specific conditions.

Below the solubility curve the solution is stable and undersaturated, meaning crystals cannot exist. Above the super-solubility curve lies the labile zone, where the solution is unstable and supersaturated, allowing both nucleation and crystal growth. In the metastable zone crystals can only grow. Operating within the metastable zone is crucial for obtaining high-quality crystals with a more uniform size distribution.

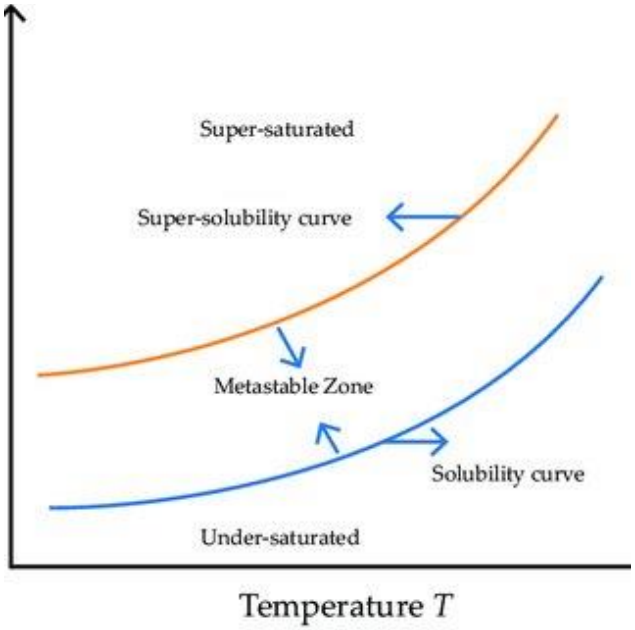

Figure 2. 1 Solubility curve and the presence of metastable and labile zones. (Dai et al., 2017)

There are two types of nucleation: Primary and secondary nucleation.

Primary nucleation can be defined as the formation of a new particle from molecules dissolved in the continuous phase. It occurs in two primary forms:

1. Homogeneous nucleation: This process is initiated solely by supersaturation.
2. Heterogeneous nucleation: Occurs with the assistance of foreign solid surfaces (impurities, dust, contaminants) which facilitate nucleation.

According to the classical nucleation theory it is possible to describe the nucleation process by examining the total Gibbs free energy of a particle (ΔG), which comprises two components: volume energy and surface energy. It can be written, for a spherical particle of radius r, as follows.

$$\Delta G = \Delta g_v \cdot \frac{4}{3}\pi r^3 + \gamma \cdot 4\pi r^2 \quad (2.\ 1)$$

The volume energy (Δg_v)is consistently negative and proportional to the cube of the particle's radius (r), whereas the surface energy (γ) is always positive and proportional to

the square of the radius. Consequently, there exists a critical radius where the total free energy reaches its maximum value.

$$r_{crit} = \frac{-2\gamma}{\Delta g_v} \tag{2. 2}$$

This critical radius (r_{crit}) defines the point at which the particle is thermodynamically favored to increase in size. A nucleus is thus defined as the smallest particle in the continuous phase with a radius greater than this critical value. (Thanh et al., 2014)

The energy barrier for heterogeneous nucleation is always smaller than the homogeneous one. They are correlated thanks to a factor based on the contact angle formed between the surface of the solid substrate and the edge of the droplet or the crystalline nucleus that is forming on the surface. Generally, it is possible to describe three situations for the energy barrier for heterogenous nucleation in comparison to the homogeneous one, looking at the contact angle (ϑ):

- $\vartheta = 0°$: there is no energy barrier.
- $0° < \vartheta < 180°$: the energy barrier is smaller than homogeneous nucleation.
- $\vartheta = 180°$: the foreign solid has not effect, so the nucleation is homogeneous.

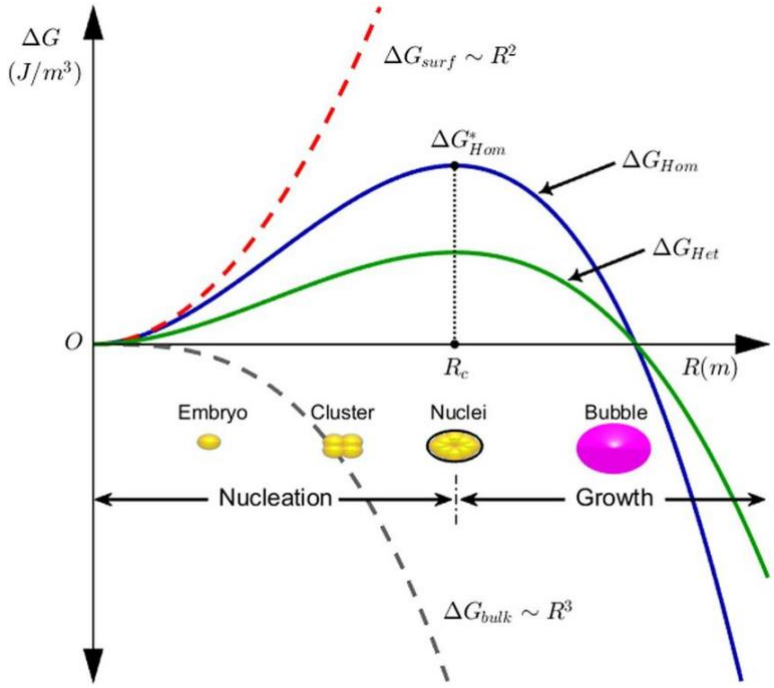

Figure 2. 2: Difference between homogeneous and heterogenous nucleation.(Gibbs Free Energy Change during Bubble Nucleation. The Surface Free... | Download Scientific Diagram, n.d.)

Crystal growth is the process by which a crystal increases in size. This occurs when material from a solution phase deposits onto the surface of an existing crystal, following the geometry of the crystal lattice. The growth of a particle involves two stages: first, a diffusion step where solute is transported from the bulk fluid through the solution's boundary layer near the crystal surface; and second, a deposition step where the solute ions or molecules adsorbed on the crystal surface are incorporated into the crystal lattice (Ray, 2023). it is possible to describe the two stages:

$$\frac{dm}{dt} = k_d\, A\, (c - c_i) = k_r\, A\, (c_i - c^*)^i \tag{2. 3}$$

Where k_d and $k_r$are mass transfer coefficients, A is the crystal surface, m is the mass deposited in time t, i is the order of integration and c^*, c_i and c are the solute concentrations at equilibrium saturation, at the interface and in the bulk solution.

The equation can be written as follows:

$$\frac{dm}{dt} = k_G\, (c - c^*)^s \tag{2. 4}$$

Where k_G is an overall crystal growth coefficient. The overall resistance $1/k_G$ can be seen as the sum of the diffusion resistance $1/k_d$ and the reaction resistance $1/k_r$.

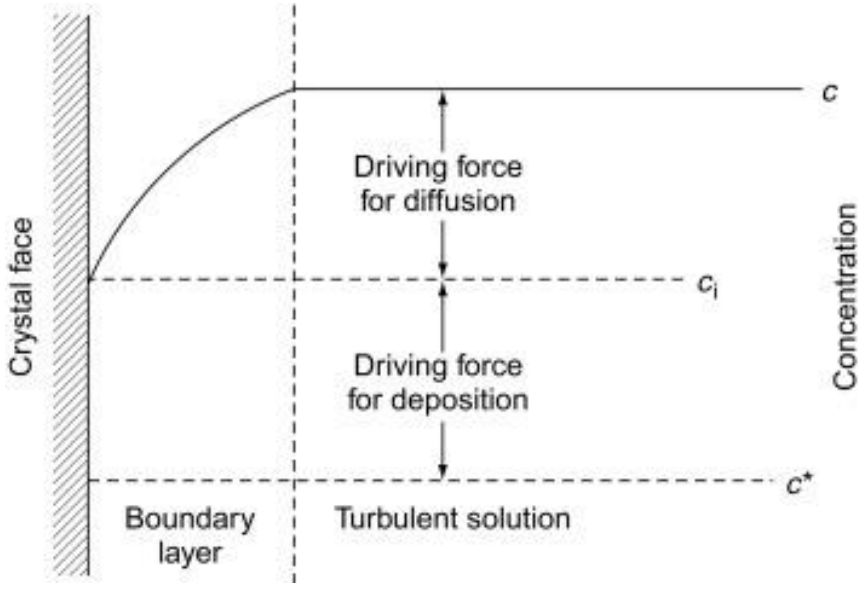

Figure 2. 3Concentration profile near the crystal surface. (Ray, 2023)

Seeding techniques involve introducing a pre-formed crystal surface onto which additional molecules can orderly aggregate, typically at a lower level of supersaturation than required for spontaneous nucleation. A seed acts as a template for molecules to assemble into crystals

with the same characteristics as the original crystal. Seeding methods are categorized into microseeding, which entails transferring microscopic crystals from a seed source to a solution without existing nuclei, and macroseeding, where pre-grown crystals are individually added to a solution already at equilibrium. The latter method enables the production of larger crystals (Stura & Wilson, 1990). In summary, seeding is a technique that facilitates the nucleation and growth of a specific crystal by introducing pre-formed seeds, leading to more controlled and efficient crystal formation.

Secondary nucleation refers to the creation of new nuclei from existing crystals, rather than from a supersaturated solution without any pre-existing crystal. It typically happens when crystal growth causes disturbances, such as collisions between crystals or shear forces in solution, leading to the creation of new nucleation sites.

2.3 Methods

Several methods have been implemented for the preparation of cocrystals and they can be divided in solution-based method (Solvent evaporation, cooling crystallization, Slurry conversion) and solid-based methods (Neat grinding, Liquid-assisted grinding,). (Guo et al., 2021; Pawar et al., 2021)

2.3.1 Solution-based methods:

In the solution-based methods it is essential to achieve cocrystal supersaturation while ensuring saturation or undersaturation of the reactants. It is important to delineate conditions for thermodynamic stability, ensuring that the cocrystals remains within a stable region, thereby preventing the crystallization of pure reactants. Therefore, it is crucial to define a three-phase diagram, which guarantees that the cocrystal stays in the thermodynamically stable region, avoiding crystallization of pure reactants.

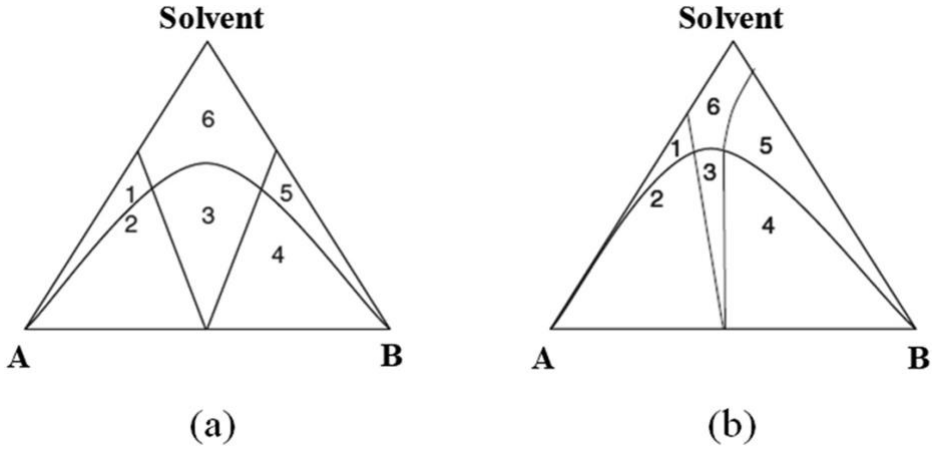

Figure 2. 4Isothermal ternary phase diagram of a cocrystal: (a) similar solubilities of the API and coformer in solvent; (b) different solubilities of the API and coformer in solvent; 1: A and solvent; 2: A and cocrystal; 3: cocrystal; 4: mixture of B and cocrystal; 5: B and solvent and 6: solution. (Guo et al., 2021)

Solution-based cocrystallization offers enhanced control and regulation of crystal properties, as well as achieving high final purity levels. Another notable benefit is its relatively straightforward scalability for large-scale industrial production of cocrystals, whether in batch or continuous operations.

- Solvent evaporation:

Several parameters influence the outcome of this method, such as temperature and evaporation rate. It's crucial to accurately determine the evaporation temperature using phase diagrams to prevent the crystallization of pure coformers. Additionally, the evaporation rate is critical, as the process duration can range from minutes to weeks.

The choice of solvent is also vital, as it impacts the solubility of the reactants. Although solvent evaporation is primarily utilized in laboratory settings or during screening processes, it is less common in industrial-scale production.

This is one of the most common methods for cocrystal formation. In this process, the cocrystal components dissolve in a suitable solvent, which subsequently evaporates. As the solvent evaporates, supersaturation occurs, leading to cocrystal nucleation and growth. While this method is straightforward and effective, it can result in undesired solvate formation or crystallization of the pure components, necessitating routine analysis and control.

- Cooling cocrystallization:

In contrast to solvent evaporation, where supersaturation is achieved through the evaporation of the solvent, this method relies on achieving supersaturation through temperature reduction. The reactants are brought into contact with a compatible solvent, forming an undersaturated solution. As temperature decreases, solubility typically decreases, leading to the precipitation of excess solute and the formation of crystals as the solution becomes supersaturated.

It's crucial to control parameters such as mass and heat transfer because crystal properties—such as size, morphology, and purity—are influenced by the degree of supersaturation determined by these factors. Cooling cocrystallization, as solvent evaporation, is more intricate than single-solute crystallization; determining the operational conditions requires a study of the stability of all crystal forms.

Cooling crystallization has been extensively employed on an industrial scale for numerous organic molecules in the pharmaceutical industries.

- Slurry cocrystallization:

The process commences with the suspension of one or both conformer crystals in a minimal amount of solvent, resulting in the formation of a slurry. It is essential to ascertain the stoichiometric ratio and maintain it for a predetermined duration. Noteworthy is the method's requirement of minimal solvent quantities and its focus on the crystallization of pure cocrystals.

During the slurry phase, each component gradually dissolves, leading to the formation of a complex that facilitates the nucleation and growth of cocrystals. Slurry cocrystallization serves as both a screening and production technique for cocrystals.

2.3.2 Solid-based methods:

While these methods necessitate only a small amount of solvent, they do require a significant input of either thermal or mechanical energy. Typically, additional treatments are required for cocrystal purification following these methods. (Guo et al., 2021)

- Neat grinding:

This method eliminates the need for a solvent, relying solely on mechanical or manual energy. Through grinding, a mobile solid surface is generated, facilitating gas diffusion and enabling the formation of cocrystals. The reactants are intricately combined via the application of pressure.

- Liquid-asisted grinding:

In this context, molecular diffusion is facilitated by the introduction of a small quantity of liquid, serving as a catalyst to expedite cocrystal formation. The choice and quantity of the liquid are pivotal because of the influence in the formation of various solid products and the crystal quality.

2.4 Reactants

The first quinolone to hit the market was derived from an isolate found in the preparation of chloroquine, exhibiting promising antibacterial properties. However, its efficacy was slowed down by poor oral absorption and limited activity against Gram-negative bacteria. Subsequent modifications, notably the addition of a piperazine ring, bolstered its effectiveness against both Gram-negative and Gram-positive species by enhancing penetration of the bacterial cell wall. Flumequine marked a pivotal advancement by introducing a fluoro-group at position 6, leading to significant efficacy against Gram-positive bacteria.(Appelbaum & Hunter, 2000)

However, the true improvement arrived with norfloxacin, which combined these advantageous features, resulting in a potent antimicrobial agent. Following its success, a plethora of fluoroquinolones were developed, showing improved gastrointestinal absorption, and enabling their use in systemic infections. Fluoroquinolones block the bacterial activity targeting two essential enzymes: DNA gyrase and Topoisomerase IV. (Drlica, 1999)

Levofloxacin stands as a potent fluoroquinolone antibiotic, representing the L-isomer of oflaxicin. Initially patented in 1985 by Daiichi Seiyaku Pharmaceutical Co.Ltd in Japan, it entered the human pharmaceutical market in 1993 (Sitovs et al., 2021). Notably, its rapid extensive penetration into bodily tissues and fluids following oral administration underscores its therapeutic efficacy against a broad spectrum of infections.

Distinguished by its enhanced pharmacological profile, oral levofloxacin demonstrates comparable antibacterial effectiveness to ofloxacin at half the daily dosage, thereby

minimizing toxicity risks. Further setting it apart, levofloxacin exhibits light sensitivity, a yellow-white coloration, odorless nature, slightly acidic and profoundly lipophilic properties.

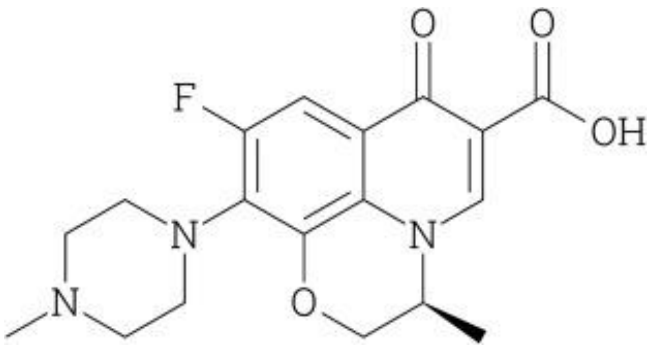

Figure 2. 5: Levofloxacin' structure. (Sitovs et al., 2021)

Flavonoids, a diverse group of natural compounds boasting varied phenolic structures, are abundant in fruits, vegetables, grains, bark, roots, stems, flowers, tea, and wine. In contemporary times, their significance extends to pharmaceutical, nutraceutical, and cosmetic realms. Renowned for their antioxidative, anti-inflammatory, anti-mutagenic, and anti-carcinogenic attributes, flavonoids also excel in modulating crucial cellular enzyme functions. Their impact spans across the biological spectrum, influencing plants, animals, and bacteria alike.

In the botanical realm, flavonoids contribute to the vibrant hues and fragrances of flowers, while in fruits, they entice pollinators, facilitating spore germination. This multifaceted group comprises various classes such as anthocyanis, flavones, flavonols, flavonones, isoflavonoids, and chalcones. (Panche et al., 2016)

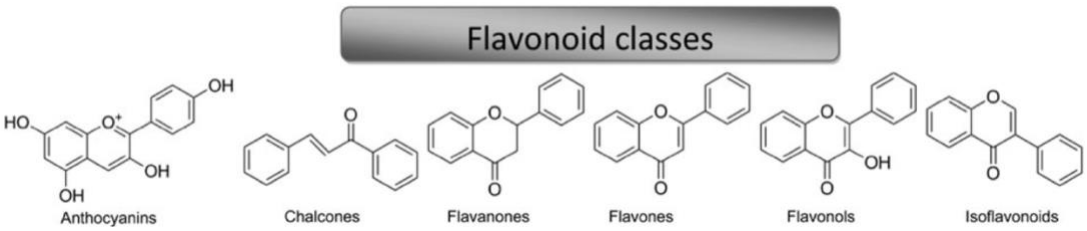

Figure 2. 6: Flavonoid classes. (Panche et al., 2016)

The term "quercetin" finds its roots in the Latin word "quercetum," which translates to Oak Forest. Interestingly, this compound cannot be synthesized within the human body.(Victor et al., 2016)

Quercetin belongs to the flavonol class, one of the six flavonoid compounds. It manifests as brilliant citron-yellow needle crystals, insoluble in cold water, sparingly soluble in hot water, yet soluble in alcohol and lipids. Its limited solubility presents a challenge, leading to low oral bioavailability. Consequently, novel strategies like cocrystallization are being explored to enhance its absorption.

In response to harmful stimuli, the body initiates inflammation as a protective mechanism. Quercetin demonstrates remarkable abilities to modulate inflammation. Like other flavonoids, quercetin showcases a broad spectrum of biological activities, potentially beneficial for cardiovascular health. It inhibits platelet aggregation, enhances endothelial function, and reduces the risk of mortality linked to low-density protein. Moreover, quercetin mitigates cardiac hypertrophy by reducing blood pressure through vasorelaxant properties.

Beyond cardiovascular health, quercetin holds promise in modulating neuronal function, potentially mitigating age-related neurodegeneration. Its potent anticarcinogenic properties, acting as an apoptosis inducer, impede tumor growth and malignant cell spread. Studies suggest quercetin's efficacy in inhibiting gastric acid secretion and gastric cell lipid peroxidation, indicating gastroprotective potential.

Furthermore, quercetin exhibits antibacterial effects against various strains, notably targeting gastrointestinal, respiratory, urinary, and dermal systems. Its anti-infective and antireplicative properties might contribute to its antiviral characteristics. Notably, quercetin also exerts anti-allergy effects by inhibiting histamine release from mast cells, acting akin to a natural antihistamine. (Y. Li et al., n.d.)

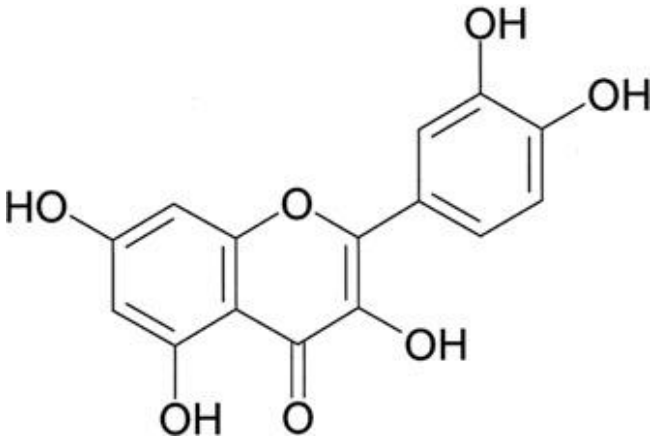

Figure 2. 7: Quercetin' structure.(Wu et al., 2003)

2.5 Contact angle

For a gas-liquid-solid contact line the contact angle is the angle drawn in the liquid phase, which is made between the solid surface and the tangent to the liquid-gas surface. This phenomenon occurs when a liquid droplet is placed on a solid material. Due to the interplay of surface tension and the attraction between the liquid and the surface, the liquid adopts a domed shape. This angle is used to quantify the wettability of a material. In thermodynamic equilibrium the contact angle is related to the interfacial energies, thanks to Young's equation. For a given system of solid, liquid and gas, at specific temperature and pressure, has a unique equilibrium contact angle.

$$cos\theta_c = \frac{Y_{SG} - Y_{SL}}{Y_{LG}} \quad (2.\ 5)$$

Where:

- θ_c is the contact angle.
- Y_{SG} is the solid-gas interfacial energy.
- Y_{LG} is the liquid-gas interfacial energy.
- $Y_{SL}$is the liquid-solid interfacial energy.

Notably, under ideal conditions of perfect smoothness and homogeneity of the surface, the contact angle becomes a thermodynamic state variable, independent of system size or geometry.

For a gas-liquid-solid interface, the contact angle defines the angle formed within the liquid phase, between the solid surface and the tangent to the liquid-gas interface, as illustrated in Figure 2.8 (Kwok & Neumann, 1999)

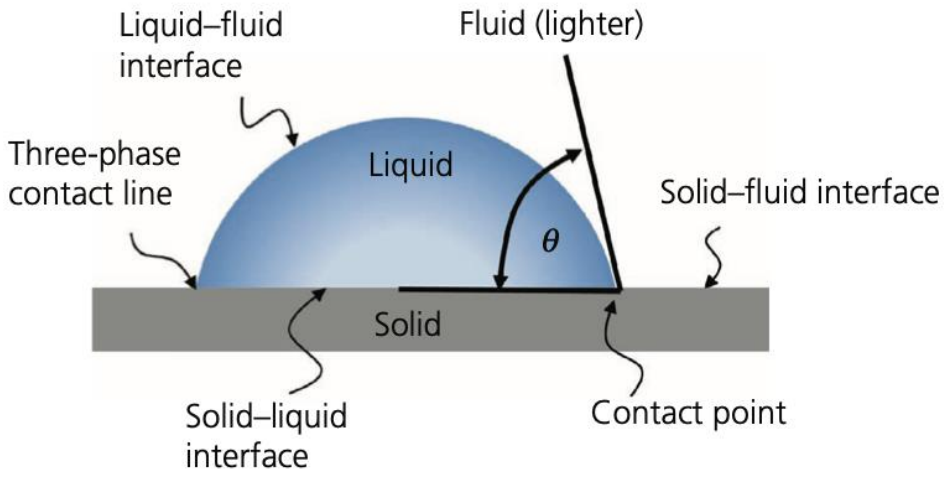

Figure 2. 8: Contact angle representation. (Marmur et al., 2017)

Young's equation retains its validity even when the gas phase is replaced with a second immiscible liquid.

Wettability of a surface is characterized by the contact angle, distinguishing between scenarios where the liquid wets the solid and where it does not (as shown in *figure 2.9*):

- $\theta_c = 0°$: perfect wetting, the liquid spreads entirely over the solid surface without achieving equilibrium.
- $0° < \theta_c < 90°$: High wetting.
- $90° < \theta_c < 180°$: low wetting.
- $\theta_c = 180°$: non-wetting.

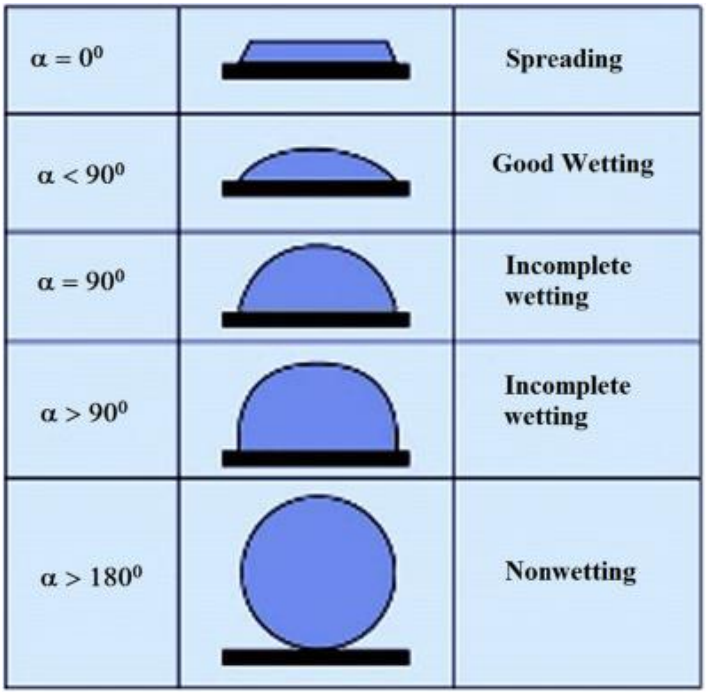

Figure 2. 9: Different values of contact angle. (Giridhar et al., 2017)

However, the theoretical framework of Young's equation presupposes an ideally smooth surface, a condition often unattainable due to factors like surface roughness or heterogeneity. Introducing micro-roughness, typically on the scale up to 20 nm, necessitates modification of Young's equation by incorporating a roughness factor, defined as the ratio between real and perfectly smooth surface areas. Surface roughening accentuates surface properties based on the initial wetting behavior. If the surface was already wet by the liquid the wettability increases, otherwise decreases. Most of the surfaces do not possess ideal symmetry, so they should be considered as three-dimensional systems. In this situation the apparent contact angle could vary from point to point.(Wolansky & Marmur, 1999)
When the heterogeneities exceed a few microns, achieving thermodynamic equilibrium becomes impractical due to barriers encountered. Consequently, the contact angle manifests different values:

- θ_{ad}: the angle measured just before the advancement of the contact line.
- θ_{rec}: the angle measured just before the receding of the contact line.

The disparity between these angles defines the hysteresis associated with the system.(Butt et al., 2022)

2.6 Analytical techniques:

Various techniques were employed in this study to gather information on the different cocrystals formed. The following sections provide a brief overview of these techniques.

- X-ray diffraction:

X-ray diffraction (XRD) is a non-invasive technique used to examine a wide variety of materials. Since X-rays have wavelengths comparable to atomic sizes, the intensities and patterns of X-ray diffraction are utilized to obtain information about atomic structures. XRD helps in examining and characterizing the positions of atoms, their arrangement within each unit cell, and the spacing between atomic planes. When X-rays strike solid materials, they are scattered by the electrons orbiting the atomic nuclei. These scattered waves, emitted in various directions, can interfere constructively or destructively. Diffraction occurs when the interference is constructive. There is a relationship between periodicity and diffraction: longer periodicities result in lower diffraction angles, and shorter periodicities result in higher diffraction angles. Amorphous materials, lacking a periodic arrangement, display only a broad peak at a certain diffraction angle on the XRD graph. In contrast, crystalline materials exhibit multiple peaks corresponding to their periodic atomic arrangement.(Ali et al., 2022)

Bragg's law relates the wavelength of the radiation to the diffraction angle and the lattice spacing in a crystalline sample.

Figure 2.10 illustrates a beam of parallel X-rays penetrating a set of parallel lattice plans spaced at a distance d and with an angle of incidence θ.

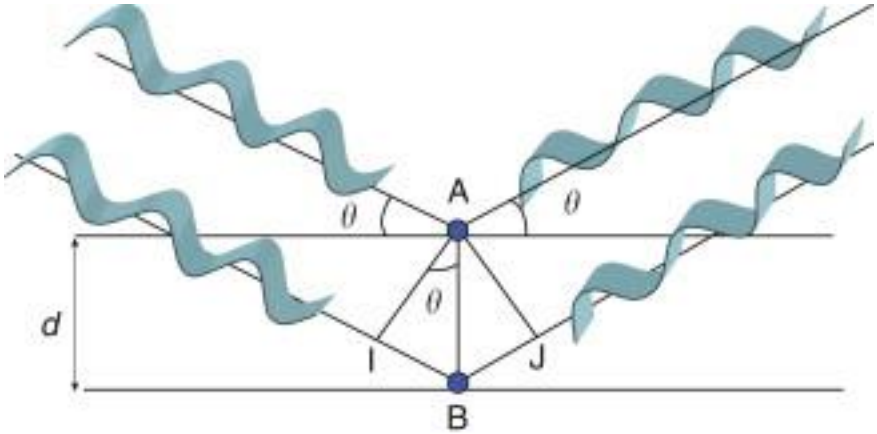

Figure 2. 10: X-ray diffraction following Bragg's law.(Le Pevelen, 2010)

Bragg's law is here reported:

$$n\lambda = 2d\ sin\theta \tag{2. 6}$$

Where d is the spacing between atomic plates, λ characterizes the X-ray wavelength, θ indicates the diffraction beam angle and n denotes the order of diffraction.

An X-ray diffraction instrument typically consists of three main components: an X-ray source, a sample holder and a detector. The X-rays generated by the source strike the sample and then they are diffracted to finally enter in the detector. In powder X-ray diffraction (PXRD) the diffraction pattern is obtained from a powdered sample of the material, rather than from an individual crystal. A powder diffractogram displays the scattered intensity versus the Bragg angle (2θ). It contains several peaks characterized by their intensity, profile and position. Because of all orientations are present, due to the random disposition of the small crystals with respect to each other, it is only necessary to vary the angle of incidence and the angle of diffraction. This allows for the recording of diffraction data over a range of 2θ values. Phase identification is achieved by converting the diffraction peaks to d -spacings and comparing them with standard reference patterns(Bunaciu et al., 2015). During this work PXRD was useful to identify the different cocrystal structures and to allow a direct comparison between them.

- Raman Spectroscopy:

Various spectroscopic methods have been utilized to characterize samples, all relying on phenomena such as emission, absorption, fluorescence, or scattering. Raman spectroscopy, a non-destructive vibrational spectroscopy technique, is used to obtain molecule-specific information. In Raman spectroscopy, a sample is exposed to photons from a monochromatic laser beam, resulting in scattered photons. Two scenarios can arise from the scattered light:

- Inelastic scattering: The scattered light differs in color, frequency, and wavelength from the incident light due to energy transfer between the molecule and scattered photons. If the frequency of the scattered light is lower than that of the incident light, indicating that the

sample has gained energy, this is referred to as "Stokes-Raman scattering." Conversely, if the frequency is higher, it is called "anti-Stokes Raman scattering".

- Elastic scattering: The scattered light retains the same frequency, wavelength, and color as the original light. (Mulvaney & Keating, 2000)

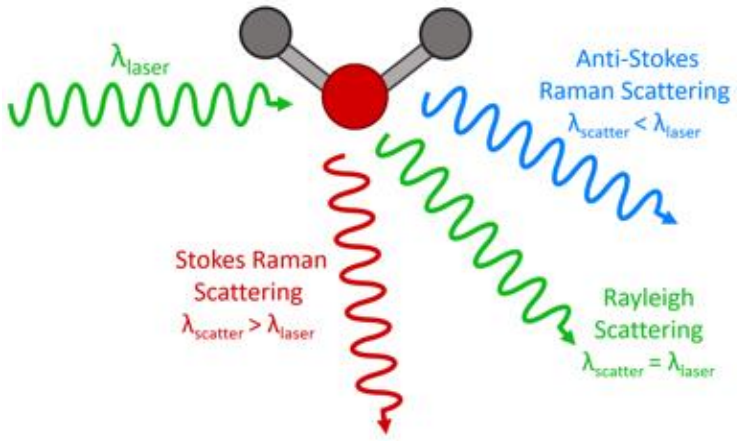

Figure 2. 11: Different scattering processes. (Smith & Dent, 2019)

When a monochromatic radiation hits a sample, it scatters in all directions after interacting with the sample's molecules. Most of the scattered radiation has a frequency equal to the incident radiation (elastic scattering), while only a small fraction causes inelastic scattering. The wavelength shift of the scattered light depends on the chemical composition of the scattering molecules. The molecular vibrations, which displace atoms from their equilibrium positions, cause changes in molecular polarizability, and the Raman scattering intensity is proportional to these changes. These molecular vibrations correspond to specific frequencies and depends on the type of bond involved.

A Raman spectrometer consists of a sample holder, a light source, monochromator and a detector. The light source, with specific frequency and wavelength, strikes the sample, causing molecular vibrations and subsequent Raman scattering. The scattered light is collected by the detector to determine its frequency. A Raman spectrum is presented as an intensity-versus-wavelength shift graph, with the wavelength shift measured in reciprocal centimeters (cm^{-1}). Since different molecules will absorb different frequencies of light due to their unique bonds and vibration frequencies, each molecule has a distinct Raman spectrum. This technique can be used to detect impurities in the sample or to identify a

material (Bumbrah & Sharma, 2016). Raman spectroscopy allowed to characterize the principal peaks of the cocrystals and to identify the presence of new intermolecular interactions by a direct comparison with the reactants.

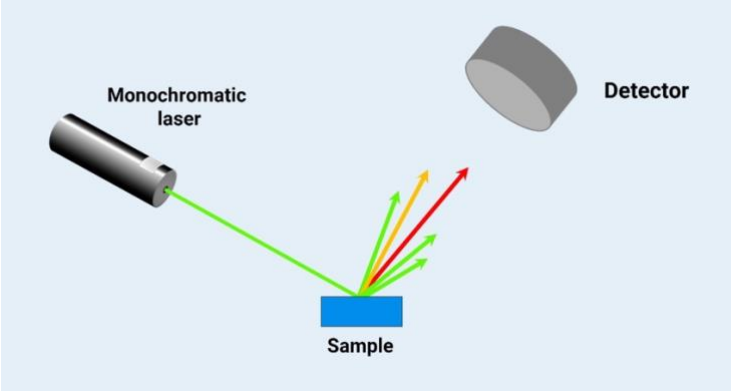

Figure 2. 12: Operating principle of Raman spectroscopy. *(*Guide to Raman Spectroscopy | Bruker*, n.d.)*

- Thermogravimetric analysis:

Thermogravimetric analysis (TGA) is a thermal analysis technique used to study changes in the physical or chemical properties of a sample in response to a controlled temperature program. The analysis is conducted within a closed furnace equipped with an analyzer that contains a highly sensitive microbalance. This microbalance is sensitive to physical phenomena such as decomposition, degradation, oxidation, and surface adsorption.

A controlled atmosphere is maintained during the analysis using a purge gas, typically nitrogen, which enters through a capillary tube at the bottom of the furnace and exits from the top. Additionally, the sample pan is isolated from the heating and cooling elements by a protective tube, ensuring accurate measurements.(Saadatkhah et al., 2019)

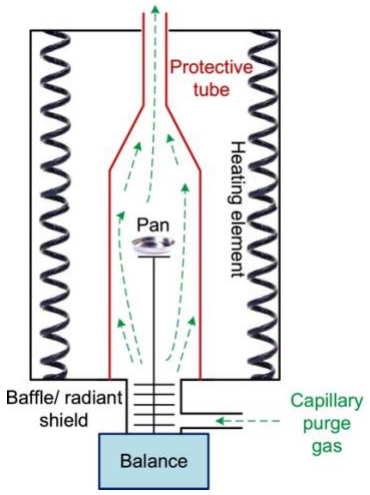

Figure 2. 13: representation of the TGA instrument. (Saadatkhah et al., 2019)

The results of a thermogravimetric analysis are displayed in a thermogram, which is a graphical representation showing the sample's mass change (y-axis) against the temperature program or the time during which the analysis is conducted (x-axis). Each material exhibits unique thermograms depending on its properties and the specific temperature program used.

Typically, mass loss below 150°C is attributed to the loss of physisorbed water or low molecular weight volatile compounds. As the temperature increases to around 250°C, chemisorbed water is removed. Further temperature increases lead to the decomposition of the material or the formation of ash in non-volatile inorganic substances.

A limitation of this technique is that it does not reveal the mechanisms of degradation, only the degradation temperature. Additionally, state transitions cannot be observed in a thermogram obtained with TGA, as these transitions do not involve a change in mass. Therefore, TGA is often coupled with differential scanning calorimetry (DSC) to provide a more comprehensive analysis (Mansfield et al., n.d.). The combination of these two techniques enabled the study of solvent loss in the cocrystal structures and allowed for the determination of the temperature at which this occurs, along with the associated degradation phenomena.

- Differential Scanning Calorimetry:

Differential Scanning Calorimetry (DSC) is another thermal analysis technique commonly used to characterize polymers, pharmaceuticals, glass, and ceramic materials. DSC is

typically employed to identify melting, crystallization, and glass transition temperatures, as well as the associated changes in enthalpy and entropy. It is particularly useful for determining the heat capacity of materials, facilitating the characterization of their thermodynamic properties.

A differential scanning calorimeter consists of two identical sample positions: one for the sample being analyzed and the other for a reference sample. This setup enables the identification of thermal events specific to the sample. The temperature is controlled by a heat reservoir, and two thermocouples connected in series measure the temperature difference between the sample and the reference. This configuration allows for the determination of the difference in heat flow between the sample and the reference.

Since the heat flow is not an absolute value, the presence of a reference is essential for accurate measurements. (Kodal et al., 2019)

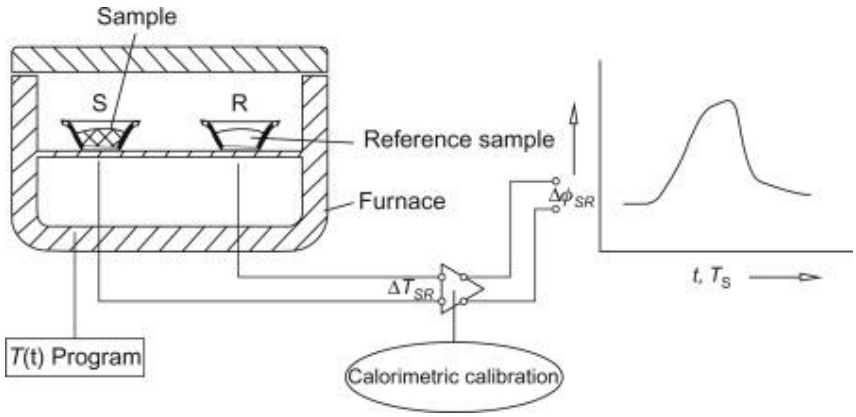

Figure 2. 14: Working principle of a differential scanning calorimeter. (Kodal et al., 2019)

A typical graph obtained by a DSC is composed by the difference of heat flow between the sample and the reference (y-axis) versus temperature or time (x-axis). During this analysis it is common to see some peaks arise due to the transitions of the material. These transitions can be exothermic or endothermic, depending on the direction of the peak. It is possible to calculate the enthalpy by integrating the area subtended by the peak and multiplying by a calorimetric constant.

A typical graph obtained from DSC displays the difference in heat flow between the sample and the reference (y-axis) plotted against temperature or time (x-axis). During the analysis, peaks commonly appear, indicating material transitions. These transitions can be either exothermic or endothermic, depending on the direction of the peak.

The enthalpy change associated with these transitions can be calculated by integrating the area under the peak and multiplying it by a calorimetric constant.(Spink, 2008)

2.7 Lambert-Beer law:

The Lambert-Beer law states that, under ideal conditions, the absorbance of a solution containing an absorbing substance is directly proportional to the substance's concentration. (Mosorov, 2017). This means that as the concentration of the absorbing substance increases, the absorbance also increases, because a more concentrated solution absorbs more light than a diluted one.

A spectrophotometer is the instrument used to measure absorbance by assessing the intensity of light, defined as the number of photons, passing through the solution at a specific wavelength. It measures the intensity of the incoming light (I_0) and the outgoing light (I). The ratio of these two values is called transmittance (T), which represents the fraction of photons passing through the solution. Absorbance (A) is then calculated from transmittance using the following formula:

$$A = -log_{10}(T) \tag{2. 7}$$

This formula quantifies the amount of light absorbed by the solution.

When light of an appropriate wavelength encounters the solution, a highly concentrated solution will typically show high absorbance and low transmittance, while a diluted solution will show the opposite. This proportional relationship between concentration and absorbance allows for the determination of a solution's concentration based on its absorbance.(Delgado, 2022)

Additionally, absorbance is dependent not only on the concentration but also on the path length (L) of the light through the solution. Given these factors, the Lambert-Beer law can be expressed as:

$$A = \varepsilon \cdot L \cdot c \tag{2.8}$$

Where:

- A is the absorbance of the substance.
- ε is the proportionality constant.
- L is the path length of the light.
- c is the concentration of the absorbing species in the solution.

2.8 Dissolution models

Understanding the dissolution behavior of a pharmaceutical product is essential, as only dissolved drug molecules, ions, or atoms can diffuse within the human body (Siepmann & Siepmann, 2013) . This section provides an overview of the primary diffusion models:

2.10.1 Zero order kinetics:

This model applies to drug dissolution from dosage forms that do not disintegrate and release the drug in a controlled manner. The equation is expressed as:

$$W_0 - W_t = k\,t \tag{2. 9}$$

Where W_0 is the initial amount of drug, $W_t$is the amount at time t, and k is a proportionality constant. By dividing both sides of the equation by W_0 it is obtained:

$$f_t = k_0\,t \tag{2. 10}$$

Here, f represents the fraction of drug dissolved at time t, and k_0 is the zero-order release constant.

If the dissolution profile follows a zero-order model, the plot of f_t versus time will be linear.(Costa & Sousa Lobo, 2001; Lokhandwala et al., 2013; R, 2014)

2.10.2 First order kinetics:

Like the previous model, the first-order model describes the release using the following equation:

$$\frac{dC(t)}{dt} = -k_1\, C(t)$$

(2. 11)

Where $C(t)$ is the drug concentration at time t, and k_1 is the first order release constant. The equation can be linearized as:

$$\ln C(t) = \ln C_0 - k_1\, t$$

(2. 12)

Where C_0 is the initial concentration of the drug. It was assumed that the initial time is equal to 0.

If the plot of the logarithm of concentration versus time yields a straight line, this indicates that the model follows first-order kinetics. (Costa & Sousa Lobo, 2001; Lokhandwala et al., 2013; R, 2014)

2.10.3 Weibull model

The Weibull model is empirical, and it lacks theoretical basis. It can be successfully applied to almost any dissolution curves. The Weibull equation describes the accumulated fraction of the drug released at time t, f(t), as a function of two parameters: a, the time scale of the process, and b, the shape parameter. the curve can be S-shaped if b>1, parabolic if b<1 or exponential if b=1. The equation is:

$$f(t) = 1 - e^{-a\,(t-Ti)^b}$$

(2. 13)

Where Ti is the lag time before the dissolution takes place, in most cases is equal to zero. The main criticism of this model is its lack of a kinetic foundation, allowing it to describe but not characterize the dissolution kinetics. (Costa & Sousa Lobo, 2001; Lokhandwala et al., 2013; R, 2014)

2.10.4 Higuchi model

proposed in 1961, the Higuchi model gained popularity for its straightforward theorical derivation and applicability across various fields. It is typically used for drugs dissolved or dispersed in a polymeric matrix. The model's assumptions include:

- The Initial concentration of the active ingredient in the matrix is higher than its solubility.
- Diffusion is one-dimensional.
- The Drug's dimensions are smaller than the thickness of the system.
- Diffusivity is constant.

The released drug concentration depends on the square root of time, expressed as:

$$f(t) = \sqrt{D\ (2A - C_s)C_s t}$$

(2. 14)

Where f(t) is the release drug principle over the time t, D is the diffusivity, A is the surface area, and C is the solubility. n

The Higuchi model is often simplified to:

$$f(t) = K_H t^{1/2}$$

(2. 15)

Where Kh is the Higuchi dissolution constant. This model describes drug release as a diffusion process governed by Fick's law, dependent on the square root of time. It is particularly useful for describing drug dissolution from various modified-release dosage forms, such as transdermal systems and matrix tablets containing soluble drugs (Costa & Sousa Lobo, 2001; Lokhandwala et al., 2013; R, 2014)

2.10.5 Korsmeyer-Peppas model:

Korsmeyer-Peppas model is semi-empirical and can be written as:

$$f(t) = k\ t^n$$

(2. 16)

Where the constant k represents the structural and geometrical characteristics of the drug dosage form, and n the release exponent that indicates the drug release mechanism.

If n=0.5 the mechanism follows Fickian diffusion, while for 0.5<n<1, it indicates a non Fickian model. To determine the value of n only the fraction f(t) < 0.6 should be used, and the model should be applied only if the release occurs in a one-dimensional manner. (Costa & Sousa Lobo, 2001; Lokhandwala et al., 2013; R, 2014)

2.10.6 Dispersive kinetics:

The model presented here is a novel semi-empirical approach designed to study and characterize complex dissolution kinetics. The concept behind the model's development centers on variations in the activation energy barrier, which can occur in certain cases due to the influence of molecular kinetic energies on the rate-determining step of the dissolution process. In these instances, the rate is assumed to involve two-dimensional nucleation. Dispersive kinetics introduces a time dependency in both the rate constant and the activation energy. Two dispersive kinetic models have been formulated, each based on two physically relevant fitting parameters. These models can be classified as either acceleratory, where the reaction rate increases, or deceleratory, if the conversion rate decreases. Acceleratory transients are typically used to describe heterogeneous systems, such as some nucleation and growth rate-limited polymorphic phase transformations conducted under slurry conditions. Deceleratory transients are commonly applied to study homogeneous conversions, such as the decomposition of various types of crystals. In this work, the focus is on the decelaratory kinetics, making it interesting to explore the dissolution model. Most dispersive kinetics are characterized by sigmoidal x-t transients and dissolution kinetics can usually be approximated as two-dimensional. The equation of the decelerator model is presented below:

$$x = e^{(\alpha t)(e^{-\beta t^2}-1)} \qquad (2.\ 17)$$

Where x is the amount remaining in the system at time t, and p=1-x is the dissolved amount at time t. the parameters α and β are the two fit parameters of the model, respectively with units of $(time)^{-1}$ and $(time)^{-2}$. (Skrdla, 2009, 2007)

3 Materials and methods

3.1 Materials

Levofloxacin was purchased from TCI Europe (TCI Europe N.V., Belgium-Tokyo Chemical Industry, Japan), while Quercetin was purchased from Sigma-Aldrich (Merck, Massachusetts, U.S.). Before using them, a check was made. No further purification was applied.

3.2 Slurry crystallization

The cocrystals of levofloxacin (LEVO) and quercetin (QUE) were synthetized via slurring at room temperature for 72 hours in the dark, with a stoichiometric ratio 1:1, using four different solvents: methanol (MeOH), ethanol (EtOH), 1-propanol (1PR) and isopropanol (IPA). The suspensions were kept under stirring (around 250 rpm) in a 10 mL glass vial closed with a PE pressure plug. Two different scales were adopted: 92.6 mg of LEVO and 84.6 mg of QUE in 2 μl of solvent (MeOH, EtOH, 1PR, IPA) and 261.3 mg of LEVO and 238.7 mg of QUE in 4 μl of solvent. Different stoichiometric ratios, particularly 1:2 and 1:3 (LEVO:QUE) , were tested to verify whether the crystal was indeed a cocrystal and not a solid solution. The quantities involved were 28.3 mg of LEVO and 51.7 mg for a stoichiometric ratio 1:2 (LEVO:QUE) and 21.4 mg and 58.6 mg for a stoichiometric ratio 1:3 (LEVO:QUE) in 2 μl of solvent (IPA, EtOH). The use of a seeding was necessary in the case of the cocrystal obtained in a slurry solution with ethanol due to the presence of contaminations.

3.3 Power X-ray Diffraction (PXRD)

PXRD patterns has been collected using Bragg-Brentano geometry on an Empyrean diffractometer (Malvern Panalytical, U.K.). Diffraction patterns have been obtained at 2θ range 4-40° and 0.0001 as minimum 2θ step size, thanks to a CuK_α radiation with a wavelength (λ) of 1.54 Å. The instrument operated at a current of 40 mA and with a voltage of 40 kV with a Soller slit of 0.04 rad, anti-scatter slit of $^1/_2$ and a divergence slit of $^1/_4$. the samples have been disposed on a sample holder called “zero-background”. The sample must form a flat and homogeneous surface to avoid phenomena of preferential orientation of the crystalline phase.

3.4 Raman spectroscopy

Raman spectroscopy was performed with a LabRAM HR Evolution spectrometer (Horiba, Japan). Each sample has been placed in a glass slide at room temperature and then brought into focus thanks to a lens (Olympus 10x). A 785 nm and a Synapse Plus detector (Horiba) were used to perform the measurements. Scans of the 200-1700 cm^{-1} spectral region were recorded, with an acquisition time of 10 s and an accumulation number of 40.

3.5Differential scanning calorimetry

Heat flow measurements have been performed using a Mettler Toledo DSC 1 (Mettler Toledo, USA). Approximately 3 mg of each sample were weighed and sealed in an aluminum pan, while an identical and empty pan was used as reference. Each sample was heated up from 20 °C to 350 °C with a rate of 10 °C/min.

3.6 Thermogravimetric analysis

Thermogravimetric analysis has been performed using a Mettler Toledo 1600 (Mettler Toledo, USA) instrument, using Argon to maintain an inert atmosphere. Approximately 6 mg of each sample were weighed and disposed on an aluminum pan with a temperature program from 20°C to 400°C with a heating rate of 10 °C/min.

3.7 Contact angle measurement

Contact angle measurements have been recorded thanks to a drop shape analyzer DSA25 (Kruss Scientific) equipped with a micro syringe and a high-speed camera. The samples analyzed are compressed discs with the diameter of 1 cm, realized putting the powder between the plates of a hydraulic press. After the powder has been under a pressure of 200 bar for 30 seconds. The measurements have been conducted either with water and sunflower oil and in both cases a volume drop of 2 μl has been deposited on the powder surface thanks to the micro syringe and the behavior has been recorded with the camera. The choice of these solvents has been made because of the different polarity (water is polar, sunflower oil is a-polar). Drop side has been analyzed with Young-Laplace method thanks to Kruss Advance 1.12.0.35401 software, allowing in this way to record contact angles between the disc surface and the drop.

3.8 Crystal16

Measurement of drug solubility is one of the key elements of active pharmaceutical ingredient (API) characterization during the drug discovery and development process.

The solubility investigation was performed with a Crystal16 parallel crystallizer (Technobis Crystallization Systems) equipped with a 645 nm-wavelength laser for turbidity measurement of solutions. The Crystal16 can concurrently handle 16 samples distributed across four blocks, with each set of four samples sharing identical temperature profiles. For the experiments, varying amounts of cocrystals (ranging from 1 to 15 mg) were introduced into 1 mL of solvent within 1.5 mL glass vials, depending on the solvent type. In the vials it is also a present a little magnet to ensure mechanical agitation with a speed of 780 rpm, ideal for powders.

The Crystal16 was calibrated and subsequently used to introduce samples into each vial at room temperature, after which the vials were returned to the Crystal16 for the experiment. The temperature profile during the experiments involved ramping up to a maximum temperature, depending on the boiling temperature of the solvent applied, followed by cooling to 0 °C for 3 runs, with a speed of $\pm$0.2°C/s. The samples were maintained at each extreme temperature for 30 minutes. The transmissivity values were recorded over time and temperature using the Crystal16 software, and subsequently exported for detailed analysis to assess partial solubility and the impact of experimental parameters. Figure 3.1 displays an example of the temperature profile set up and the transmissivity values recorded. This figure is referred to the experiment of the cocrystal obtained by ethanol as solvent (LEVOQUE_EtOH) in ethanol.

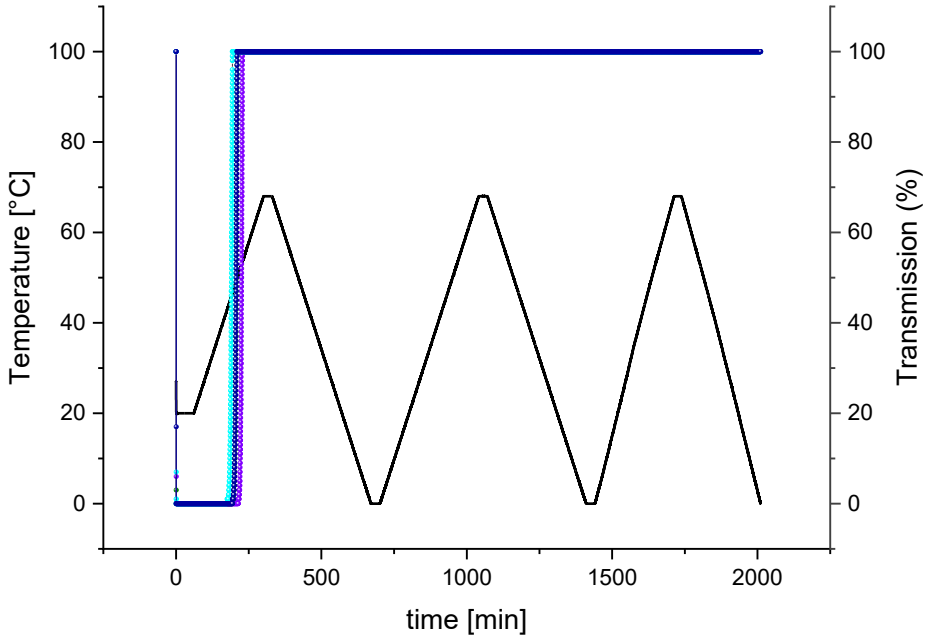

Figure 3. 1 Crystal 16 Temperature profile and transmissivity values recorded for different cocenntrations of LEVOQUE_EtOH in EtOH. From left to right: 10.14 mg/g (cyan), 11.79 mg/g (green), 12.17 mg/g (blue), 13.69 mg/g (violet)

The data exported from the software is available as supplementary data file. With the assistance of the CrystalClear software, the solubility points were then fitted to the van't Hoff equation to obtain the solubility curves (Amrihesari et al., 2023). These points, also called clear points, correspond to a transmissivity value of 100% (solution completely clear). Crystal clear belongs to the Crystal family, a collection of agile software development methodologies that can be used for different software projects depending upon size, complexity and criticality. Crystal clear is designed for the small projects. (Anwer et al., 2017)

The temperature dependence of how much a substance dissolves can be explained by an enthalpic factor known here as the van't Hoff enthalpy of solution (also referred to as apparent enthalpy of solution, enthalpy of dissolution, or heat of solution). This van't Hoff enthalpy of solution is a measurable thermodynamic property that shows good correlation with other physical characteristics. Nordstrom and Rasmuson (2006a, 2006b, 2006c) investigated the van't Hoff enthalpy of solution and observed a strong relationship with the molar solubility in organic solvents at a constant temperature. (Nordström & Rasmuson, 2009). Solubility data have been then linearized following van't Hoff equation:

$$\ln x = -\frac{\Delta H}{R}\left(\frac{1}{T} - \frac{1}{T_0}\right)$$

(3. 1)

Where x is the molar fraction of the component, ΔH is the dissolution enthalpy, R is the gas constant, T_0 is the initial temperature and T is the saturation temperature of the molar fraction x, both expressed in Kelvin.

Van't Hoff linearization allows to extrapolate solubilities values at different temperatures from the ones analyzed.

3.9 Dissolution tests

To conduct dissolution tests, a dialysis bag is prepared. The membrane is cut from a dialysis tubing cellulose membrane with a molecular weight cut-off of 14,000 Da (Sigma-Aldrich, Cesano Maderno, Italy). The membrane is then immersed in milli Q water, for at least 10 minutes, to ensure proper functioning. A specific amount of powder (either cocrystals or pure components), sieved in a sieve with the diameter of 500 μm, is placed inside the membrane along with a glass marble to prevent floating and ensure the powder remains submerged in the solution. The membrane is then sealed on both sides.

The dialysis bag is placed in a baker with 100 ml of milli Q water or an acid solution at pH 1 (obtained with hydrochloric acid 37% w/w), at room temperature. The pH 1 value was settled to simulate the effect in the human stomach. The moment the bag is introduced into the baker is considered the initial time (t0). The setup is maintained under slow agitation (around 85 rpm) to ensure a homogeneous solution, thus maintaining a consistent concentration of the powder throughout the solution. At specific time intervals from t0, 1 ml samples are withdrawn, and the same volume is immediately replaced with either water or hydrochloric acid, depending on the experiment. The extracted samples are analyzed in a Multiskan Sky high UV/Vis Microplate Spectrophotometer (ThermoFisher Scientific).

It is crucial to identify the wavelength of the Levofloxacin, the substance known to be released into the solution. Quercetin is known to be insoluble in water and preliminary tests have shown that by the end of the experiment, only Quercetin remains in the dialysis bag while Levofloxacin is entirely in the solution. This necessitates identifying the typical wavelength of Levofloxacin.

To determine this, known quantities of Levofloxacin are dissolved and samples are taken at various times. The blank (containing only the solvent) is analyzed to calibrate the

instrument. A scan is then conducted over the desired wavelength region (220-500 nm). The spectrophotometer produces a graph with absorbance values on the y-axis and wavelengths on the x-axis. Peaks in the graph indicate wavelengths where the substance absorbs light most strongly. The tallest peak represents the wavelength at which the powder absorbs the most light, corresponding to the typical wavelength of the substance. In this case the value is 289 nm, as shown in the figure below.

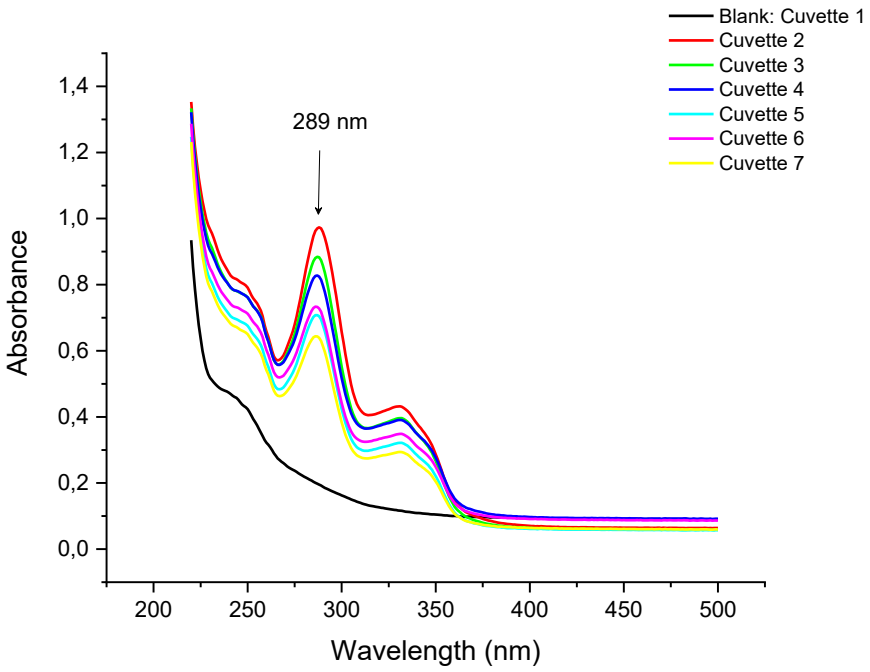

Figure 3. 2 Levofloxacin wavelength detection

Determining the extinction factor (ε) of Levofloxacin is essential for calculations during the experiments. To achieve this, known quantities of levofloxacin were dissolved, and their absorbance values were recorded. A graph plotting concentration versus absorbance was created, and the extinction coefficient was determined from the slope of the resulting line. This is done for both the solvent of interest: milli Q water and pH 1 solution. Identical cuvettes were used throughout the experiment to ensure a consistent optical path length, which is accounted for in the extinction factor.

Starting with a concentration of 10 mg/ml of Levofloxacin, a series of dilutions was prepared to ensure that absorbance values remained around 1, thus adhering to the linear range of Lambert-Beer law. Multiple data points were collected and plotted on a concentration versus absorbance graph. The data were then fitted with a linear fit. The fit

was deemed acceptable with an R^2 value of 0.9843. consequently, the slope of the resulting line, as indicated by the linear equation, was taken as the extinction factor.

Table 3.1 Concentration and absorbance values obtained by several dilutions to obtain Levofloxacin extinction factor

Ci	Levo(µL)	Water(µL)	Levo(mg)	[Levo]i(mg/µL)	[Levo]i(mg/mL)	A
C1	2	1998	0.02	0.00001	0.01	1.028
C2	900	100	0.009	0.000009	0.009	0.931
C3	900	100	0.0081	0.0000081	0.0081	0.849
C4	900	100	0.00729	0.00000729	0.00729	0.733
C5	900	100	0.006561	0.000006561	0.006561	0.714
C6	900	100	0.0059049	5.9049E-06	0.0059049	0.65

.

Table 3.1 presents the dilutions made and the corresponding concentrations, along with the absorbance value. To clarify the procedure:

Starting with a stock solution of 10 mg/ml (0.01 mg/µl) of Levofloxacin, a first dilution is prepared by mixing 2 µl of the stock solution with 1998 µl of Milli Q water. The amount of Levofloxacin in the diluted solution is calculated by multiplying the volume by the concentration. This allows for the determination of the actual concentration of Levofloxacin in the cuvette, expressed in both mg/ml and mg/µl. The absorbance values are then measured using a spectrophotometer. This procedure is repeated for each subsequent dilution.

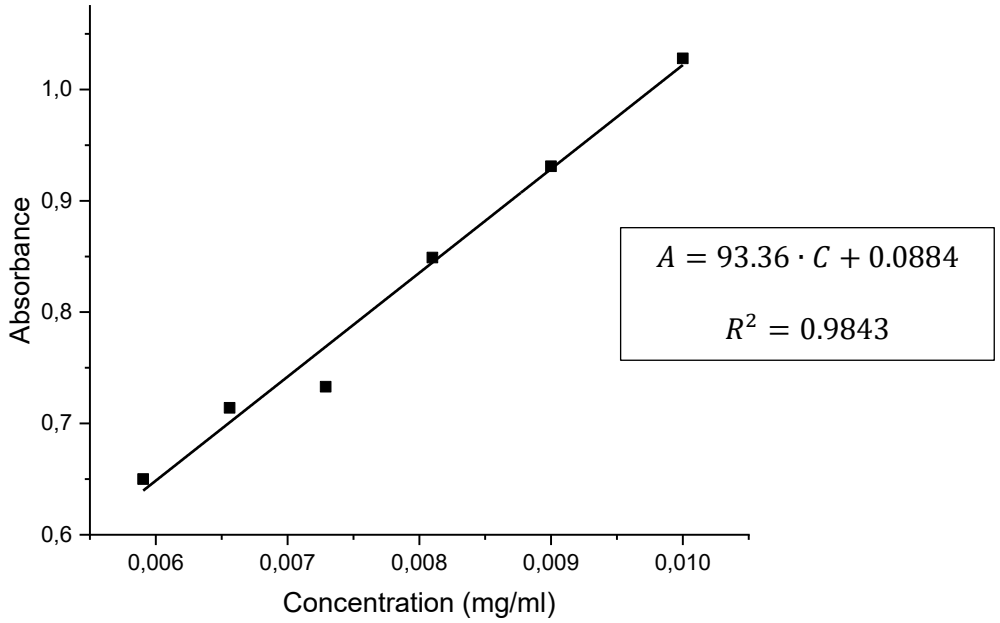

Figure 3. 3 Linear fit of concentration vs absorbance values

The equation obtained with the linear fitting is as follows:

$$A = 93.36 \cdot C + 0.0884$$

(3. 2)

This indicates that the extinction coefficient of Levofloxacin in a pH 1 solution is 93.36 ml/(mg·cm). The same procedure was applied using Milli-Q water, resulting in an extinction coefficient of 72.10 ml/(mg·cm). This suggests that the dissolution rate of Levofloxacin is faster in a pH 1 solution compared to Milli-Q water.

After collecting the samples at specific times, they were analyzed using a Multiskan Sky high UV/Vis Microplate Spectrophotometer (ThermoFisher Scientific). The absorbance values were obtained by setting the wavelength specific to Levofloxacin. Prior to testing the samples, a blank sample containing the solvent of interest (either milli-Q water or the solution at pH 1) was analyzed to assess its contribution to the absorbance value. The absorbance values of the samples were then adjusted by subtracting the absorbance value of the blank, resulting in what is referred to as the corrected absorbance. This corrected absorbance was then used to calculate the concentration by dividing it by the extinction coefficient of Levofloxacin. The dissolved mass of Levofloxacin was determined by multiplying this concentration by the volume of the solution. Additionally, it was accounted

for that each 1 ml sample withdrawn was replaced by 1 ml of solvent when calculating the dissolved mass.

Natural polysaccharides attract attention as pharmaceutical excipients due to their biocompatibility, low toxicity and low cost. Among these, cellulose nanocrystals (CNCs) have increased interest due to their large surface area, high hydrophilicity, high tensile strength and stiffness, and lightweight (Almeida et al., 2024; Mishra, 2024). Mannitol exhibits low moldability and a high dissolution rate and less sensitivity to humidity. Combinations of mannitol and microcrystalline cellulose or nanocrystalline cellulose are frequently used in fast dissolving/disintegrating tablets (Joseph, 2007). In this work tablets of either cocrystals, physical mixture and levofloxacin were realized to study the change of the dissolution event. The tablets contained 5% w/w of CNCs, 20% w/w of mannitol and 75% w/w of either cocrystals, physical mixture and levofloxacin, realized putting the powders between the plates of a hydraulic press under a pressure of 200 bar for 30 seconds and discs with the diameter of 1 cm. Before the powders were sieved in a sieve with the diameter of 500 μm. Figure 3.4 displays one of the tablets used in this work of LEVOQUE_EtOH.

Figure 3. 4 Tablet of LEVOQUE_EtOH

Various dissolution models (zero order, first order, Higuchi and Weibull) were tested to identify the one that best represented the experimental data collected. Among these, the best fit was shown by the deceleratory model, reason why it was used during the calculations. The dissolved mass at each time is divided by the initial concentration, referred to here as p. From this, the value of x is calculated as

$$x = 1 - p$$

(3. 3)

Using the model's formula, the beta parameter is determined for each time point, based on an assumed alpha value from the literature

$$\beta = -\frac{\ln(x)}{\big((\alpha t) + 1\big)t^2}$$

(3.4)

The model formula is then applied to generate the data, and the deviation from the actual values is calculated.

$$x = e^{(\alpha t)(e^{-\beta t^2} - 1)}$$

(3.5)

the absolute error is then determined, followed by the calculation of quadratic errors, which are summed together. the Excel 'Solver' tool is then used to minimize this error by adjusting the alpha and beta values. This is done to ensure the convergence, because usually numerical methods are strongly dependent from the initial values.

4 Results and discussion

4.1 PXRD results

All the cocrystals analyzed in this work were obtained via slurry over 72 hours, covered with aluminum foil, to prevent light sensitive starting materials to degrade. Figure 4.1 illustrates a comparison between the diffractograms of the cocrystals and those of the original reagents, levofloxacin and quercetin, as obtained through PXRD analysis. This comparison reveals that the combination of levofloxacin and quercetin, in a slurry solution, produces new compounds rather than a physical mixture, which would have shown as overlapping diffraction patterns of the individual reagents.

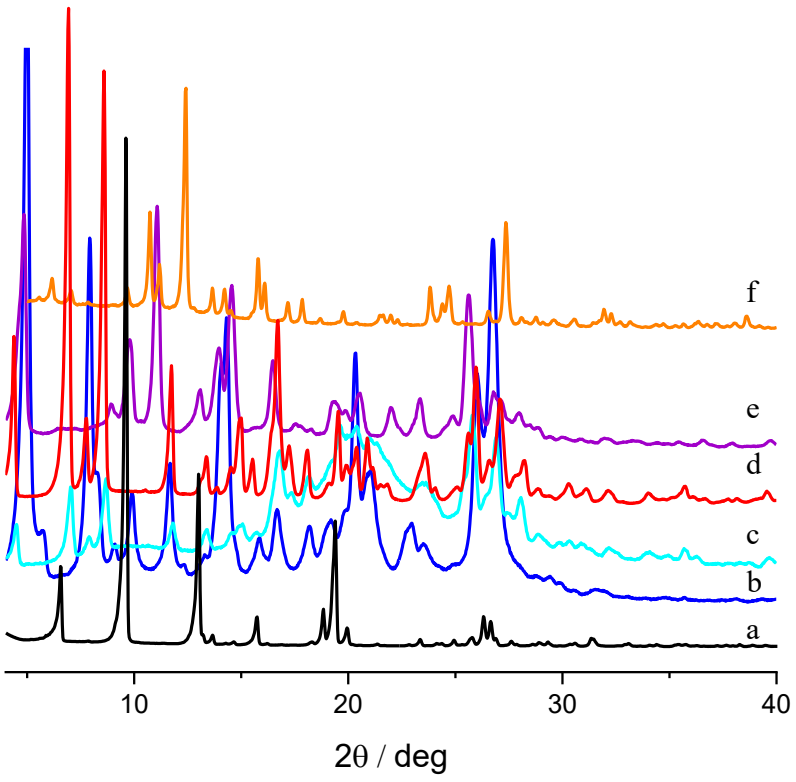

Figure 4. 1 PXRD patterns at room temperature. From bottom to top: LEVO (a, black), LEVOQUE_EtOH (b,blue),), LEVOQUE_1PR (c,cyan), LEVOQUE_IPA (d,red), LEVOQUE_MeOH (e,violet), QUE (f,orange)

A comparison between the solvated and the desolvated structures was conducted. The diffractograms of LEVOQUE_EtOH and LEVOQUE_MeOH revealed shifts in peak position, indicating that the two forms are structurally distinct, as depicted in figures 4.2

and 4.3. The absence of ethanol and methanol results in different structural arrangements, referred to here LEVOQUE_FORM I and LEVOQUE_FORM III, respectively.

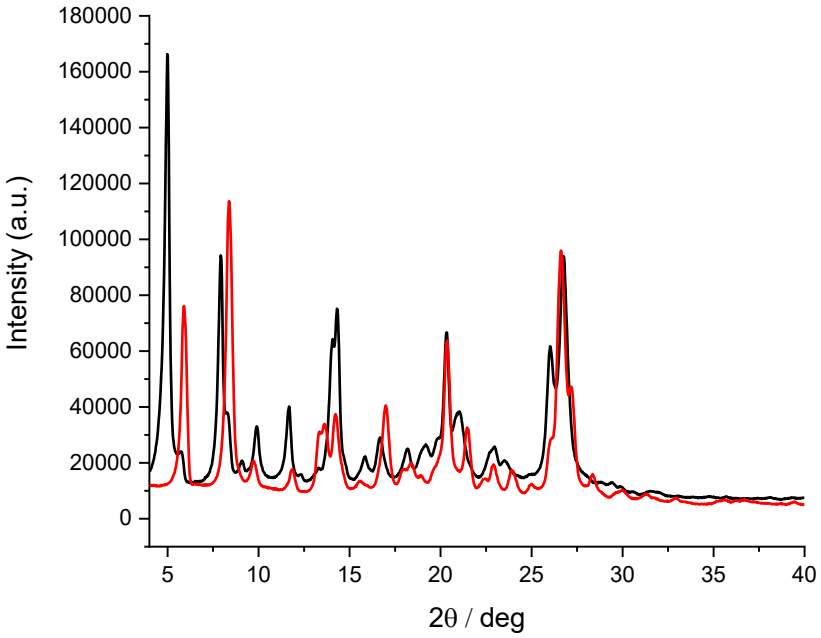

Figure 4. 2 PXRD comparison between LEVOQUE_EtOH (black) and LEVOQUE_FORM I (red)

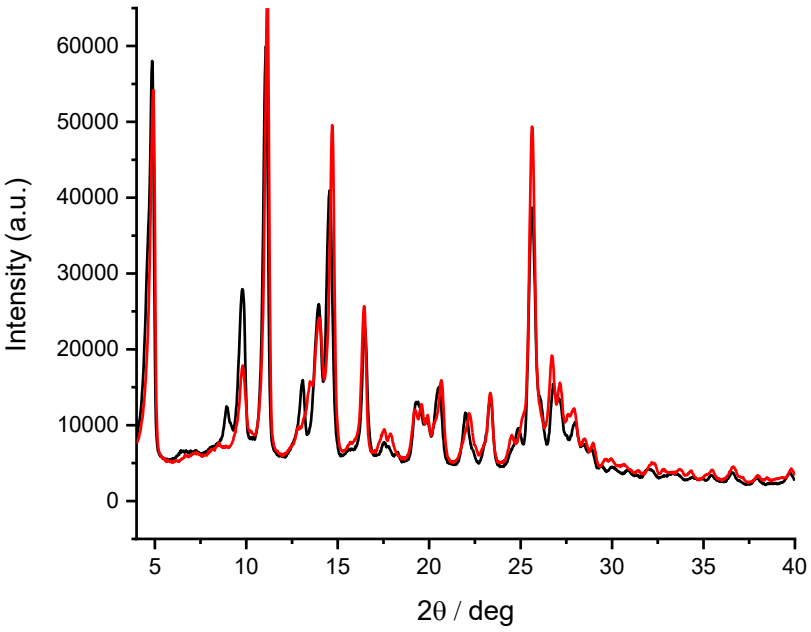

Figure 4. 3 PXRD comparison between LEVOQUE_MeOH (black) and LEVOQUE_FORM III (red)

However, for LEVOQUE_IPA and LEVOQUE_1PR no differences were observed between the diffractograms of the solvated and desolvated structures, referred to here LEVOQUE_FORM II (IPA) and LEVOQUE_FORM II (1PR). In these cases, the desolvation process maintains the original crystal packing without altering the arrangement (figures 4.4 and 4.5). This leads to the question: "is it truly a solvate?". While the answer is complex, thermal analysis provided further insights into this concept. The diffractograms of LEVOQUE_FORM II (IPA) and LEVOQUE_FORM II (1PR) showed an almost complete overlap of the peaks, indicating that the two compounds have isomorphic crystal structure as showed in figure 4.6.

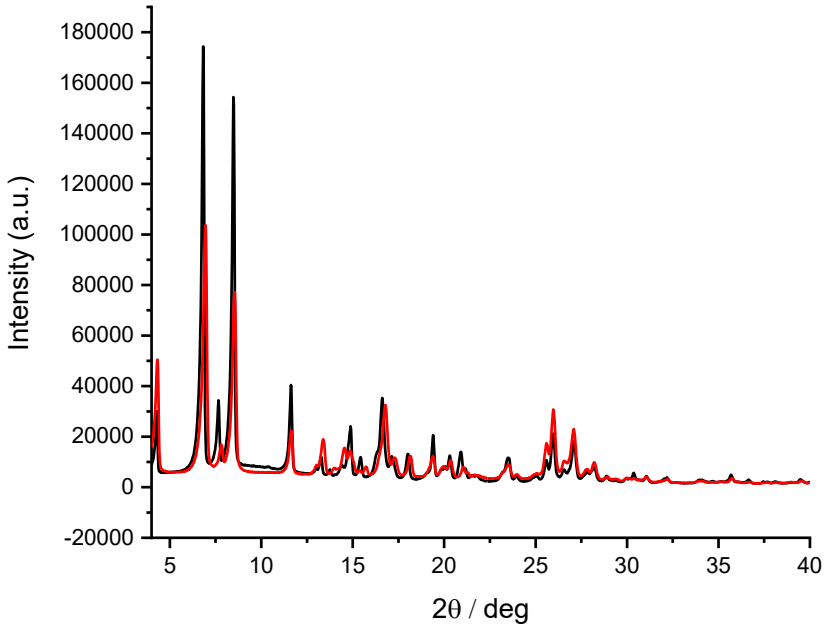

Figure 4. 4 PXRD comparison between LEVOQUE_IPA (black) and LEVOQUE_FORM II (IPA) (red)

.

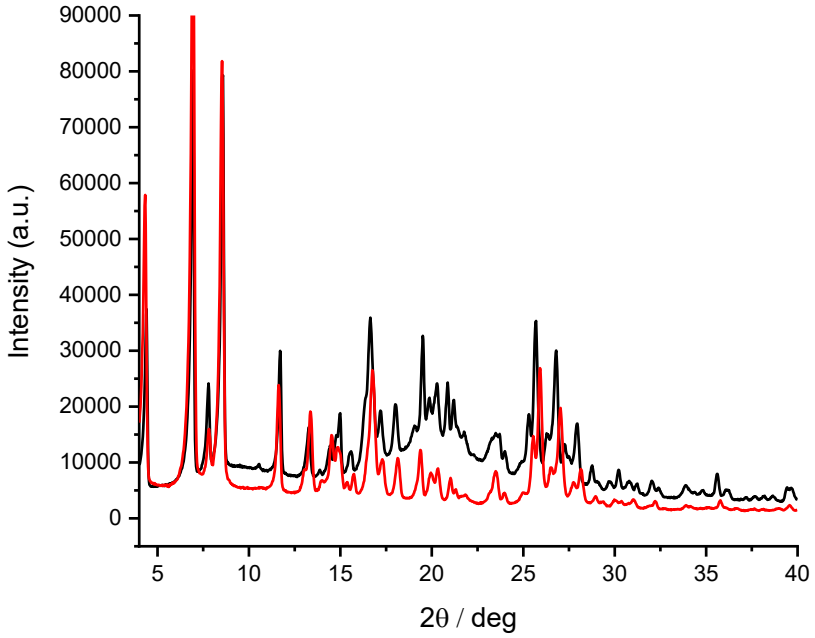

Figure 4. 5 PXRD comparison between LEVOQUE_1PR (black) and LEVOQUE_FORM II (1PR) (red)

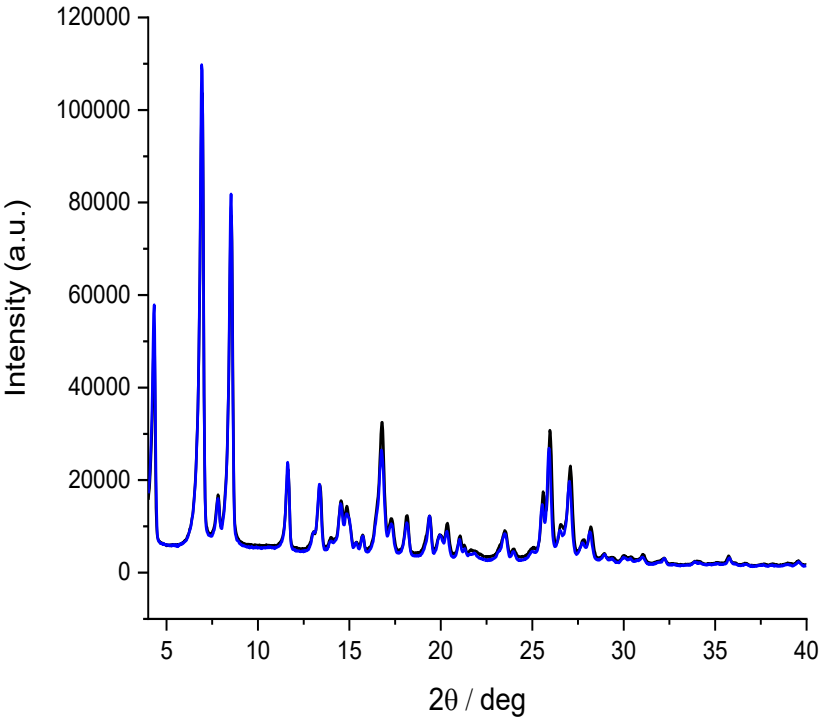

Figure 4. 6 PXRD comparison between LEVOQUE_FORM II (IPA) (black) and LEVOQUE_FORM II (1PR) (blue).

In Figure 4.7 are summarized the various forms identified during this study. Over time, all these forms tend to convert to LEVOQUE_FORM II.

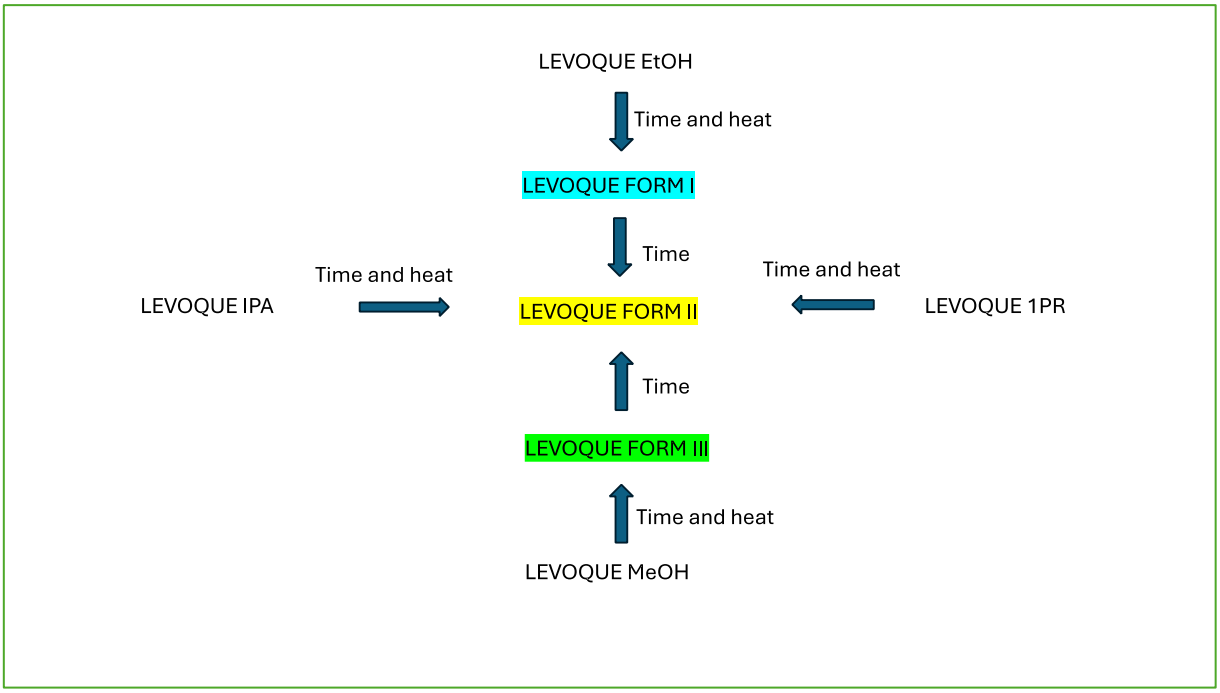

Figure 4. 7 schematic of the various cocrystals forms.

To be sure that the structure obtained is a cocrystal and not a solid solution a change of the stoichiometric ratio has been made. A solid solution consists in a homogeneous solid-phase mixture where two or more substances coexist within in a single phase. Solid solutions can be categorized based on their miscibility (continuous or discontinuous) and the distribution of solvate molecules within the solvent (substitutional, interstitial, or amorphous). In a continuous solid solution, the components are fully miscible in all proportions, whereas in discontinuous solid solutions, the solubility of each component is limited. Classical solid solutions exhibit a crystalline structure, where solute molecules can either replace solvent molecules in the crystal lattice (substitutional) or occupy the interstitial spaces between them (interstitial). In an amorphous solid solution, the solute molecules are irregularly dispersed within the amorphous solvent.(Leuner & Dressman, 2000)

Usually, this kind of test requires to change the most abundant component seen in the structure, reason why it was decided to change the quercetin quantity. Particularly a test with the cocrystals obtained with ethanol and isopropanol was made, with a stoichiometric ratio of 1:2 and 1:3 (LEVO: QUE). Three possible scenarios were identified:

1) The pattern observed by PXRD analysis is the same.
2) The pattern observed by PXRD is completely different.

3) The pattern observed by PXRD is different, particularly it is composed by the pattern obtained with the stoichiometric ratio 1:1 plus the excess of quercetin.

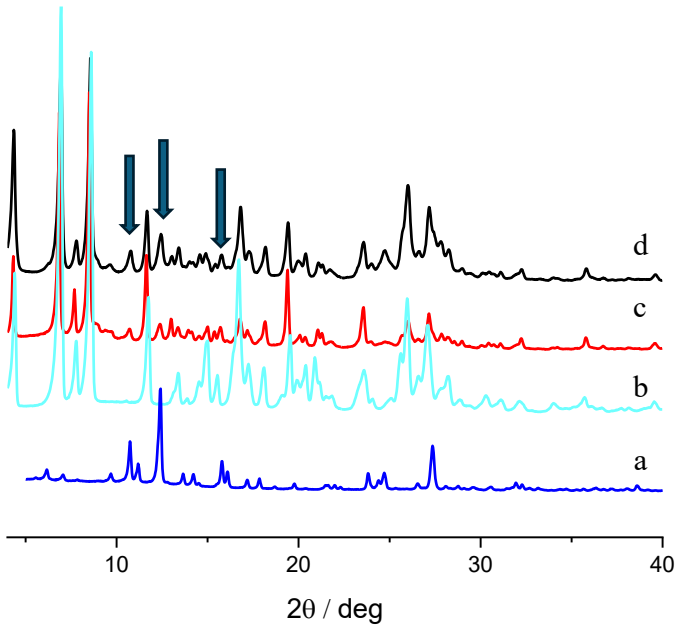

Figure 4. 8 PXRD analysis. From bottom to top: QUE (a,blue), LEVOQUE_IPA (b,green), LEVOQUE_IPA_1:2 (LEVO:QUE) (c,red), LEVOQUE_IPA_1:3 (LEVO:QUE) (d,black)

Figure 4.8 depicts a comparison of the diffractograms for different stoichiometric ratios of the components obtained under slurry conditions using isopropanol as solvent, and the diffractogram of quercetin. The arrows highlight the peaks indicating an excess of quercetin in the structure when the stoichiometric ratio was altered. This observation supports the conclusion that the system corresponds to the third scenario among the three previously described, confirming that a cocrystal with a specific order is formed rather than a solid structure between levofloxacin and quercetin. It is possible to observe the same in the case of ethanol as solvent, as showed in Figure 4.9.

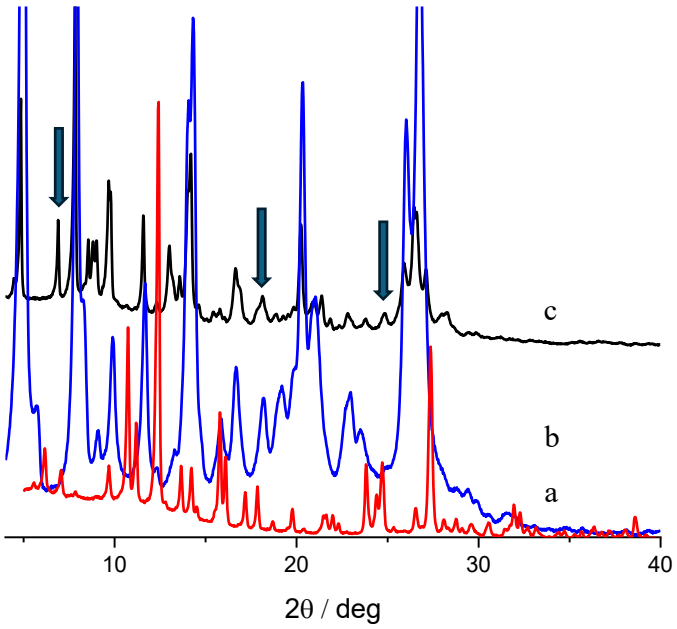

Figure 4. 9 PXRD analysis. From bottom to top: QUE (a,red), LEVOQUE_EtOH (b,blue), LEVOQUE_EtOH_1:2 (LEVO:QUE) (c,black)

During this thesis, the use of seeding became essential because the LEVOQUE_EtOH cocrystal could not be obtained in a pure form and was contaminated, hence referred to as LEVOQUE_EtOH mixture. Specifically, the cocrystal displayed peaks characteristic of the LEVOQUE_IPA cocrystal, which were not originally present. To resolve this, a seed of the correct form was introduced under slurry conditions. This seed, stored in the fridge to prevent transformation into a different polymorphic form, acted as a template. By reducing the nucleation energy barrier, the seed directed the cocrystallization process toward the desired form.

In Figure 4.10 it is possible to observe the contamination mentioned above. With the arrows are highlighted the common peaks between LEVOQUE_EtOH_mixture and LEVOQUE_IPA.

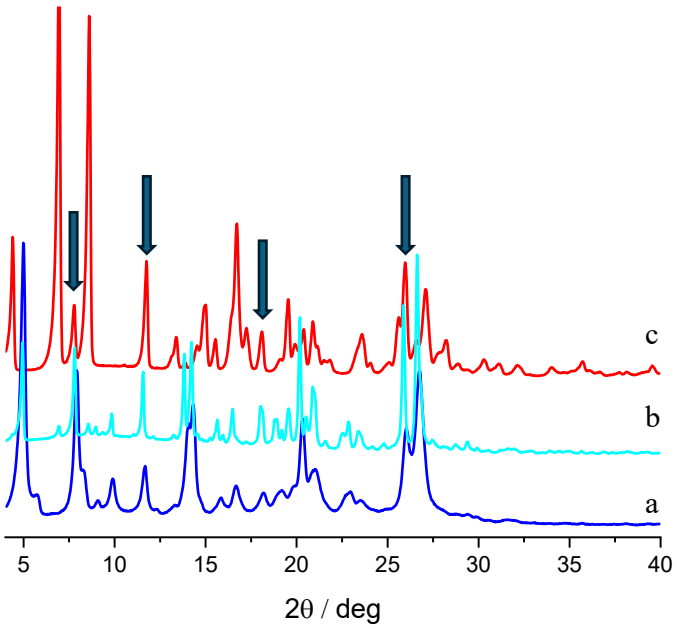

Figure 4. 10 LEVOQUE_EtOH_mixture: the need of a seeding. From bottom to top: LEVOQUE_EtOH (a,blue), LEVOQUE_EtOH_mixture (b,cyan), LEVOQUE_IPA (c,red)

4.2 Thermal analysis

Different polymorphic forms of the cocrystals were obtained during this work. In this section the differential scanning calorimetry results and the thermogravimetric analyses are presented with the aim to distinguish between the solvated structures and the desolvated ones. These analyses were useful to define the absence of impurities, the thermal stability and the melting points for each cocrystal. in the following figures the results for the differential scanning calorimetry and the thermal gravimetrical analysis are depicted. In all cases, except for LEVOQUE_MeOH, it was possible to detect the solvent loss from the structure, indicating the transition from the solvated form to the desolvated one. This show the presence of the solvent in all the structure, ensuring that also LEVOQUE_IPA and LEVOQUE_1PR are solvated and the desolvation process maintains the crystal packing structure. LEVOQUE_MeOH displays no changes in the thermogram until the occurrence of the degradation phenomena, as a matter of fact it already desolvates at room temperature. For LEVOQUE_IPA, LEVOQUE_1PR and LEVOQUE_MeOH endothermic peaks were shown by the DSC, followed by a significant weight loss in the thermogram. This happens respectively around 150 °C (for LEVOQUE_IPA), 160°C (LEVOQUE_1PR) and 170°C

(LEVOQUE_MeOH). For LEVOQUE_EtOH it was not possible to detect marked endothermic peaks like the other cases, but a slight heat flow change around 120°C. LEVOQUE_EtOH partly desolvates at room temperature.

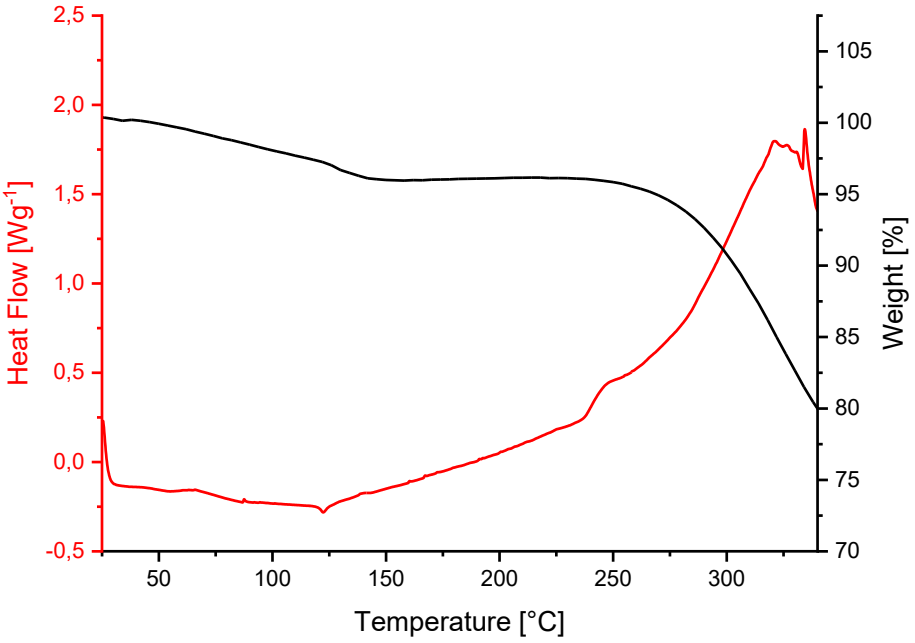

Figure 4. 11 DSC (red) and TGA (black) for LEVOQUE_EtOH

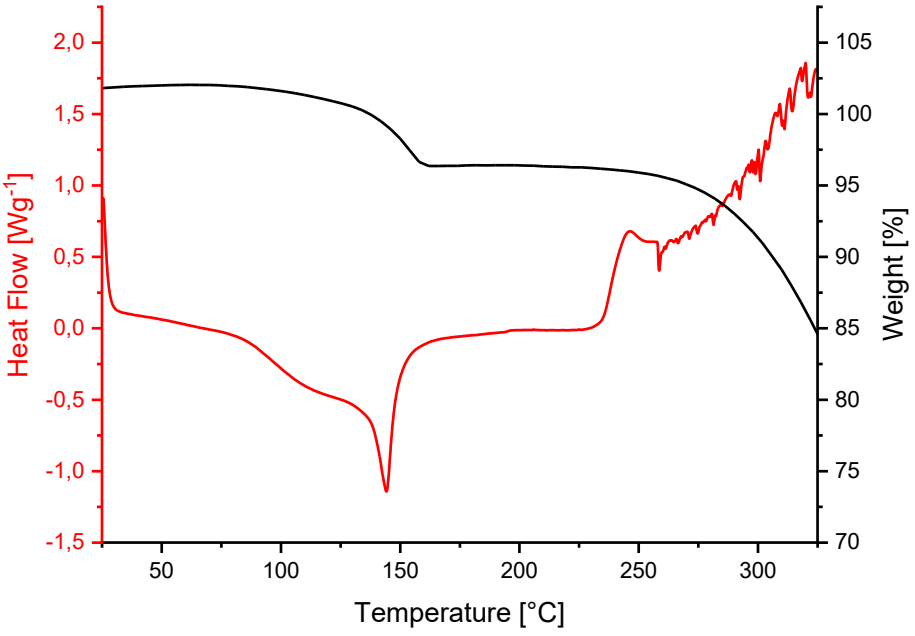

Figure 4. 12 DSC (red) and TGA (black) for LEVOQUE_IPA

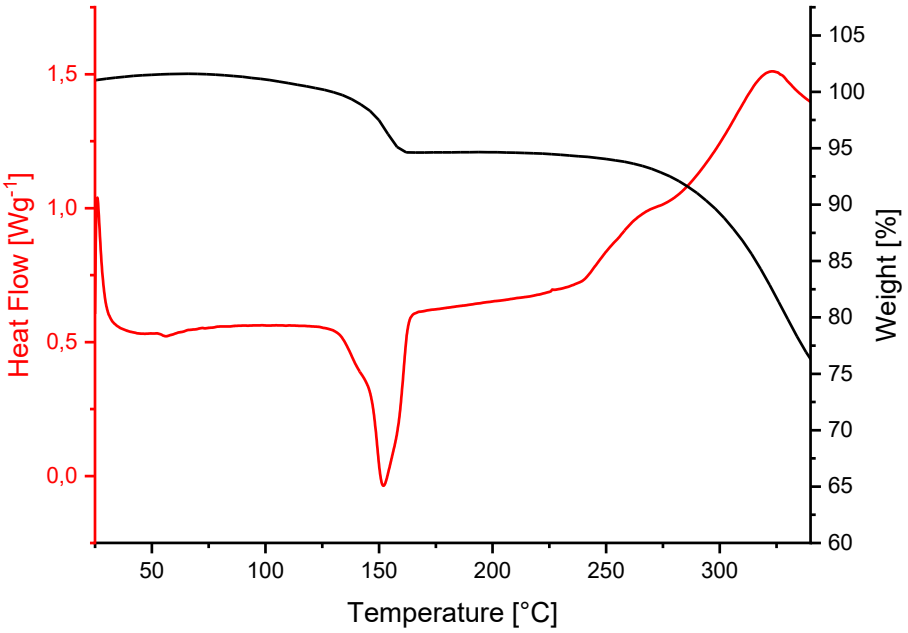

Figure 4. 13 DSC (red) and TGA (black) for LEVOQUE_1PR

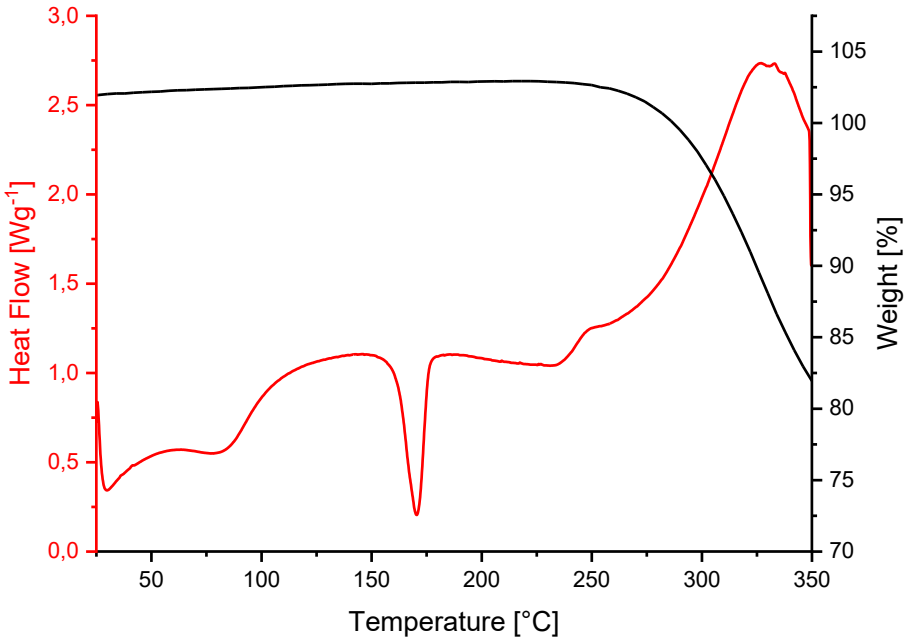

Figure 4. 14 DSC (red) and TGA (black) for LEVOQUE_MeOH

4.3 Raman spectroscopy

In Figure 4.15 the Raman spectrum of quercetin is reported and in Figure 4.16 the structure with every ring nominated.

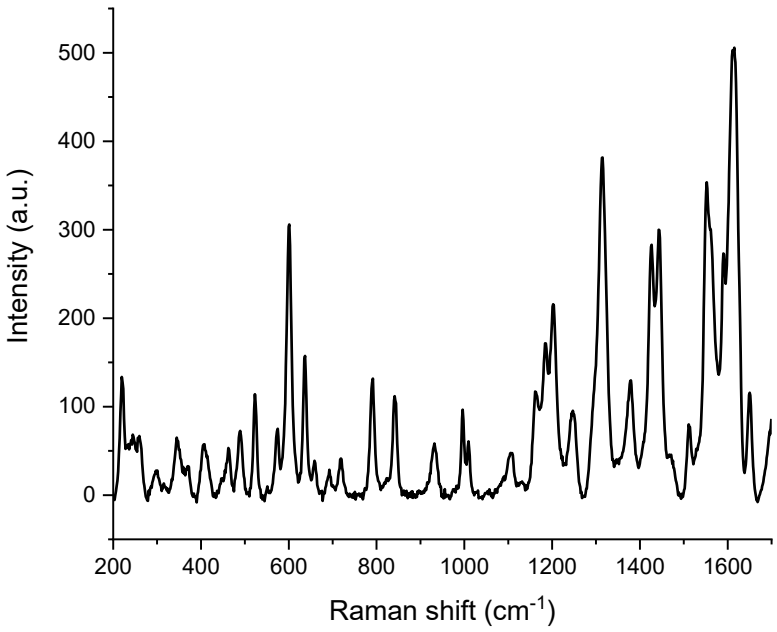

Figure 4. 15 Raman spectrum of quercetin

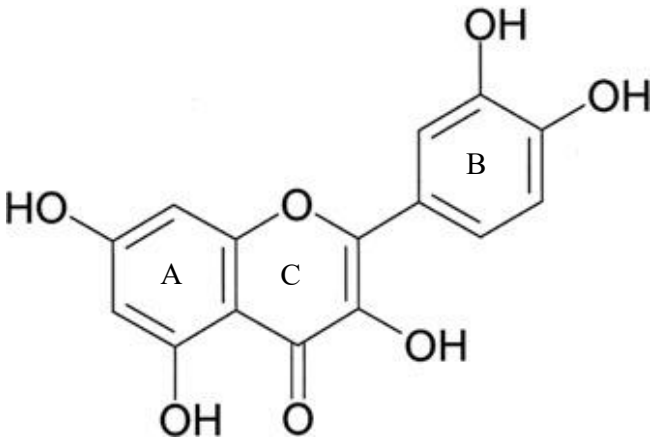

Figure 4. 16 Quercetin' structure. (Wu et al., 2003)

From the Raman spectrum of quercetin, it is possible to identify sone typical frequencies (Cieślik-Boczula et al., 2012; Numata & Tanaka, 2011):

- 1615 cm^-1: C=O stretch
- 1552 cm^-1, 1443 cm^-1, 1427 cm^-1: O-H bend
- 1315 cm^-1: Ring deformation (ring B)

- 1161 cm^-1: C-H bend (ring B)
- 841 cm^-1, 601 cm^-1: Ring stretch (ring B, C)
- 791 cm^-1: O-H stretch (ring A)

In Figure 4.17 the Raman spectrum of levofloxacin is reported and in Figure 4.18 the structure.

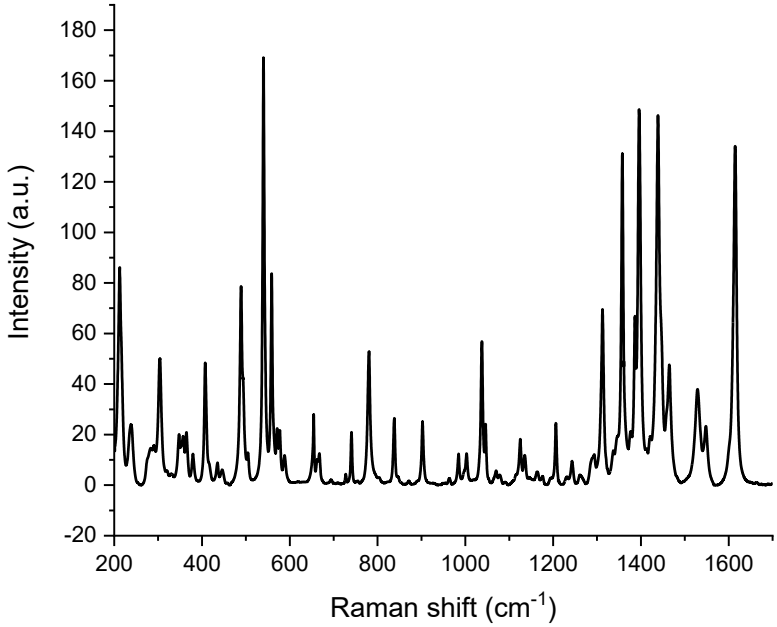

Figure 4. 17 Raman spectrum of levofloxacin

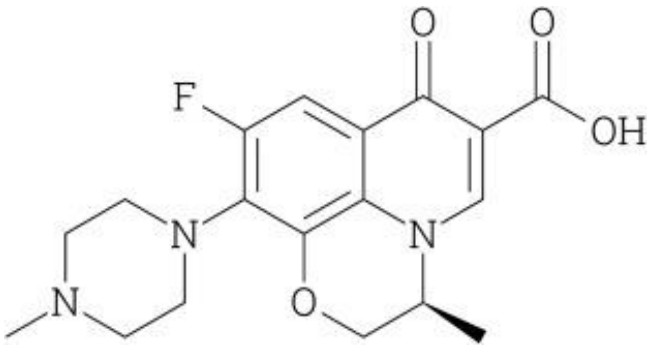

Figure 4. 18 Levofloxacin' structure. (Sitovs et al., 2021)

From the Raman spectrum of levofloxacin, it is possible to identify sone typical frequencies (N. Li et al., 2021; Liu et al., 2015; Sinha & Biswas, 2020):

- 1615 cm^-1: C=C stretching and C=N stretching.
- 1548 cm^-1: v C=C.
- 1439 cm^-1: CH2 bending and CH2 wag.

- 1396 cm^-1: OH bend.
- 902 cm: v C-C.

Levofloxacin is the only quinolone to have two peaks in the region around 1400 cm^-1, so it can be recognized immediately from its isomer oflaxacin.

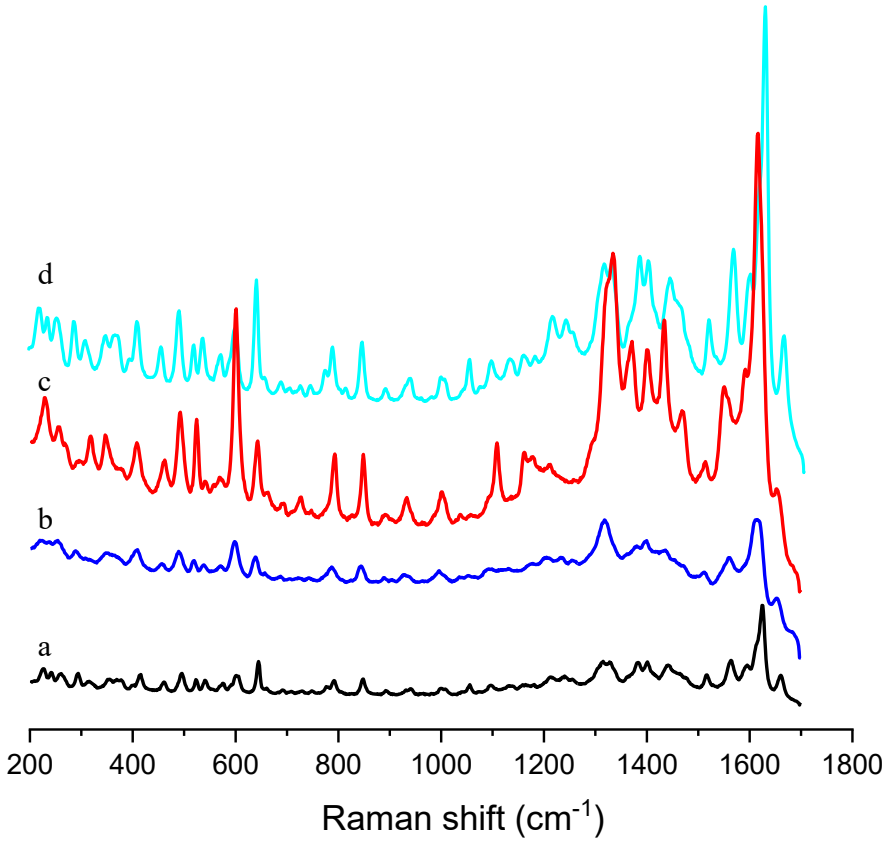

Figure 4. 19 Raman spectroscopy of cocrystals. From bottom to top: LEVOQUE_1PR (a,black), LEVOQUE_EtOH (b,blue), LEVOQUE_MeOH (c,red), LEVOQUE_IPA (d,cyan)

Figure 4.19 depicts the Raman spectroscopy analysis for the four different cocrystals. It is possible to see a shift in the double bond's frequencies due to the formation of new intermolecular interactions, confirming what has already been told with the PXRD analysis: the formation of a new crystal form rather than a physical mixture. Particularly there is a shift from 1615 cm^-1 to 1625 cm^-1, frequence typically associated to the formation of an amide group or C(O)N (Barmpalexis et al., 2018). It is possible to find some of the original reactants' peaks such 1315 cm^-1 and 791 cm^-1 for quercetin, showing the presence of the

original rings of quercetin B and C, or 1439 cm^-1 for levofloxacin. The shift of the other positions is due to a different disposal of the cocrystals, slightly different between the four different cocrystals studied in this work (Barmpalexis et al., 2018).

4.4 Contact angle measurements

Contact angle measurements are applied to investigate the wettability of the cocrystals by a liquid, in this work a drop of 2 μl of water or sunflower oil.

It must be considered that the contact angle is a surface property. The tablets realized weighted between 100 and 120 mg, but it was impossible to realize perfect homogeneous surfaces, this bringing to also some differences of recorded values in the same cocrystal class analyzed.

table 4. 1Contact angle values

Component	**Contact angle value**	
	water	oil
LEVOQUE_FORM I	105.9°	20.2°
LEVOQUE_IPA	105.3°	24.4°
LEVOQUE_FORM II (IPA)	112.3°	19.1°
LEVOQUE_1PR	104.2°	33.6°
LEVOQUE_FORM II (1PR)	110.8°	17.2°
LEVOQUE_FORM III	106.8°	25.4°
LEVO	61.4° (0 s) 46.2 ° (2 s)	36.4°

Table 4.1 shows all the contact angle values measured for each cocrystal and for levofloxacin. It is clear that all cocrystals exhibit contact angles greater than 90° when in contact with a 2 µl drop of water, indicating a strong tendency for the cocrystal surfaces to repel water. In contrast, the contact angle with a drop of sunflower oil is very low, demonstrating good wettability. For the cocrystals obtained using 1-propanol and isopropanol as solvents, contact angle measurements were taken for both the solvated and desolvated structures. The desolvated structures showed higher contact angles with water and lower ones with sunflower oil compared to the solvated forms. This change can be attributed to the loss of isopropanol/1-propanol during heat treatment. Since isopropanol and 1-propanol contain a polar hydroxyl group, their presence could improve wettability with water and decrease it with sunflower oil. However, it is more likely that the observed

differences are due to variations in the exposed surface areas between the solvated and desolvated samples, which were not perfectly identical.

Ethanol and methanol are highly volatile solvents, and they are believed to leave the structure quickly, limiting the analysis to the desolvated forms, LEVOQUE_FORM I and LEVOQUE_FORM III. This is why no heat treatment was needed for the study of contact angles for the cocrystals obtained from methanol and ethanol. The recorded contact angle values align with the other cases. A similar analysis was conducted for levofloxacin. When wetted by a 2 µl drop of water, levofloxacin showed a much lower contact angle (61.4°), indicating good wettability. After two seconds, the contact angle decreased further to 46.2°. When wetted with sunflower oil, levofloxacin exhibited a higher contact angle than the cocrystals. This difference can be attributed to the presence of quercetin in the cocrystal structure, which is known for its very low wettability. Figure 4.20 displays an example of the contact angle result obtained by the high-speed camera for a sample of LEVOQUE_IPA wet by a 2 µl drop of water. In this case it can be clearly seen the domed shape assumed by the drop, due to the low wettability with the cocrystal surface. All the images of the contact angle values are reported in appendix B.

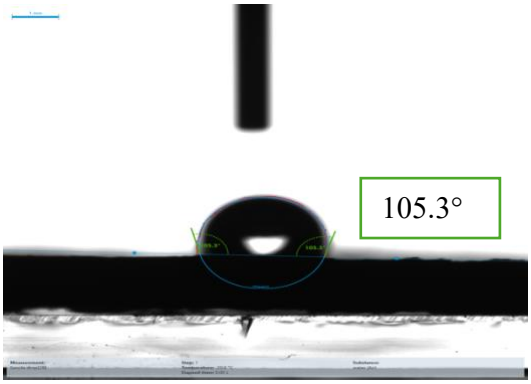

Figure 4. 20 Contact angle measurement for a tablet of LEVOQUE_IPA wet by a 2 µl droplet of water

4.5 Solubility measurements

Solubility refers to the maximum amount of solute that can be dissolved in a certain amount of solvent at a specific temperature. Solubility tests were performed to obtain data for crystallization experiments and synthesis scale up. Each-crystal solubility profile was studied in the respective solvent of crystallization. The experimental points were obtained thanks to the Crystal 16 tool and analyzed with the Crystal Clear system, as already discussed in paragraph 3.7.

table 4. 2 Test conditions for solubility test for the four different cocrystals

Component	Concentration range (mg/g)	Max Temperature reached (°C)
LEVOQUE_FORM I	2.66-13.69	65
LEVOQUE_FORM III	3.91-13.76	52
LEVOQUE_FORM II (IPA)	3.69-13.36	75
LEVOQUE_FORM II (1PR)	2.61-11.19	75

Table 4.2 presents the test conditions for the four different cocrystals, including the concentration range (from minimum to maximum) in mg/g and the maximum temperature reached during each experiment. The variation in temperature set up is attributed to the different boiling points of the solvents used for the solubility tests.

Figure 4.21 displays the comparison of the four different van't Hoff solubility curves.

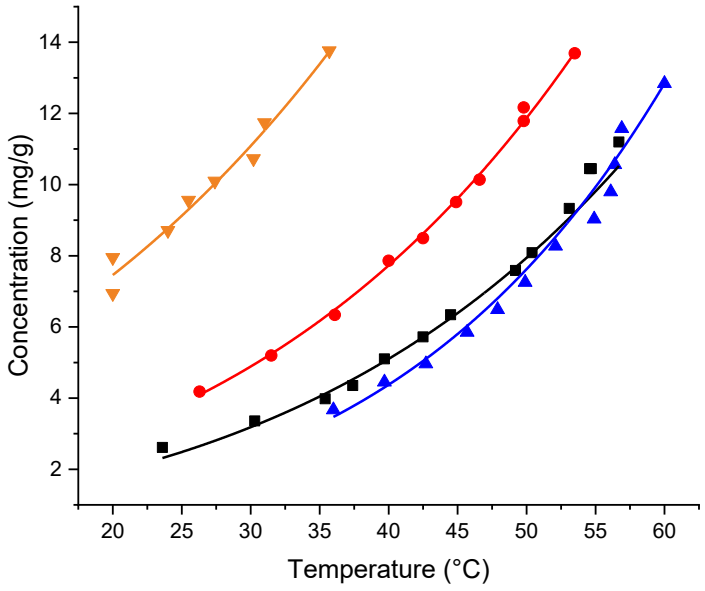

Figure 4. 21 van't Hoff solubility curves for the four different cocrystals. From left to right: LEVOQUE_MeOH in MeOH (orange), LEVOQUE_EtOH in EtOH (red), LEVOQUE_1PR in 1PR (black) and LEVOQUE_IPA in IPA (blue)

The data points were all approximated using the van't Hoff equation. It is evident that the solubility of LEVOQUE_FORM I in methanol occurs at lower temperatures and higher concentrations compared to the other forms. LEVOQUE_FORM II (IPA) requires a higher temperature to dissolve than the other cases. Between 55°C and 60 °C, the solubility curves

of LEVOQUE_FORM II (IPA) and LEVOQUE_FORM II (1PR) intersect, indicating that both forms have the same solubility within this temperature range. The equations were subsequently linearized according to the van't Hoff linearization.

table 4. 3 Van't Hoff equations for the solubility tests of each cocrystal and the corresponding R^2

Component	Van't Hoff equation	R^2
LEVOQUE_FORM I	$y = 15.9204 - \frac{4343.0785}{x + 273}$	0.997
LEVOQUE_FORM III	$y = 14.0228 - \frac{3519.9767}{x + 273}$	0.975
LEVOQUE_FORM II (IPA)	$y = 19.3972 - \frac{5609.2248}{x + 273}$	0.978
LEVOQUE_FORM II (1PR)	$y = 15.9251 - \frac{4474.4739}{x + 273}$	0.990

Table 4.3 shows the equations generated by the software along with the corresponding R^2 values, where y stands for concentration (mg/g) and x for temperature (°C). The fit was deemed highly acceptable due to the high R^2 values.

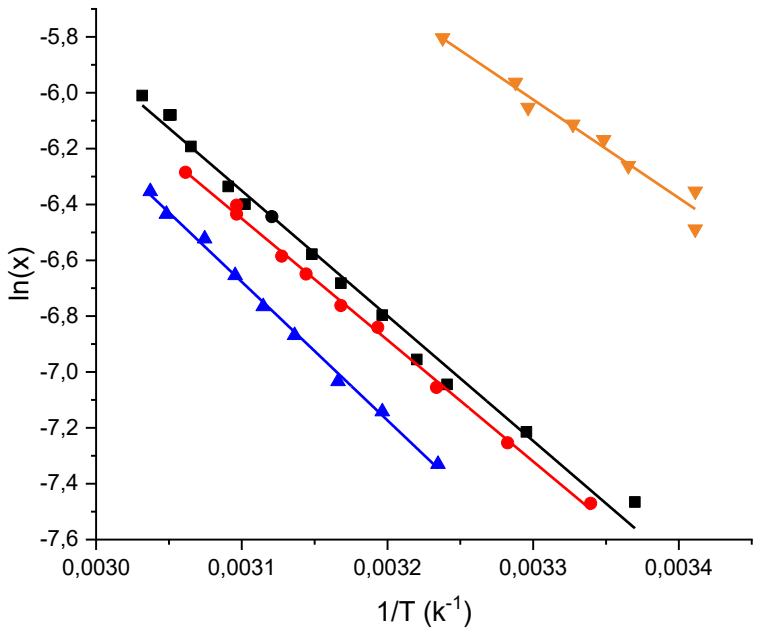

Figure 4. 22 Linearized van't Hoff solubility curves for the four different cocrystals. From left to right: LEVOQUE_IPA in IPA (blue), LEVOQUE_EtOH in EtOH (red), LEVOQUE_1PR in 1PR (black) and LEVOQUE_MeOH in MeOH

It is possible to visualize the linearized solubility curves from figure 4.22 and the respective equations from table 4.4.

table 4. 4 Linearized van't Hoff equations of each cocrystal and the corresponding R^2

Component	Van't Hoff equation linearized	R^2
LEVOQUE_FORM I	$\ln(x) = 7.026 - \frac{4347.250}{T}$	0.998
LEVOQUE_FORM III	$\ln(x) = 5.603 - \frac{3523.497}{T}$	0.964
LEVOQUE_FORM II (IPA)	$\ln(x) = 8.698 - \frac{4959.637}{T}$	0.997
LEVOQUE_FORM II (1PR)	$\ln(x) = 7.533 - \frac{4478.760}{T}$	0.990

From the linearized equations, the solution enthalpies were calculated, and all the values were found to be positive, indicating that the process is endothermic. A higher enthalpy value signifies a greater energy requirement to transition from the solid state to the dissolved state. As a result, lower temperatures are associated with low solubility. An increase in temperature leads to a more significant rise in solubility for compounds with higher solution enthalpies. The highest van't Hoff enthalpy value is achieved by LEVOQUE_IPA in isopropanol and the lowest by LEVOQUE_MeOH in methanol. All the values are reported in table 4.5.

table 4. 5 Comparison between the solubility tests

Cocrystal	solvent	Enthalpy J/mol
LEVOQUE_FORM III	Methanol	29294
LEVOQUE_FORM I	Ethanol	36143
LEVOQUE_FORM II (1PR)	1-propanol	37236
LEVOQUE_FORM II (IPA)	Isopropanol	41234

The solubility study of LEVOQUE_IPA in isopropanol revealed unusual transmissivity readings. During the second temperature cycle applied by the system, an initial increase in transmissivity was observed, followed by a sudden decrease, even as the temperature continued to increase. This behavior may be due to a polymorphic transformation into a less soluble form. Figure 4.23 shows the transmissivity reading mentioned above.

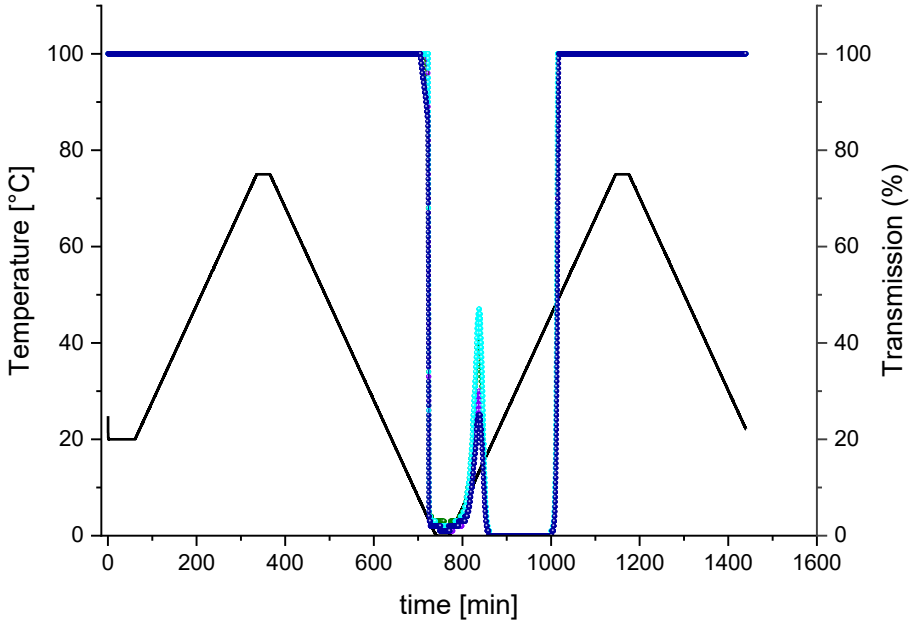

Figure 4. 23 Crystal 16 Temperature profile and transmissivity values recorded for different cocnentrations of LEVOQUE_IPA in IPA. From left to right: 9.80 mg/g (cyan), 10.56 mg/g (green), 11.58 mg/g (blue), 13.36 mg/g (violet)

4.6 Dissolution rate measurements

Dissolution tests were performed to assess the release rate of levofloxacin. A comparison was made between all the cocrystals, the physical mixture and pure levofloxacin to evaluate the API release. This comparison was carried on for both milli Q water and pH1 solution. Both powders and tablets containing mannitol and cellulose nanocrystals were tested. At specific time intervals, 1 ml samples were taken, with an equivalent volume of the appropriate solvent (milli Q water or pH1 solution) added to maintain the same volume. During the first four hours, samples were withdrawn every 30 minutes to closely monitor the initial release. Subsequently, samples were collected hourly on the same day, and then twice daily in the following days.

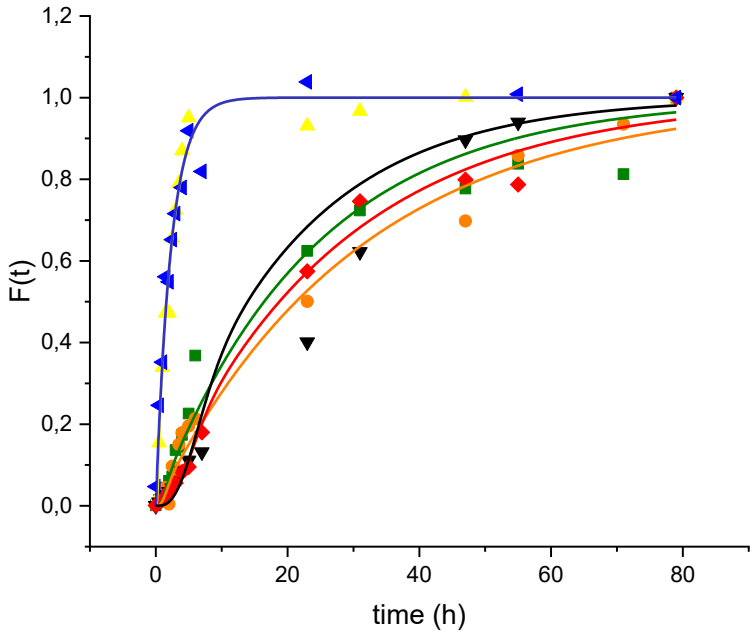

Figure 4. 24 Dissolution tests for powders in milli-Q water. From left to right: LEVO (blue), QUE (yellow), LEVOQUE_FORM I (black), LEVOQUE_FORM II (1PR) (green), LEVOQUE_FORM II (IPA) (red), LEVOQUE_FORM III (orange).

Figure 4.24 displays the results of the dissolution tests in milli-Q water. It is possible to see that both the absolute levofloxacin and the physical mixture achieved the maximum release in 23 hours, while the cocrystals needed more time, around 3 days. This is an important observation because it may allow a control on the release of the active pharmaceutical ingredient, in particular if we are looking for a sustained release modality. There was not a significant difference between the different kind of cocrystals, although it can be highlighted that LEVOQUE_FORM I seemed to be the fastest one, while LEVOQUE_FORM III seemed to be the slowest one. The curve presented are generated following the deceleratory model, as already explained in the previous section. This model does not allow a direct comparison between the different curves, because it is strongly dependent on both the fit parameters, alpha and beta. It is showed from the author himself to be challenging to do a comparison between the parameters. In table 4.6 are reported all the values calculated for these curves.

table 4. 6 Fit parameters for the deceleratory model of the dissolution tests for tablets in milli-Q water.

Specie	α (h^-1)	ß (h^-2)
LEVO	0.43	72
LEVO + QUE	0.427	61.2
LEVOQUE_IPA	0.037	0.041
LEVOQUE_1PR	0.0432	0.438
LEVOQUE_MeOH	0.0326	0.442
LEVOQUE_EtOH	0.0396	0.026

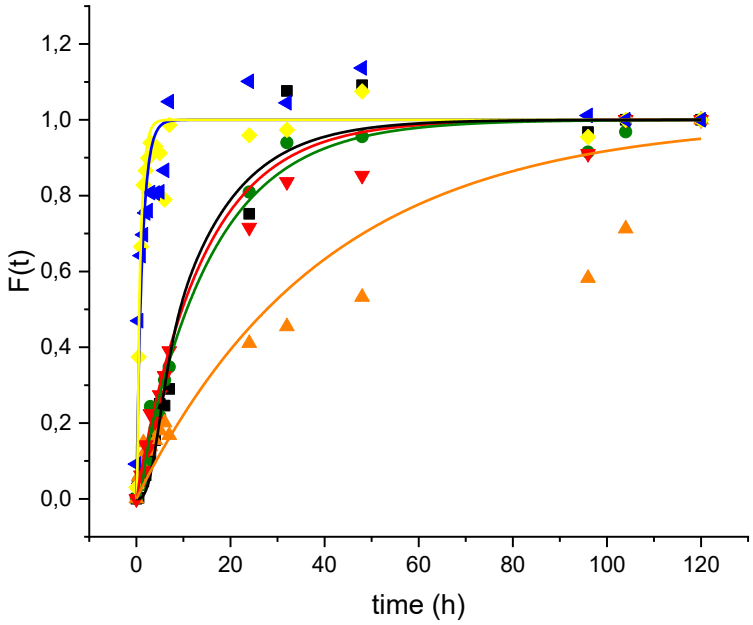

Figure 4. 25 Dissolution tests for powders in pH 1 solution. From left to right: LEVO (blue), QUE (yellow), LEVOQUE_FORM I (black), LEVOQUE_FORM II (IPA) (red), LEVOQUE_FORM II (1PR) (green), LEVOQUE_FORM III (orange).

Figure 4.25 presents the dissolution test results in the pH1 solution as modeled by the deceleratory model. It is evident that both levofloxacin and the physical mixture reach the peak dissolution within 7 hours, whereas the cocrystals require at least 32 hours. Notably, LEVOQUE_FORM III exhibits a much slower dissolution rate, taking up to 120 hours. The dissolution rate is notably higher than in milli-Q water, which is fully consistent with the exctinction factors calculated in section 3.8. Table 4.7 shows the fit parameters of the deceleratory model of the dissolution tests in pH 1 solution.

table 4. 7 Fit parameters for the deceleratory model of the dissolution tests for tablets in pH 1 solution.

Specie	α (h^-1)	ß (h^-2)
LEVO	0.8116	59.7942
LEVO + QUE	1.1844	7.0656
LEVOQUE_IPA	0.0713	11.8805
LEVOQUE_1PR	0.0646	0.4230
LEVOQUE_MeOH	0.0250	45.3616
LEVOQUE_EtOH	0.0777	0.0375

Tablets containing levofloxacin, cocrystals or the physical mixture were produced to study how the dissolution behavior differs from that of the powders. The tables were composed of 75% w/w levofloxacin/cocrystals/physical mixture, 20% w/w mannitol and 5% w/w cellulose nanocrystals. The powder blend with this composition was sieved using a 500 µm sieve and then compressed using a hydraulic press at 200 bar for 30 seconds.

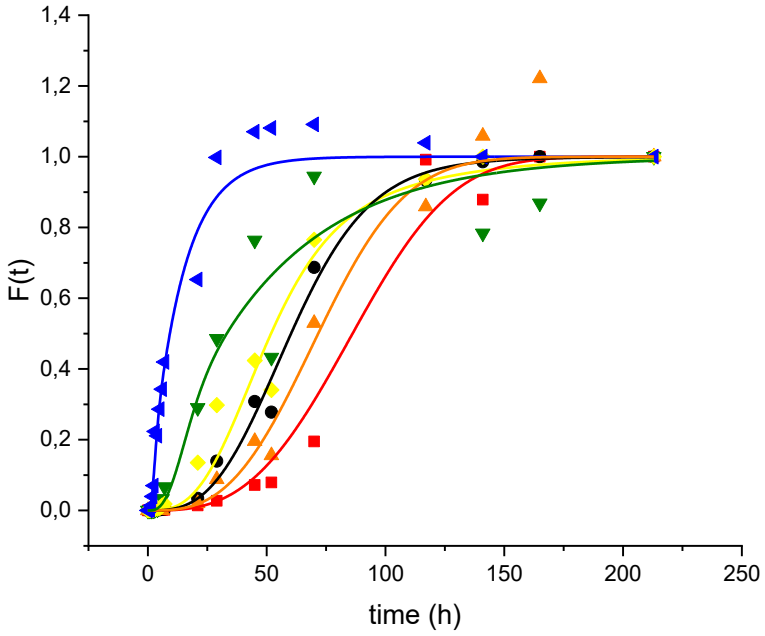

Figure 4. 26 Dissolution tests for tablets in milli-Q water. From left to right: LEVO (blue), LEVOQUE_FORM II (1PR) (green), LEVO+QUE (yellow), LEVOQUE_FORM I (black), LEVOQUE_FORM III (orange), LEVOQUE_FORM II (IPA) (red).

Figure 4.26 displays the dissolution results for the tablets dissolved in milli-Q water. This time levofloxacin and the physical mixture behave differently. Levofloxacin tablets reach the maximum dissolution at 7 hours, while the physical mixture needs 32 hours. The cocrystals show a similar behavior.

table 4. 8 Fit parameters for the deceleratory model of the dissolution tests for powders in milli-Q water.

Specie	α (h^-1)	ß (h^-2)
LEVO	0.0749	0.1365
LEVO + QUE	1.1844	7.0656
LEVOQUE_IPA	0.0713	11.8805
LEVOQUE_1PR	0.0646	0.4230
LEVOQUE_MeOH	0.0250	45.3616
LEVOQUE_EtOH	0.0777	0.0375

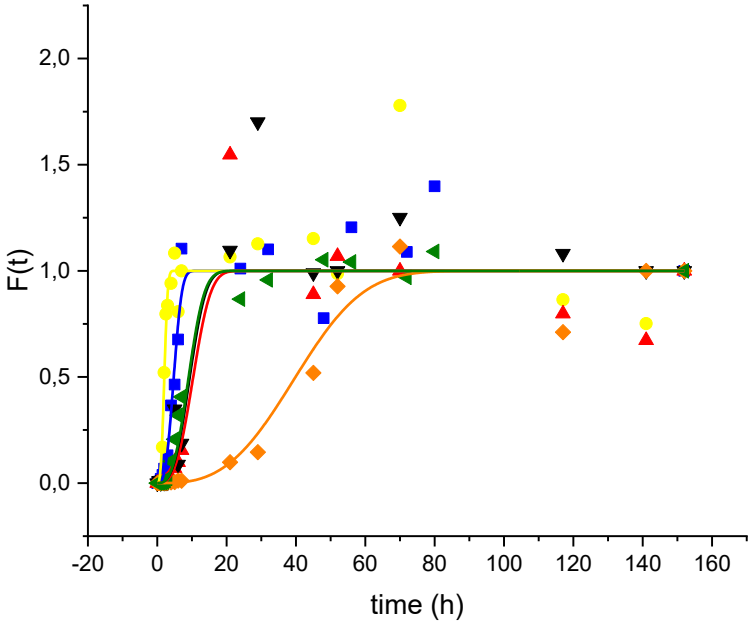

Figure 4. 27 Dissolution tests for tablets in pH 1 solution. From left to right: LEVO+QUE (yellow), LEVO (blue) LEVOQUE_FORM II (1PR) (green), LEVOQUE_FORM I (black), LEVOQUE_FORM II (IPA) (red); LEVOQUE_FORM III (orange).

Figure 4.27 shows the dissolution rates of the tablets in pH1 solution. LEVO+QUE reaches the dissolution peak in 2.5 hours, while LEVO in 7 hours. The cocrystals keep showing a slowed down behavior in comparison to pure Levofloxacin, due to the intermolecular interactions formed with the quercetin. LEVOQUE_FORM III shows a very different dissolution curve, reaching the maximum in 52 hours, while the other cocrystals need 21 hours. it is possible to observe that some points exceed the unit value, this is because the

assumption of homogeneity conditions due to perfect mixing are not always realistic and the value automatically becomes dependent on the position of the measurement.

table 4. 9Fit parameters for the deceleratory model of the dissolution tests for powders in pH1 solution

Specie	α (h^-1)	ß (h^-2)
LEVO	19.8521	0.0003
LEVO + QUE	104.7412	0.0013
LEVOQUE_IPA	9.5771	8.5279E-05
LEVOQUE_1PR	1.2299	0.0008
LEVOQUE_MeOH	10.9289	1.0009E-06
LEVOQUE_EtOH	9.5771	8.5279E-05

.

4.6.5 Comparison between the different cases for LEVOQUE_FORM I

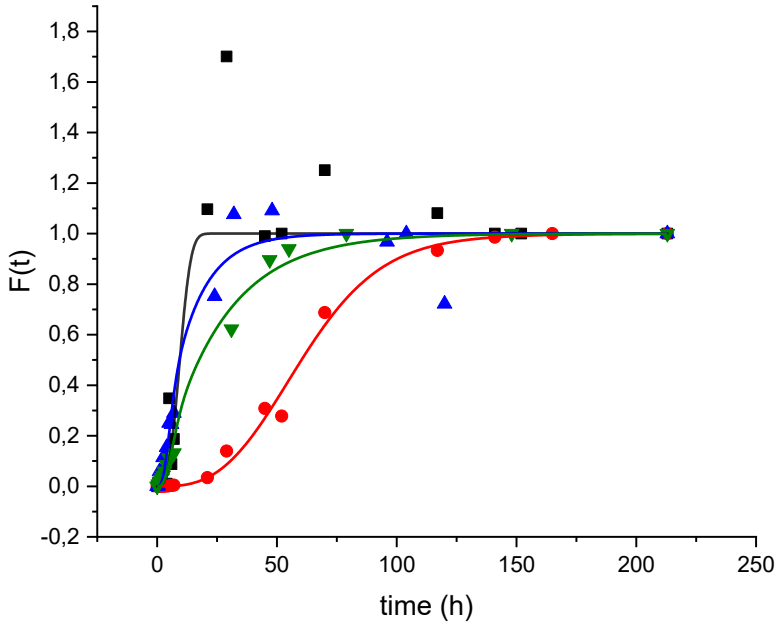

Figure 4. 28 Comparison between the different cases for LEVOQUE_FORM I. From left to right: tablet in pH1 solution (black), powder in pH1 solution (blue), powder in milli-Q water (green) and tablets in milli-Q water (red).

Figure 4.28 shows a comparison of the four different dissolution tests conducted in this study for LEVOQUE_FORM I. It is evident that the tablet containing 75% w/w LEVOQUE_FORM I, 20% mannitol and 5% CNCs in pH1 solution exhibited the fastest dissolution profile, whereas in milli-Q water it had the slowest. Overall, it can be concluded that the dissolution rate was higher in the pH 1 solution. This was anticipated when the

extinction coefficients in the Lambert-Beer law were calculated for levofloxacin, as the coefficient in pH 1 solution was higher than in milli Q water. The tablets in pH 1 solution reached the maximum dissolution value after 21 hours, while in milli-Q they took 117 hours. For the powders, the peak was reached in pH 1 solution after 32 hours and in milli Q water after 79 hours. A similar trend was observed with the other cocrystals. Tablets displayed the fastest dissolution rate, making them suitable for oral dispersion of the API.

5 Conclusion

The focus of this work was to show how crystal engineering could be used to design novel materials with several different properties. Taking into account the work previously done by (Uivarosi et al., 2024), where a LEVOQUE cocrystal in Ethanol was firstly obtained and tested against the pathogen *H. Pylori*----in this work four different solvents (methanol, ethanol, 1-propanol and isopropanol) were used to obtain four corresponding cocrystal solvates and their desolvated version. The goal was to observe the differences in term of physical-chemical properties and dissolution profiles. Different structures were visualized from the powder x-ray diffraction and the Raman spectroscopy. Differential scanning calorimetry and thermogravimetric analysis techniques were applied to obtain information on the samples' thermal behavior. The complete characterization allowed to determine the presence of solvated and desolvated structures. The desolvated structure formed in the synthesis from ethanol was called FORM I, from isopropanol and 1-propanol FORM II and from methanol FORM III. With time all these forms tend to convert to FORM II, the most stable polymorph found for this system. Different stoichiometric ratios were used to confirm stoichiometry and the cocrystal nature of the novel crystal forms. Contact angle measurements were also conducted, evidencing that the presence of quercetin in the structure increases hydrophobicity in comparison with pure levofloxacin. Solubility tests were performed to obtain data for crystallization experiments and synthesis scale up and for the scope each cocrystal solubility was studied in the respective solvent of crystallization. Dissolution tests of both powders of the cocrystals, physical mixture and pure levofloxacin in milli Q water and pH 1 solution were performed, and it was observed that in pH 1 solution the dissolution profiles are generally faster. Dissolution profiles of tablets formulated with excipients were also collected a preliminary study on tentative novel formulations. Cocrystals showed a slower dissolution rate than levofloxacin and physical mixture. This could be an advantage in terms of a sustained release, a strategy in which the active pharmaceutical ingredient is released gradually over an extended period. Crystal engineering is a powerful tool in designing sustained release formulations, as it allows control over physical properties of the drug, such as solubility and dissolution rate, by modifying the crystal structure. Cocrystals can be engineered to include an opportune conformer that provides an additional therapeutic effect or enhances the sustained release properties. The choice of one of the cocrystals presented in this thesis could be made by looking at the desired release rate of the API.

Appendix A: Model's choice

Dissolution model

Various dissolution models were tested to identify the one that best represented the experimental data collected. This section explains the calculations performed for each of the models presented. The data reported are derived from LEVOQUE_EtOH dissolution in milli-Q water. The choice is completely random. All the result are detailed in Section 4.5.

Zero order model

The dissolved mass at each time is divided by the initial concentration, which matches the concentration at the final time. The data are then plotted over time. If the plot forms a straight line, it indicates that the zero order model accurately describes the dissolution process. The model constant can be determined from the slop of this line.

First order model

The calculation for the first model involved several steps:

- First, the dissolved mass of levofloxacin was calculated at each time point of interest.
- By subtracting this value from, the mass of levofloxacin remaining in the dialysis bag was determined.
- The logarithm of the unreleased mass was then plotted against time. The slope of the resulting curve was used to calculate the kinetic constant, k_1.
- With the kinetic constant determined, the unreleased concentration over time was calculated using the following equation:

$$C(t) = C_0 \, e^{(-k_1 t)} \tag{A.1}$$

Higuchi model

The dissolved mass at each time is divided by the initial concentration and plotted against the square root of time. if the resulting points form a straight line, it indicates that the Higuchi model can accurately describe the dissolution process. The Higuchi constant can be derived from the slop of this line.

Different models were investigated during this work to try to better understand the dissolution rate of the samples analyzed. This section is dedicated to show the different considerations that brought to the effective choose of the model. Just as an example the dissolution of

LEVOQUE_FORM I in milli-Q water is considered. The models here presented are the zero order, the first order and the Higuchi.

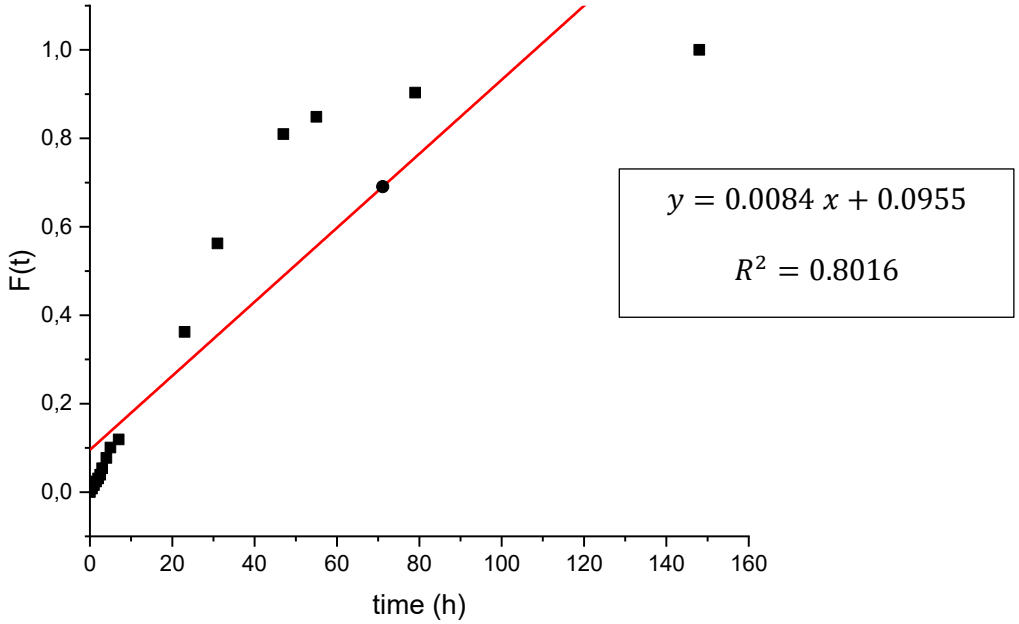

Figure A. 1 zero-order model for LEVOQUE_FORM I in milli-Q water

Figure A.1 displays the zero order for LEVOQUE_FORM I in milli-Q water. To ensure that the model is correct the points should have been disponed on a line. From this applied model is possible to observe that the active ingredient does not dissolve with a constant rate over time. The released concentration of levofloxacin does not increase linearly over time and the dissolution rate changes over time. This could suggest that other parameters may influence the dissolution rate, as the decreasing surface area of the solute.

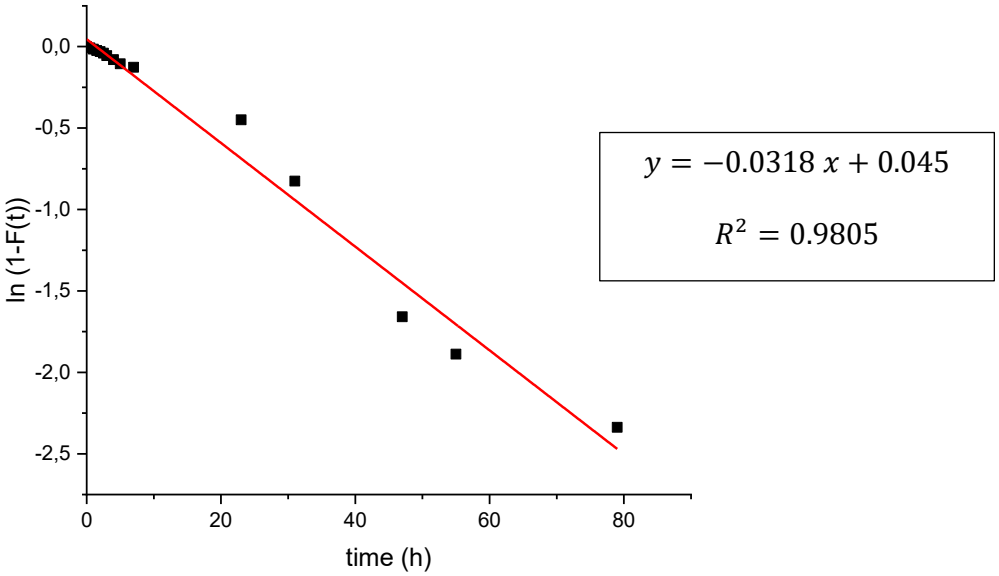

Figure A. 2 first-order model for LEVOQUE_FORM I in milli-Q water

Figure A.2 shows the logarithmic plot of the released concentration over time. Although it seems to be a good approximation, because it's near to a linear line, it can be seen from figure A.3 that the real values are very different from the calculated ones. This allowed to say that the model is not a correct interpretation of the results.

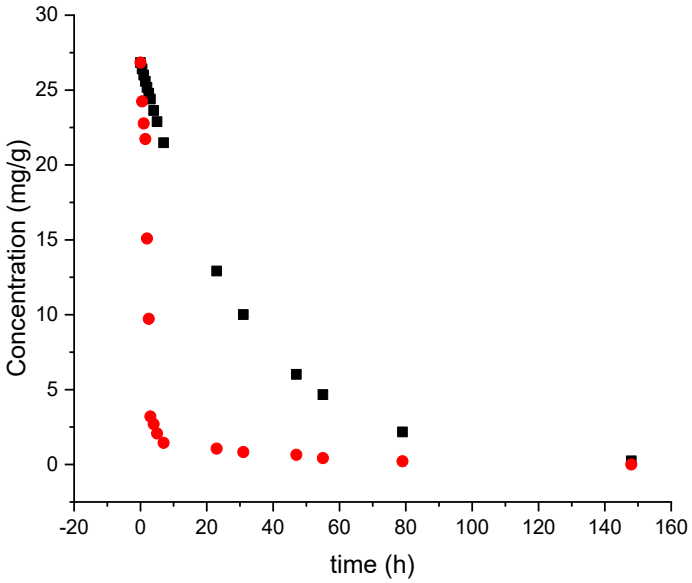

Figure A. 3 Comparison between the first order model (black) and the experiment (red) for LEVOQUE_FORM I in milli-Q water

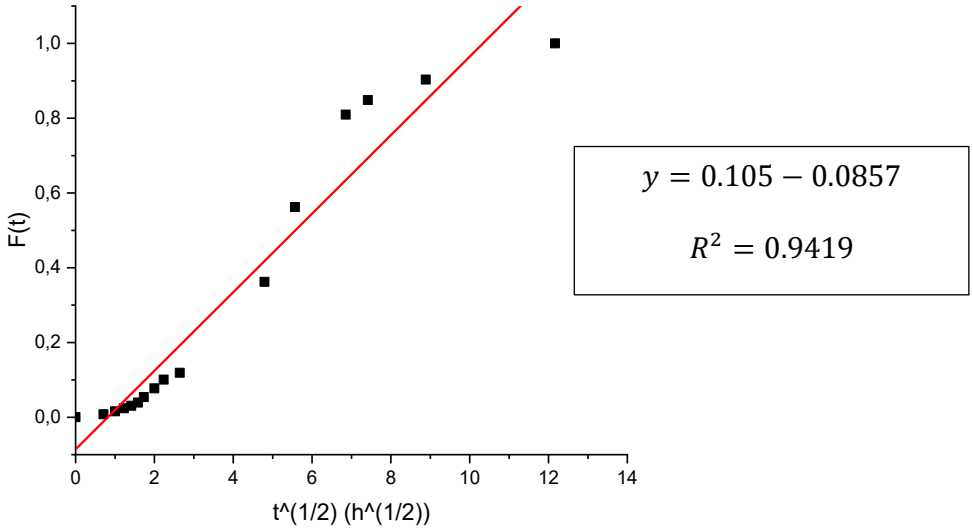

Figure A. 4 Higuchi model for LEVOQUE_FORM I in milli-Q water

Figure A.4 presents the released concentration over the square root of time. From the slope of the line the Higuchi constant was obtained. The Higuchi model was then used to calculate the model expected values. It was then made a comparison between the calculated and the real values, showing that the model is not appropriate for this kind of release (figure A.5).

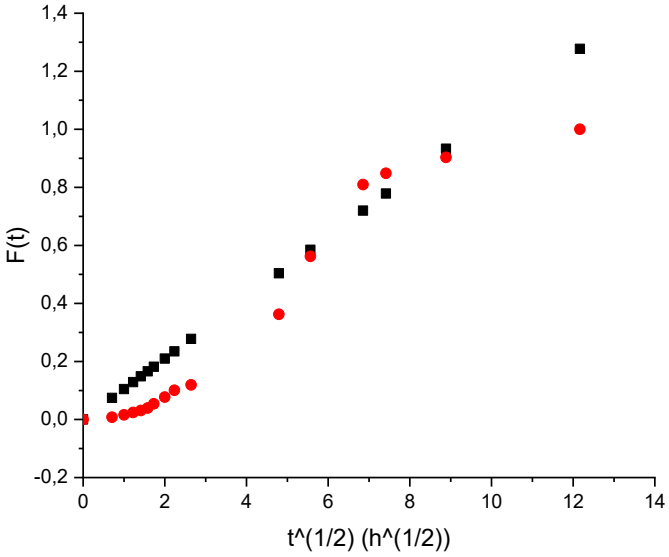

Figure A. 5 Comparison between the Higuchi model(black) and the experiments (red) for LEVOQUE_FORM I in milli-Q water

Deceleratory model

Figure A.6 displays the dispersive kinetic model, particularly the deceleratory model. The observation of asymmetric, sigmoidal dissolution profiles could be attributed to a variation in

the activation energy of the classic kinetic constant. This model appeared as a better fit for the dissolution profiles obtained for the analyzed samples.

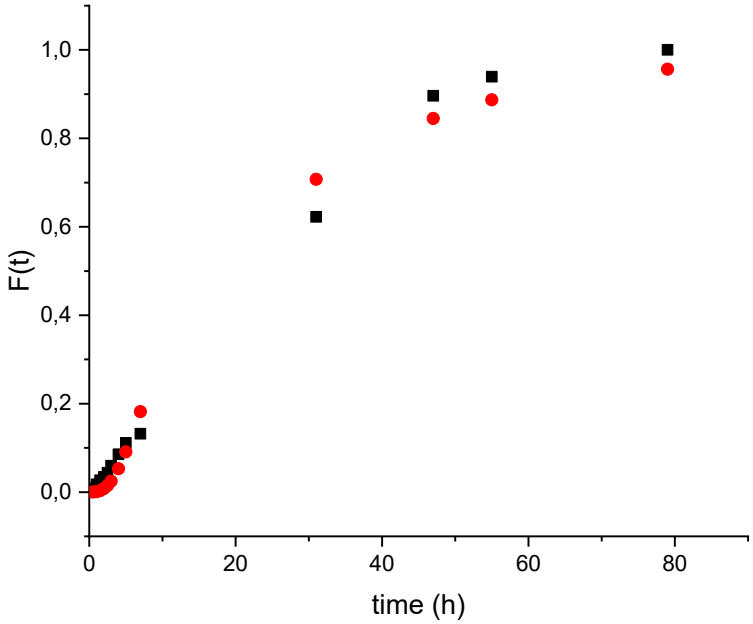

Figure A. 6 Comparison between deceleratory model (red) and the experiment (black) for LEVOQUE_FORM I in milli-Q water

Appendix B: Contact angle images

Figure B. 1 Contact angle measurement for a tablet of LEVOQUE_IPA wet by a 2 µl droplet of sunflower oil.

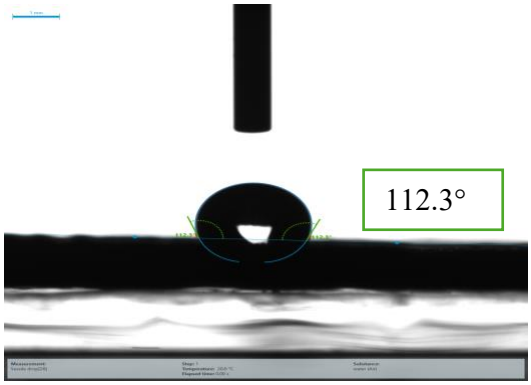

Figure B. 2 Contact angle measurement for a tablet of LEVOQUE_FORM II (IPA) wet by a 2 µl droplet of water

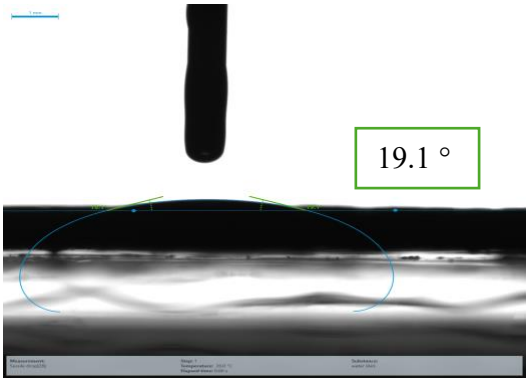

Figure B. 3 Contact angle measurement for a tablet of LEVOQUE_FORM II (IPA) wet by a 2 µl droplet of sunflower oil

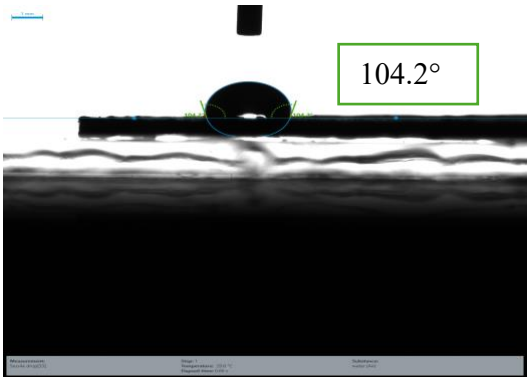

Figure B. 4 Contact angle measurement for a tablet of LEVOQUE_1PR wet by a 2 µl droplet of water

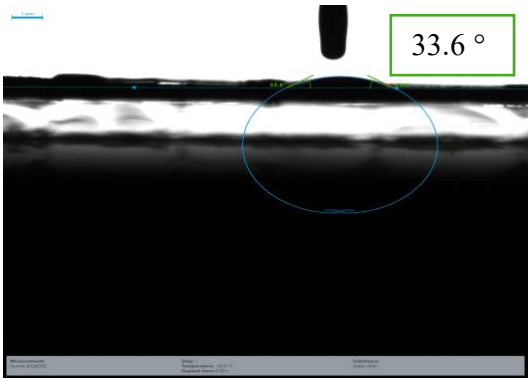

Figure B. 5 Contact angle measurement for a tablet of LEVOQUE_1PR wet by a 2 µl droplet of sunflower oil

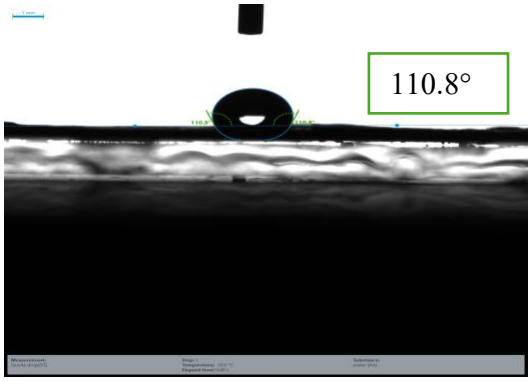

Figure B. 6 Contact angle measurement for a tablet of LEVOQUE_FORM II (1PR) wet by a 2 µl droplet of water

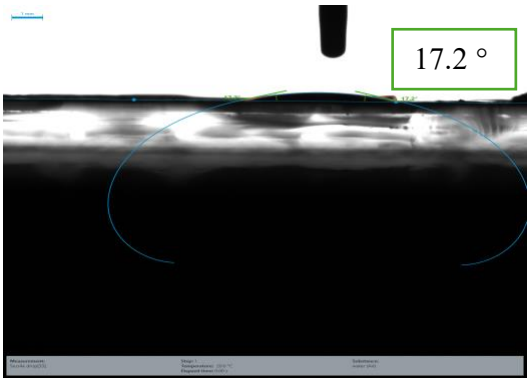

Figure B. 7 Contact angle measurement for a tablet of LEVOQUE_FORM II (1PR) wet by a 2 µl droplet of sunflower oil

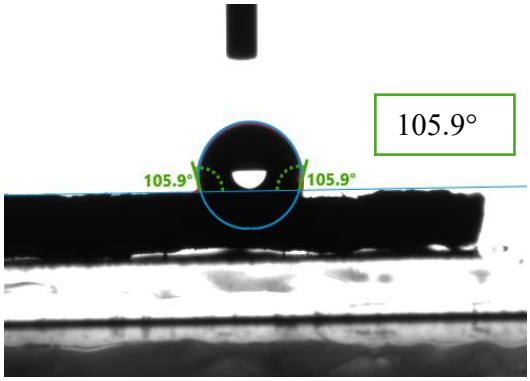

Figure B. 8 Contact angle measurement for a tablet of LEVOQUE_FORM I wet by a 2 µl droplet of water

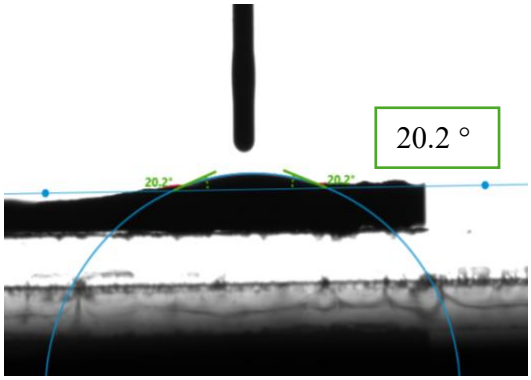

Figure B. 9 Contact angle measurement for a tablet of LEVOQUE_EtOH wet by a 2 µl droplet of sunflower oil

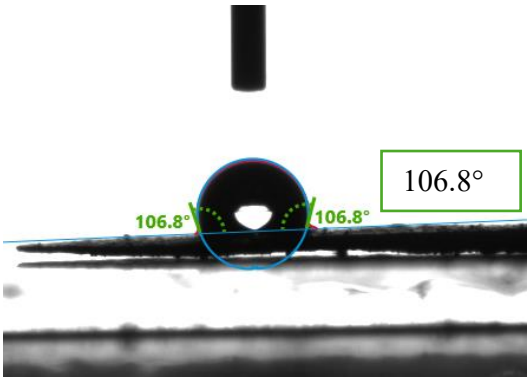

Figure B. 10 Contact angle measurement for a tablet of LEVOQUE_FORM III wet by a 2 µl droplet of water

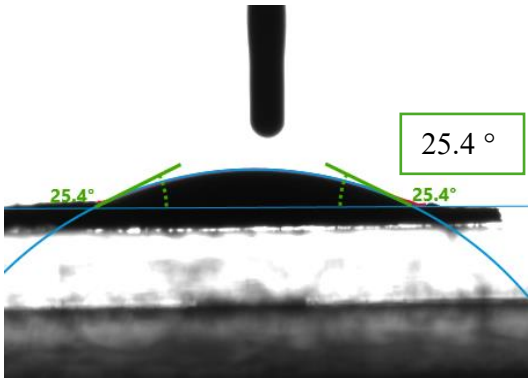

Figure B. 11 Contact angle measurement for a tablet of LEVOQUE_FORM III wet by a 2 µl droplet of sunflower oil

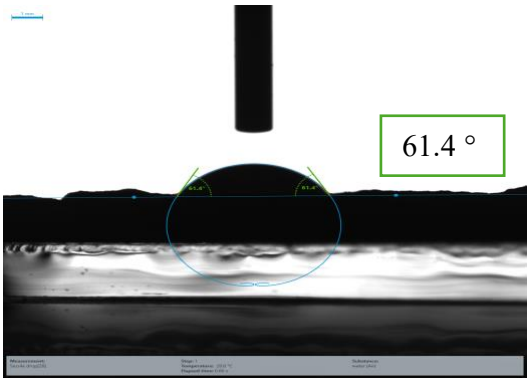

Figure B. 12 Contact angle measurement for a tablet of LEVO wet by a 2 µl droplet water at t0.

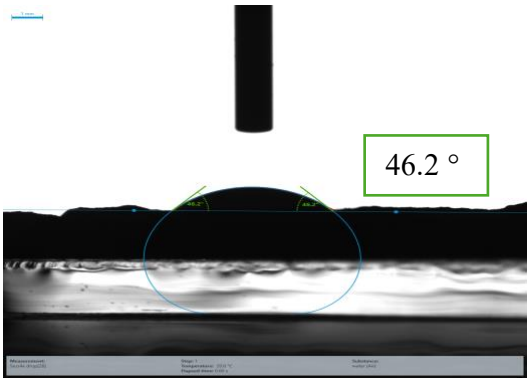

Figure B. 13 Contact angle measurement for a tablet of LEVO wet by a 2 µl droplet water at t0.

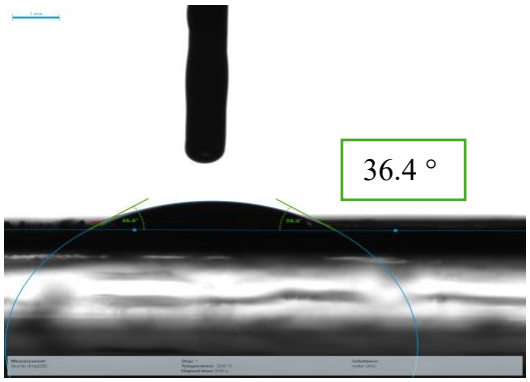

Figure B. 14 Contact angle measurement for a tablet of LEVO wet by a 2 µl droplet water at t0.

References

Ali, A., Wai Chiang, Y., & Santos, R. M. (2022). *Citation: minerals X-ray Diffraction Techniques for Mineral Characterization: A Review for Engineers of the Fundamentals, Applications, and Research Directions*. https://doi.org/10.3390/min12020205

Almeida, S. L., Lazo, R. L., Carneiro, J., Caldonazo, A., Pires, C., Andreazza, I. F., & Murakami, F. S. (2024). Cellulose nanocrystals as an innovative superdisintegrant for oral dispersible tablets. *Journal of Drug Delivery Science and Technology*, *96*, 105694. https://doi.org/10.1016/J.JDDST.2024.105694

Amrihesari, M., Murry, A., & Brettmann, B. (2023). Towards standardized polymer solubility measurements using a parallel crystallizer. *Polymer*, *278*, 125983. https://doi.org/10.1016/J.POLYMER.2023.125983

Anwer, F., Aftab, S., Waheed, U., & Muhammad, S. S. (2017). Agile Software Development Models TDD, FDD, DSDM, and Crystal Methods: A Survey. *INTERNATIONAL JOURNAL OF MULTIDISCIPLINARY SCIENCES AND ENGINEERING*.

Appelbaum, P. C., & Hunter, P. A. (2000). The fluoroquinolone antibacterials: past, present and future perspectives. *International Journal of Antimicrobial Agents*, *16*(1), 5–15. https://doi.org/10.1016/S0924-8579(00)00192-8

Barmpalexis, P., Karagianni, A., Nikolakakis, I., & Kachrimanis, K. (2018). Artificial neural networks (ANNs) and partial least squares (PLS) regression in the quantitative analysis of cocrystal formulations by Raman and ATR-FTIR spectroscopy. *Journal of Pharmaceutical and Biomedical Analysis*, *158*, 214–224. https://doi.org/10.1016/J.JPBA.2018.06.004

Bumbrah, G. S., & Sharma, R. M. (2016). Raman spectroscopy – Basic principle, instrumentation and selected applications for the characterization of drugs of abuse. *Egyptian Journal of Forensic Sciences*, *6*(3), 209–215. https://doi.org/10.1016/J.EJFS.2015.06.001

Bunaciu, A. A., Udriştioiu, E. gabriela, & Aboul-Enein, H. Y. (2015). X-Ray Diffraction: Instrumentation and Applications. *Critical Reviews in Analytical Chemistry*, *45*(4), 289–299. https://doi.org/10.1080/10408347.2014.949616

Butt, H. J., Liu, J., Koynov, K., Straub, B., Hinduja, C., Roismann, I., Berger, R., Li, X., Vollmer, D., Steffen, W., & Kappl, M. (2022). Contact angle hysteresis. *Current Opinion in Colloid & Interface Science*, *59*, 101574. https://doi.org/10.1016/J.COCIS.2022.101574

Cieślik-Boczula, K., Maniewska, J., Grynkiewicz, G., Szeja, W., Koll, A., & Hendrich, A. B. (2012). Interaction of quercetin, genistein and its derivatives with lipid bilayers – An ATR IR-spectroscopic study. *Vibrational Spectroscopy*, *62*, 64–69. https://doi.org/10.1016/J.VIBSPEC.2012.05.010

Costa, P., & Sousa Lobo, J. M. (2001). Modeling and comparison of dissolution profiles. *European Journal of Pharmaceutical Sciences*, *13*(2), 123–133. https://doi.org/10.1016/S0928-0987(01)00095-1

Dai, H., Lu, X., Peng, Y., Yang, Z., & Zhu, H. (2017). Characteristics of metastable zone in the crystallization process: A case study of sparingly soluble hydroxyapatite. *Desalination and Water Treatment*, *62*. https://doi.org/10.5004/dwt.2017.1647

Delgado, R. (2022). *Misuse of Beer-Lambert Law and other calibration curves*. https://doi.org/10.1098/rsos.211103

Desiraju, G. R., Vittal, J. J., & Ramanan, A. (2011). *Crystal Engineering*. https://doi.org/10.1142/8060

Drlica, K. (1999). Mechanism of fluoroquinolone action. *Current Opinion in Microbiology*, *2*(5), 504–508. https://doi.org/10.1016/S1369-5274(99)00008-9

Fda, Cder, Stewart, & Felicia. (2018). *Regulatory Classification of Pharmaceutical Co-Crystals Guidance for Industry*. http://www.fda.gov/Drugs/GuidanceComplianceRegulatoryInformation/Guidances/default.htm

Gibbs free energy change during bubble nucleation. The surface free... | Download Scientific Diagram. (n.d.). Retrieved July 25, 2024, from https://www.researchgate.net/figure/Gibbs-free-energy-change-during-bubble-nucleation-The-surface-free-energy-G-sur-f_fig2_328206118

Giridhar, G., Manepalli, R. K. N. R., & Apparao, G. (2017). Contact Angle Measurement Techniques for Nanomaterials. *Thermal and Rheological Measurement Techniques for Nanomaterials Characterization*, *3*, 173–195. https://doi.org/10.1016/B978-0-323-46139-9.00008-6

Gonzá Lez, A. S., Casado, J., & Ngel Lanas, A. ´. (n.d.). *Fighting the Antibiotic Crisis: Flavonoids as Promising Antibacterial Drugs Against Helicobacter pylori Infection*. https://doi.org/10.3389/fcimb.2021.709749

Guide to Raman Spectroscopy | Bruker. (n.d.). Retrieved July 25, 2024, from https://www.bruker.com/en/products-and-solutions/infrared-and-raman/raman-spectrometers/what-is-raman-spectroscopy.html

Guo, M., Sun, X., Chen, J., & Cai, T. (2021). Pharmaceutical cocrystals: A review of preparations, physicochemical properties and applications. *Acta Pharmaceutica Sinica B*, *11*(8), 2537–2564. https://doi.org/10.1016/J.APSB.2021.03.030

Joseph, A. (2007). Novel co-processed excipients of mannitol and microcrystalline cellulose for preparing fast dissolving tablets of glipizide Indian Journal of Pharmaceutical Sciences Scientifi c Publication of the Indian Pharmaceutical Association. *Article in Indian Journal of Pharmaceutical Sciences*. https://doi.org/10.4103/0250-474X.38467

Kavanagh, O. N., Croker, D. M., Walker, G. M., & Zaworotko, M. J. (2019). Pharmaceutical cocrystals: from serendipity to design to application. *Drug Discovery Today*, *24*(3), 796–804. https://doi.org/10.1016/J.DRUDIS.2018.11.023

Kodal, M., Karakaya, N., Wis, A. A., & Ozkoc, G. (2019). Thermal Properties (DSC, TMA, TGA, DTA) of Rubber Nanocomposites Containing Carbon Nanofillers. *Carbon-Based Nanofillers and Their Rubber Nanocomposites: Fundamentals and Applications*, 325–366. https://doi.org/10.1016/B978-0-12-817342-8.00011-1

Kwok, D. Y., & Neumann, A. W. (1999). Contact angle measurement and contact angle interpretation. *Advances in Colloid and Interface Science*, *81*(3), 167–249. https://doi.org/10.1016/S0001-8686(98)00087-6

Le Pevelen, D. D. (2010). Small Molecule X-Ray Crystallography, Theory and Workflow. *Encyclopedia of Spectroscopy and Spectrometry, Second Edition*, 2559–2576. https://doi.org/10.1016/B978-0-12-374413-5.00359-6

Leuner, C., & Dressman, J. (2000). Improving drug solubility for oral delivery using solid dispersions. In *European Journal of Pharmaceutics and Biopharmaceutics* (Vol. 50, Issue 1). https://doi.org/10.1016/S0939-6411(00)00076-X

Li, N., Han, S., Lin, S., Sha, X. Y., & Hasi, W. (2021). Fabrication of an AAO-based surface-enhanced Raman scattering substrate for the identification of levofloxacin in milk. *New Journal of Chemistry*, *45*(17), 7571–7577. https://doi.org/10.1039/D1NJ00642H

Li, Y., Yao, J., Han, C., Yang, J., Chaudhry, M. T., Wang, S., Liu, H., & Yin, Y. (n.d.). *nutrients Quercetin, Inflammation and Immunity*. https://doi.org/10.3390/nu8030167

Liu, S., Huang, J., Chen, Z., Chen, N., Pang, F., Wang, T., & Hu, L. (2015). *Raman spectroscopy measurement of levofloxacin lactate in blood using an optical fiber nano-probe*. https://doi.org/10.1002/jrs.4629

Lokhandwala, H., Deshpande, A., & Deshpande, S. (2013). KINETIC MODELING AND DISSOLUTION PROFILES COMPARISON: AN OVERVIEW drug release kinetic models, model dependent method, model independent method, statistical model, pairwise comparison. *Int J Pharm Bio Sci*, *4*(1), 728–737. www.ijpbs.net

Mansfield, E., Kar, A., & Hooker, S. A. (n.d.). *Applications of TGA in quality control of SWCNTs*. https://doi.org/10.1007/s00216-009-3319-2

Marmur, A., Volpe, C. Della, Siboni, S., Amirfazli, A., & Drelich, J. W. (2017). Contact angles and wettability: Towards common and accurate terminology. *Surface Innovations*, *5*(1). https://doi.org/10.1680/jsuin.17.00002

Mishra, S. (2024). *New Excipient For Oral Drug Delivery: CNC Derived From Sugarcane Bagasse-Derived Microcrystalline Cellulose*. https://doi.org/10.1021/acsomega.4c00497

Mosorov, V. (2017). The Lambert-Beer law in time domain form and its application. *Applied Radiation and Isotopes*, *128*, 1–5. https://doi.org/10.1016/J.APRADISO.2017.06.039

Mulvaney, S. P., & Keating, C. D. (2000). *Raman Spectroscopy*. https://doi.org/10.1021/a10000155

Nordström, F. L., & Rasmuson, Å. C. (2009). Prediction of solubility curves and melting properties of organic and pharmaceutical compounds. *European Journal of Pharmaceutical Sciences*, *36*(2–3), 330–344. https://doi.org/10.1016/J.EJPS.2008.10.009

Numata, Y., & Tanaka, H. (2011). Quantitative analysis of quercetin using Raman spectroscopy. *Food Chemistry*, *126*(2), 751–755. https://doi.org/10.1016/J.FOODCHEM.2010.11.059

Panche, A. N., Diwan, A. D., & Chandra, S. R. (2016). Flavonoids: an overview. *Journal of Nutritional Science*, *5*, 1–15. https://doi.org/10.1017/jns.2016.41

Pawar, N., Saha, A., Nandan, N., & Parambil, J. V. (2021). *Solution Cocrystallization: A Scalable Approach for Cocrystal Production*. https://doi.org/10.3390/cryst11030303

R, K. A. (2014). Mathematical Models of Drug Dissolution: A Review. *Scholars Academic Journal of Pharmacy (SAJP)*, *3*(5), 388–396. www.saspublisher.com

Ray, A. K. (2023). Crystallisation. In *Coulson and Richardson's Chemical Engineering: Volume 2B: Separation Processes* (Vol. 2B). https://doi.org/10.1016/B978-0-08-101097-6.00006-7

Rissanen, Kari. (2021). *Hot topics in crystal engineering*.

Saadatkhah, N., Adrián, |, Garcia, C., Ackermann, S., Leclerc, P., Latifi, | Mohammad, Samih, | Said, Patience, G. S., Chaouki, | Jamal, & Chaouki, J. (2019). *Experimental methods in chemical engineering: Thermogravimetric analysis-TGA*. https://doi.org/10.1002/cjce.23673

Siepmann, J., & Siepmann, F. (2013). Mathematical modeling of drug dissolution. *International Journal of Pharmaceutics*, *453*(1), 12–24. https://doi.org/10.1016/J.IJPHARM.2013.04.044

Sinha, R. K., & Biswas, P. (2020). Structural elucidation of Levofloxacin and Ciprofloxacin using density functional theory and Raman spectroscopy with inexpensive lab-built setup. *Journal of Molecular Structure*, *1222*, 128946. https://doi.org/10.1016/J.MOLSTRUC.2020.128946

Sitovs, A., Sartini, I., & Giorgi, M. (2021). Levofloxacin in veterinary medicine: a literature review. *Research in Veterinary Science*, *137*, 111–126. https://doi.org/10.1016/J.RVSC.2021.04.031

Skrdla, P. J. (n.d.). *Crystallizations, Solid-State Phase Transformations and Dissolution Behavior Explained by Dispersive Kinetic Models Based on a Maxwell-Boltzmann Distribution of Activation Energies: Theory, Applications, and Practical Limitations*. https://doi.org/10.1021/jp904505w

Skrdla, P. J. (2007). A simple model for complex dissolution kinetics: A case study of norfloxacin. *Journal of Pharmaceutical and Biomedical Analysis*, *45*(2), 251–256. https://doi.org/10.1016/J.JPBA.2007.06.012

Smith, E., & Dent, G. (2019). Modern raman spectroscopy: A practical approach. *Modern Raman Spectroscopy: A Practical Approach*, 1–241. https://doi.org/10.1002/0470011831

Spink, C. H. (2008). Differential Scanning Calorimetry. *Methods in Cell Biology*, *84*, 115–141. https://doi.org/10.1016/S0091-679X(07)84005-2

Stura, E. A., & Wilson, I. A. (1990). Analytical and production seeding techniques. *Methods*, *1*(1), 38–49. https://doi.org/10.1016/S1046-2023(05)80145-8

Thanh, N. T. K., Maclean, N., & Mahiddine, S. (2014). *Mechanisms of Nucleation and Growth of Nanoparticles in Solution*. https://doi.org/10.1021/cr400544s

Uivarosi, V., Fiore, C., Antoniciello, F., Roncarati, D., Scarlato, V., Grepioni, F., & Braga, D. (2024). *Levofloxacin and Ciprofloxacin Co-Crystals with Flavonoids: Solid-State Investigation for a Multitarget Strategy against Helicobacter pylori*. https://doi.org/10.3390/pharmaceutics16020203

Victor, A., David, A., Arulmoli, R., & Parasuraman, S. (2016). *Overviews of Biological Importance of Quercetin: A Bioactive Flavonoid*. https://doi.org/10.4103/0973-7847.194044

Wolansky, G., & Marmur, A. (1999). Apparent contact angles on rough surfaces: the Wenzel equation revisited. *Colloids and Surfaces A: Physicochemical and Engineering Aspects*, *156*(1–3), 381–388. https://doi.org/10.1016/S0927-7757(99)00098-9

Wu, S. N., Chiang, H. T., Shen, A. Y., & Lo, Y. K. (2003). Differential effects of quercetin, a natural polyphenolic flavonoid, on L-type calcium current in pituitary tumor (GH3) cells and neuronal NG108-15 cells. *Journal of Cellular Physiology*, *195*(2). https://doi.org/10.1002/jcp.10244